Space Science and Engineering Cent
University of Wisconsin–Madison

Final Report on NASA contract NAGW-1745

Studying the Impact of Cold-Frontal Passages on Geomorphic Evolution of the Louisiana Coast

A REPORT from the

COOPERATIVE INSTITUTE FOR METEOROLOGICAL SATELLITE STUDIES

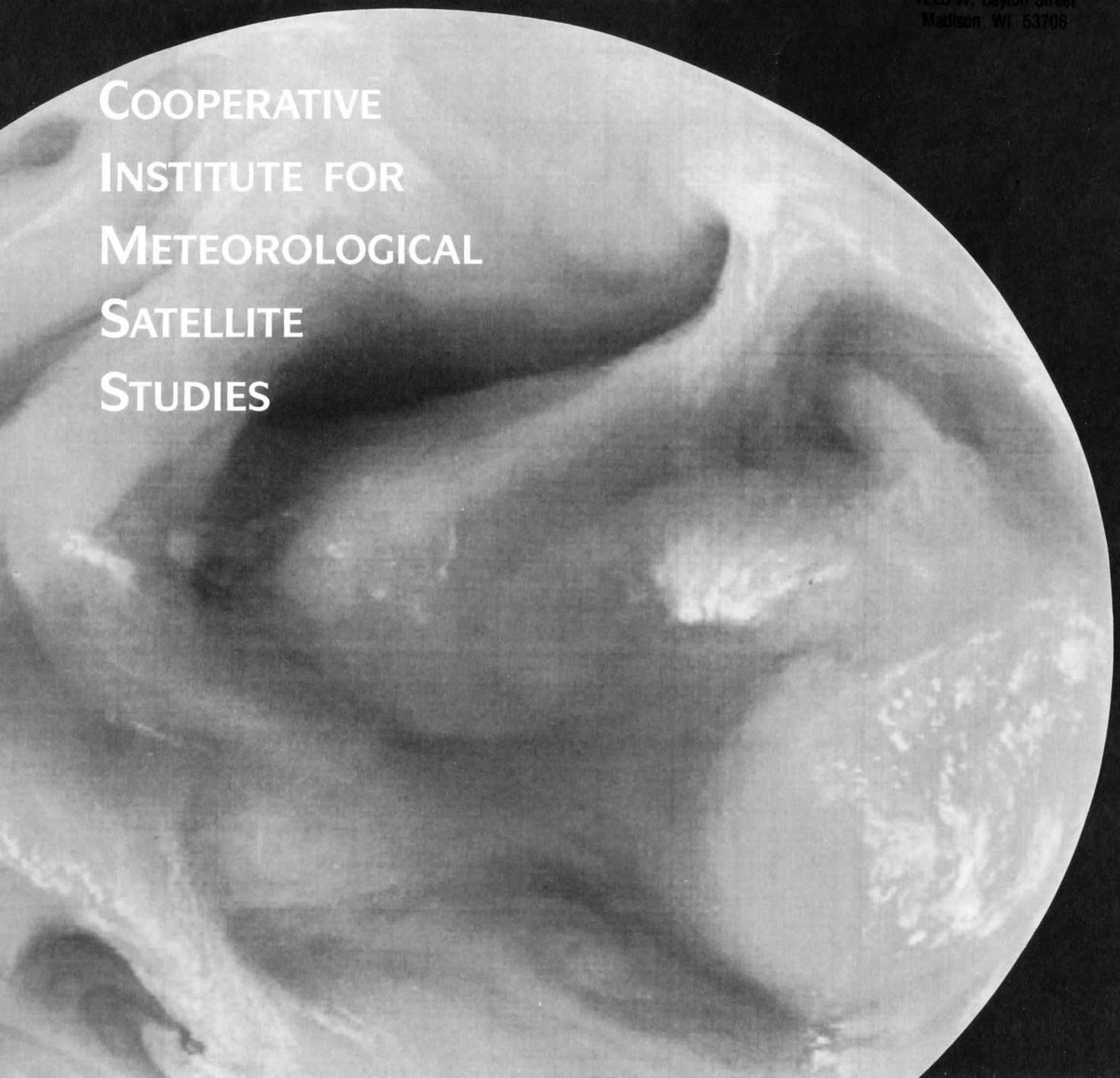

Final Report on NASA contract NAGW-1745

Studying the Impact of Cold-Frontal Passages on Geomorphic Evolution of the Louisiana Coast

for the period of 1 January 1989 to 30 June 1993

submitted by

W. Paul Menzel

Christopher C. Moeller

Cooperative Institute for Meteorological Satellite Studies (CIMSS)

University of Wisconsin

1225 West Dayton Street

Madison, Wisconsin 53706

and

Harry H. Roberts

Oscar K. Huh

Coastal Studies Institute (CSI)

Louisiana State University

308 Howe-Russell Geoscience Complex

Baton Rouge, Louisiana 70803

October 1993

Table of Contents

I. INTRODUCTION

Recent work has indicated the importance of cold front passages on coastal environments (Huh et al. 1984; Roberts et al. 1987; Moeller et al. 1991; Huh et al. 1991). Cold fronts impact coastal regions through their associated wind, temperature, and pressure patterns, causing redistribution of sediment, water level fluctuation, wave action, and by affecting water temperatures and moisture content of fresh shoreline sediment deposits (Roberts et al. 1987). The influence that cold front passages have on the Louisiana coastal environments, including land loss and land building processes, have been the primary topic of this multidisciplinary research, which combines meteorological remote sensing expertise from the University of Wisconsin with expertise in coastal processes from Louisiana State University. Coastal impacts/responses that have been investigated include the response of suspended sediment plumes (primary source of depositional material), sea surface temperature and its relationship to water depth, coastal circulation patterns, and deposition/erosion patterns along the Louisiana coast. An unexpected finding, that visible/near infrared reflectance and sea surface temperature correlate to define water types, is the subject of continuing research (under a follow-on project).

The study was designed to apply remote sensing as a primary source of information for coastal research. This approach is necessary for a comprehensive spatial study because of the difficulty of gathering surface data in coastal environments, with many regions inaccessible or impractical to reach by surface transportation. This project thus served as a testing ground for the informational content of high resolution remote sensing measurements in a coastal environment. The understandings gained from this effort will benefit the application of multispectral observations from the MODIS instrument (estimated launch in 1998).

Remote sensing data collection was supported for the Multispectral Atmospheric Mapping Sensor (MAMS) which flew at 20 km altitude on NASA's ER-2 aircraft.

MAMS scans a 37 km swath collecting 100 m spatial resolution data. The Calibrated Airborne Multispectral Scanner (CAMS) was flown on the NASA Learjet (under separate funding) at two different altitudes, swath widths, and spatial resolution (2.01 km altitude, 2.33 km wide swath, 5 m resolution; and 12.07 km altitude, 14.01 km wide swath, 30 m resolution). Experimental work using surveyed ground targets resulted in a high speed georeferencing software package developed at NASA's Stennis Space Center under NASA NAG13-4 as well as under this project. The CAMS data at the two scales and its associated color aerial photography provided excellent geomorphic detail, supplementing the MAMS larger scale multispectral observations. MAMS and CAMS collected data on the visible reflectance and thermal properties of the Louisiana coastal region ; *in situ* boat measurements of suspended sediment concentration, sea surface temperature, secchi disk depth and salinity were also collected (separate funding) to compare to the MAMS data. Other meteorological data from conventional NWS networks were collected at the University of Wisconsin and Louisiana State University.

NOAA satellite AVHRR visible and thermal imagery were also acquired before, during and after aircraft missions to provide support for aircraft and *in situ* measurement operations as well as for contextual information on environmental conditions.

II. RESEARCH ACCOMPLISHMENTS

A. MAMS data collection

MAMS was flown on NASA's ER-2 aircraft over the Louisiana coast beginning with the cold front season of 1987-88. A list of MAMS Louisiana coast flights through the end of this grant is shown in Table 1. Data quality is generally very good. In a few cases, the aircraft navigation data, which is important for earth referencing the MAMS data and collocating between data sets, was lost (recorder failure). In these cases a synthetic navigation, which utilized known ground points was applied. Results of this

Table 1. - MAMS Louisiana Coast Flight Summary

DATE	COVERAGE	*in situ*	COMMENTS
01/27/88	Type 1		clear, no navigation; light winds
08/26/88	Type 1		summer; thin cirrus
11/02/88	Type 1	X	cirrus; 12μm failure
03/30/89	Type 1		clear, prefrontal; SW wind
04/01/89	Type 1	X	clear, postfrontal; NE wind; frontal passage pair w/Mar30
04/06/89	Type 2		clear, triple overpass; transition to prefrontal; wind light from SE
12/13/89	Type 1	*	clear, postfrontal; low water;
04/15/90	Type 2		triple overpass; postfrontal; light winds
04/16/90	Type 1		transition to prefrontal; high tide; some cloud; light winds
12/04/90	Type 2	X	postfrontal; low water; data gaps; strong winds
12/05/90	Type 1	X	postfrontal; clear; light winds consecutive day pair w/Dec 4
03/30/91	Type 2		triple overpass; postfrontal; cloud streets; 11μm failed
04/01/91	Type 1		postfrontal; clear; light winds high tide
12/11/92	Type 1	X	postfrontal; light wind; no navigation; some cirrus; bad roll correction

Notes:
Thermal channel data available with 10 bit precision; others at 8 bit precision.
Type 1 flights cover full Louisiana coastline.
Type 2 flights overpass the Atchafalaya Bay region of the Louisiana coast repeatedly.
* Boat ramp water level too low to launch boat.

were good. Rare occurrences of channel data loss occurred on Nov 2 1988 and March 30 1991. These were unfortunate but quickly repaired. Bad roll correction problems can be removed during data processing, with some loss of data on the limbs of the scan.

The MAMS data sets have been split into straight line flight track segments, navigated, and archived on tape for future use. Blackbody count and data line dropouts were also replaced with averaged data for the archived data set. See Jedlovec et al., (1989) for a detailed description of the MAMS instrument.

In addition to the MAMS data collection, the NASA ER-2 aircraft collected 10 meter resolution false color infrared photographic data during most flights. These data are a useful source of information on small scale geomorphology, serving also as a verification data set for observations in MAMS data.

B. MAMS Observations and Results

1. Sediment Plume Response to Cold Front Passage

The response of the Atchafalaya River sediment plume to the prefrontal and postfrontal phases of a cold front passage has been documented using MAMS data from March 30 and April 1, 1989 (Moeller et al., 1993). Monitoring suspended sediment is a critical component for identifying potential regions of coastal progradation (and conversely erosion) as the sediment is a primary source of depositional material. MAMS visible data was corrected for atmospheric effects in order to isolate the water leaving turbidity radiance (Gumley 1990b). The sediment plume was deflected by the near surface winds of the cold front. In the prefrontal phase, southwesterly winds retarded the natural flow of the sediment plume towards the southwest, depriving the Chenier Plain coast of the sediment source. After frontal passage, northeasterly winds allowed the plume to shift back towards the west, once again hugging the Chenier Plain coast. A similar response has also been observed around the Mississippi River Birdfoot delta. These results are documented in Moeller, et al., (1993), a copy of which is included in Appendix A of this report.

2. MAMS Suspended Sediment and Sea Surface Temperature Products

Algorithms to compute suspended sediment concentration (SSC) and sea surface temperature (SST) products directly from MAMS data were generated with the help of boat collected *in situ* measurements of these quantities. MAMS visible data were atmospherically corrected using a scattering model based on Gordon et al., (1983) and

Guzzi et al., (1987) and assembled by Gumley (1990a,b). The corrected radiances were compared to boat *in situ* measurements of SSC for regression coefficient development. Regressions were meaningful, but lacked robustness (Gumley 1990a). Uncertainty associated with the absolute calibration of MAMS visible data from flight to flight complicates this effort. Increasing the regression data set and improving the regression is an ongoing effort in the follow-on project to this work. MAMS thermal data were atmospherically corrected for water vapor effects using a split window technique (Bates, et al., 1987). A comparison of SST using existing VISSR Atmospheric Sounder (VAS) SST coefficients and those developed for MAMS from boat *in situ* measurements showed little difference (< 1 K). The *in situ* data set for MAMS SST also is being expanded in the follow-on project to this work. Maps of turbidity-related reflectance and SST were produced for all case studies. Examples are shown in Moeller et al., (1989), and Moeller et al., (1993).

3. Sea Surface Temperature Response to Atmospheric Conditions

This topic was studied by comparing MAMS SST products under prefrontal and postfrontal atmospheric conditions. Results showed that in shallow bays and nearshore shallow waters (0 - 6 m deep), SSTs cooled in response to changing atmospheric temperatures associated with the cold front passage. SST was observed to drop 2 - 3 K after cold front passage in waters of 1 m depth or less, with smaller changes in waters up to 6 m depth (case study of March 30 - April 1, 1989, Moeller et al., 1993). In this particular case, air temperature dropped about 5 - 7 °C in the 36 hours following cold front passage. These results were corroborated with *in situ* buoy SST and with AVHRR SST analyses to the degree that the 1 km nadir resolution and overpass positioning of the AVHRR data would allow. This signal to water depth can be isolated in regions where no horizontal temperature advection is taking place in the water (e.g. many bay regions along the coast); the analysis is complicated by riverine and marsh influx into bays in

some regions. A solar heating effect is superimposed on the SST response to atmospheric temperature, causing shallow water warming in cold atmospheric conditions under sunny skies.

4. Observations of Progradation Along the Chenier Plain Coast

Field site survey, and aircraft photography data were used to identify regions of coastal progradation. On the Chenier Plain, significant progradation is taking place along a 14 km stretch near Freshwater Bayou Outlet. Estimates based on field survey and aircraft photography place progradation at or exceeding 60 m/yr over the last 4 years. Huh et al., (1991) documents some of this growth; a copy is included in Appendix A. Signature of this growth has also been seen in MAMS thermal data. Exposed, recent deposits of mud appear as warm features in the data. This is attributable to rapid warming of the dark mud deposits when exposed to sun, as compared to surrounding vegetated surface or nearshore shallow water. The 100 m resolution of MAMS however restricts its utility for finding small mud deposits; aircraft photography meets this need as well as serving as verification for deposition sites identified in MAMS imagery.

5. Water Types Detection

MAMS reflectance and SST products demonstrate a correlation in water scenes that is related to properties of various water types in coastal bays and estuaries. When water levels are driven down by postfrontal northerly winds, coastal marshes and bays discharge their water towards the continental shelf. The result is a mosaic of water types that exhibit contrasting reflectance (based on turbidity) and thermal characteristics. When displayed in a temperature versus reflectance format, the various water types cluster into groups. Six water types have been identified: (1) Gulf waters (warm and low turbidity), (2) Bay Waters (cool and very turbid), (3) River waters (cool and moderately turbid), (4) Fresh water marsh drainage (cool and low turbidity), (5) Salt marsh drainage

(cool, low turbidity), (6) Soil water drainage from sub-aerially exposed deltaic sand banks (very cold in mid-day, varying turbidity in shallow water, possibly a result of reflectance from the subaqueous bottom). Water typing informs the investigator not only that certain water types are present, but also indicates the patterns of dispersal (i.e. circulation patterns) of each type. This information is useful for documenting and understanding the processes affecting marsh ecology, the various scales of circulation, and the potential or probable response of local marine life to the cold front forcing. A publication is forthcoming on this topic.

6. Coastal Circulation Response to Cold Front Passage

As mentioned, cold front pattern winds affect water levels in coastal bays. Fluctuating water levels affect coastal circulation patterns by displacing marsh, bay, and other water types downgradient. Optimally, an animated set of images provides the best information, however, no currently existing satellite platform can provide the high spatial and temporal resolution necessary to monitor the fine scale motions (< 500 m, hours) that exist in coastal environments. MAMS data was used in a "snapshot" mode to infer circulation, by observing patterns of reflectance and thermal features. These inferences demonstrate the small scale detail that is present (see Moeller et al., 1993). MAMS near infrared imagery showing snapshots of coastal circulation on April 6, 1989 and December 13, 1989 are also included with this report, following this section. It demonstrates in graphic detail the wholesale circulation variability that occurs along the Louisiana coast. In the follow-on project this topic will be further explored by applying a georeferencing package designed for aircraft data (Rickman et al., 1989) and animating MAMS repeat overpass images.


MAMS
NEAR IR
6 APR 1989
TRACK E-F
13 DEC 1989
TRACK E-F

III. LIST OF PAPERS RESULTING FROM NAGW-1745

Gumley, L. E., 1990a: Atmospheric correction of Multispectral Atmospheric Mapping Sensor (MAMS) data and estimation of sediment parameters in Atchafalaya Bay, Louisiana. MS thesis, University of Wisconsin-Madison, Madison WI, 100pp.

Gumley, L. E., C. C. Moeller, and W. P. Menzel, 1990b: Monitoring of Mississippi delta coastal geomorphology using high resolution Multispectral Atmospheric Mapping Sensor (MAMS) data. **5th Australasian Remote Sensing Conference**, Perth, Australia, 738-745.*

Huh, O. K., H. H. Roberts, L. J. Rouse, and D. A. Rickman, 1991: Fine grain sediment transport and deposition in the Atchafalaya and Chenier Plain sedimentary system. **Coastal Sediments '91: Proceedings of Specialty Conference**, June 25-27, 1991, Seattle, WA, American Society of Civil Engineers, New York, NY, 817-830.*

Huh, O. K., H. H. Roberts, C. C. Moeller, and W. P. Menzel, 1993: Processes of coastal geomorphic development: land building and land loss along the Louisiana deltaic coastline. **Coastal Zone 1993: Eighth Symposium on Coastal and Ocean Management**, New Orleans, LA, July 19-23, 1993.*

Moeller, C. C., L. E. Gumley, W. P. Menzel, and K. I. Strabala, 1989: High resolution depiction of SST and SSC from MAMS data. **Fourth Conference on Satellite Meteorology and Oceanography**, AMS, Boston, MA, 208-212.*

Moeller, C. C., O. K. Huh, L. E. Gumley, and W. P. Menzel, 1991: Response of the Louisiana coastal environment to a cold front wind system. **Fifth Conference on Meteorology and Oceanography of the Coastal Zone,** AMS, Boston, MA, 124-129.*

Moeller, C.C., O. K. Huh, H. H. Roberts, L. E. Gumley, and W. P. Menzel, 1993: Response of Louisiana coastal environments to a cold front passage. Jour. of Coastal Research, Vol. 9, No. 2, 434-447.*

Rickman, D., M. C. Ochoa, K. W. Holladay and O. K. Huh, 1989: Georeferencing airborne imagery over new deltas in Louisiana. Photogrammetric Engineering and Remote Sensing, 55, 1161-1165.*

* copy included in Appendix A

IV. REFERENCES

Bates, J. J., W. L. Smith, G. S. Wade, and H. M. Woolf, 1987: An interactive method for processing and display of sea-surface temperature fields using VAS multispectral data. Bulletin of the American Meteorological Society, 68, 602-606.

Gordon, H. R., D. K. Clark, J. W. Brown, O. B. Brown, R. H. Evans, W. W. Broenkow, 1983: Phytoplankton pigment concentrations in the Middle Atlantic Bight: Comparison of ship determinations and CZCS estimates. Applied Optics, 22, 20-36.

Gumley, L. E., 1990a: Atmospheric correction of Multispectral Atmospheric Mapping Sensor (MAMS) data and estimation of sediment parameters in Atchafalaya Bay, Louisiana. MS thesis, University of Wisconsin-Madison, Madison WI, 100pp.

Gumley, L. E., C. C. Moeller, and W. P. Menzel, 1990b: Monitoring of Mississippi delta coastal geomorphology using high resolution Multispectral Atmospheric Mapping Sensor (MAMS) data. **5th Australasian Remote Sensing Conference**, Perth, Australia, 738-745.

Guzzi, R., R. Rizzi, and G. Zibordi, 1987: Atmospheric correction of data measured by a flying platform over the sea: Elements of a model and its experimental validation. Applied Optics, 26, 3043-3051.

Huh, Oscar K., Lawrence J. Rouse, Jr., and Nan Delene Walker, 1984: Cold air outbreaks over the northwestern Florida continental shelf: heat flux processes and hydrographic changes. Jour. of Geophys. Res., Vol. 89, No. C1, 717-726.

Huh, O. K., H. H. Roberts, L. J. Rouse, and D. A. Rickman, 1991: Fine grain sediment transport and deposition in the Atchafalaya and Chenier Plain sedimentary system. **Coastal Sediments '91: Proceedings of Specialty Conference**, June 25-27, 1991, Seattle, WA, American Society of Civil Engineers, New York, NY, 817-830.

Jedlovec, G. J., K. B. Batson, R. J. Atkinson, C. C. Moeller, W. P. Menzel, and M. W. James, 1989: Improved capabilities of the Multispectral Atmospheric Mapping Sensor (MAMS). NASA Technical Memorandum 100352, Marshall Space Flight Center, Huntsville, AL, 71pp.

Moeller, C. C., L. E. Gumley, W. P. Menzel, and K. I. Strabala, 1989: High resolution depiction of SST and SSC from MAMS data. **Fourth Conference on Satellite Meteorology and Oceanography**, AMS, Boston, MA, 208-212.

Moeller, C.C., O. K. Huh, H. H. Roberts, L. E. Gumley, and W. P. Menzel, 1993: Response of Louisiana coastal environments to a cold front passage. Jour. of Coastal Research, Vol. 9, No. 2, 434-447.

Rickman, D., M. C. Ochoa, K. W. Holladay and O. K. Huh, 1989: Georeferencing airborne imagery over new deltas in Louisiana. Photogrammetric Engineering and Remote Sensing, 55, 1161-1165.

Roberts, H. H., O. K. Huh, S. A. Hsu, L. J. Rouse, Jr., and D. Rickman, 1987: Impact of cold-front passages on geomorphic evolution and sediment dynamics of the complex Louisiana coast. **Coastal Sediments '87: Proceedings of Specialty Conference**, May 12-14, 1987, New Orleans, LA, American Society of Civil Engineers, New York, NY, 1950-1963.

APPENDIX A. - NASA SUPPORTED PUBLICATIONS

Journal of Coastal Research	9	2	434–447	Fort Lauderdale, Florida	Spring 1993

Response of Louisiana Coastal Environments to a Cold Front Passage

Christopher C. Moeller†, Oscar K. Huh‡, Harry H. Roberts‡, Liam E. Gumley* and W. Paul Menzel††

†Cooperative Institute for Meteorological Satellite Studies
1225 W. Dayton Street
Madison, WI 53706, U.S.A.

‡Louisiana State University
Coastal Studies Institute
Howe-Russell Geosciences Complex
Baton Rouge, LA 70803, U.S.A.

*Research and Data Systems Corporation
7855 Walker Drive, Suite 460
Greenbelt, MD 20770, U.S.A.

††NOAA/NESDIS Advanced Satellite Products Project
1225 W. Dayton Street
Madison, WI 53706, U.S.A.

ABSTRACT

MOELLER, C.C.; HUH, O.K.; ROBERTS, H.H.; GUMLEY, L.E., and MENZEL, W.P., 1993. Response of Louisiana coastal environments to a cold front passage. *Journal of Coastal Research*, 9(2), 434–447. Fort Lauderdale (Florida), ISSN 0749-0208.

The effect of a cold front passage on suspended sediment concentrations, water temperatures, and coastal circulation off Louisiana is examined via remote sensing with the Multispectral Atmospheric Mapping Sensor (MAMS). This 12 channel visible-infrared scanning spectrometer is flown on NASA's ER-2 aircraft, collecting 100 m resolution data over a 37 km swath from an altitude of 20 km. Time series charts of water temperature and suspended sediment content record the rapid (days) response of these shallow coastal waters to the cold front system of March 30–April 1, 1989. The river discharge sediment plumes stream down wind from the coast, remaining as coherent discrete water masses for up to 100 km. Detectable temperature gradients evolve rapidly in the estuarine waters in response to changing atmospheric conditions, with lowest temperatures developing in shallowest regions. Water level setup and setdown created by surface winds and barometric pressure strongly affect the exchange of river, estuarine and Gulf water. Behavior of the turbid river and estuarine discharge plumes is important as they serve as the source for new sediment deposits along the coastline. The utility of time series from high resolution, multispectral imagery in coastal environmental research, resource management, and pollution control is clear from this short term, multimission coverage.

ADDITIONAL INDEX WORDS: *Geomorphology, estuaries, sea surface temperature, suspended sediment.*

INTRODUCTION

The role of cold front weather systems in coastal geomorphology has only in recent years become a topic of research. These weather systems have been extensively studied from meteorological and climatological points of view because they affect most of the developed world. However, their importance as agents of change in coastal environments is just being recognized. Cold fronts, because of their higher frequency of occurrence, larger area of coverage, and persistent sequence of wind shifts from repeated directions of approach, are thought to be affecting the coastal environment more on a cumulative basis than the occasional tropical storm. ROBERTS *et al.* (1987) have outlined responses of various portions of the Louisiana coastline to passing cold fronts. These include deposition and erosion at different parts of the coastline, suspended sediment transport, and water level setup and wave action which alternately cause inland marsh inundation and drainage. KEMP (1986) has suggested that wave action associated with winter storms transports fluid mud in coastal waters, promoting progradation of shoreface where fluid mud is present. Understanding the mechanisms of coastal change and their response to cold front systems is necessary in order to develop effective coastal management programs.

The Multispectral Atmospheric Mapping Sensor (MAMS) has been used to study the impact of a cold front which passed through the Louisiana coastal zone on March 30–31, 1989. MAMS data was collected in daytime cloud-free conditions during the pre-frontal phase on March 30 and in day two of the post-frontal phase on April 1. MAMS has been used in previous work along the Louisiana coastline (MOELLER *et al.*, 1989)

92022 received 9 March 1992; accepted in revision 4 August 1992.

Table 1. *MAMS spectral channels.*

Channel	Bandwidth (@ 50% response)
1*	0.42–0.45 μm
2	0.45–0.52
3	0.52–0.60
4	0.57–0.67
5	0.60–0.73
6	0.65–0.83
7	0.72–0.99
8	0.83–1.05
9	3.47–3.86
10	3.47–3.86
11	10.55–12.24
12	12.32–12.71

* Not available when 10 bit infrared data are collected

and is well suited to monitor the coastal environment because of its 100 meter resolution in 12 spectral channels. The 12 visible/infrared channels are shown in Table 1. MAMS flies onboard NASA's ER-2 high altitude aircraft, scanning a 37 km swath from an altitude of 20 km. Calibration of infrared channels is accomplished by viewing two onboard blackbodies of known temperature during each scan. Visible calibration is accomplished by laboratory procedure. For detailed information on the MAMS spectrometer, see JEDLOVEC *et al.* (1989).

LOUISIANA COAST

Figure 1 shows the Louisiana coastal region and study sites. Three regions, the Atchafalaya Bay, the Chenier Plain, and the Chandeleur Islands (barrier islands) are circled in Figure 1 as locations of primary interest to the study. The Atchafalaya Bay is a region of new delta growth. Clays, silts and fine sands are transported by the Atchafalaya River, a distributary of the Mississippi River, into the Atchafalaya Bay. The sands and coarse silts are deposited in a series of delta lobes surrounding the mouths of both the Atchafalaya River and the Wax Lake Outlet. Clays and fine silts largely remain in suspension and are transported seaward and along shore by discharge inertia, and westward by prevailing coastal currents. These fine grained sediments drift westward in a sediment plume or mud stream where they are either deposited on the shoreface or settle out on the seafloor fronting the Chenier Plain. New deposits of fluid mud and mud congealed to clay have been found along the Chenier Plain (HUH *et al.*, 1991). Since 1987, a stretch over 14 km long along the Chenier Plain has been prograding seaward at the rate of some 60 meters per year (HUH *et al.*, 1991). This land is being formed when storm wave and surge action throw fluid mud onshore. The fluid mud supply has two possible immediate sources:

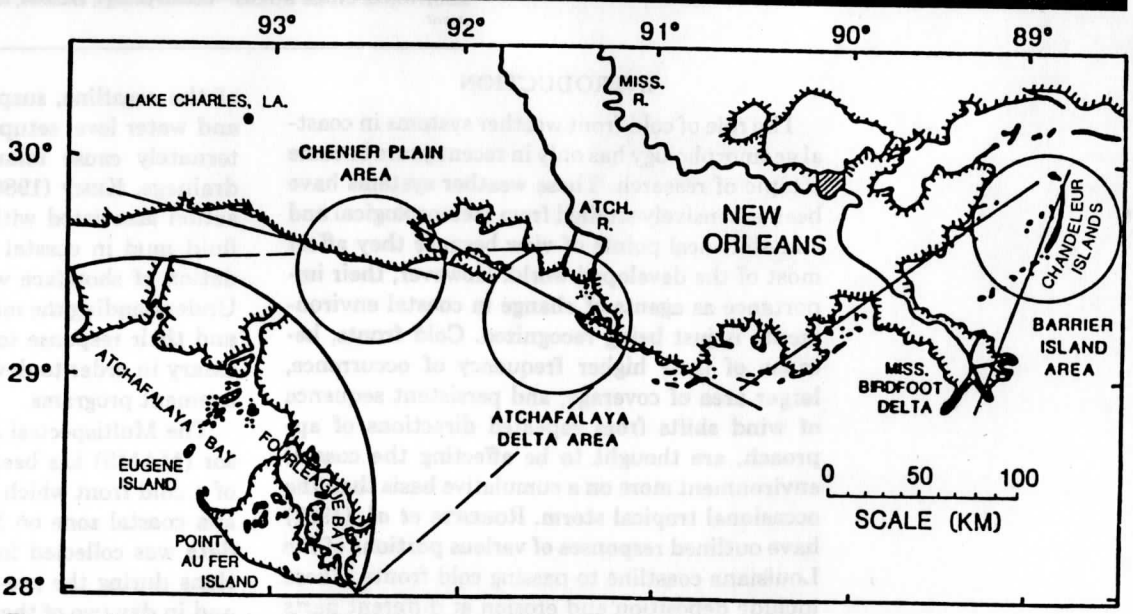

Figure 1. Louisiana coastal region with MAMS flight tracks (long thin lines) and primary areas of interest (circled) in the study. The Atchafalaya Delta area is expanded in the lower left hand corner for detail.

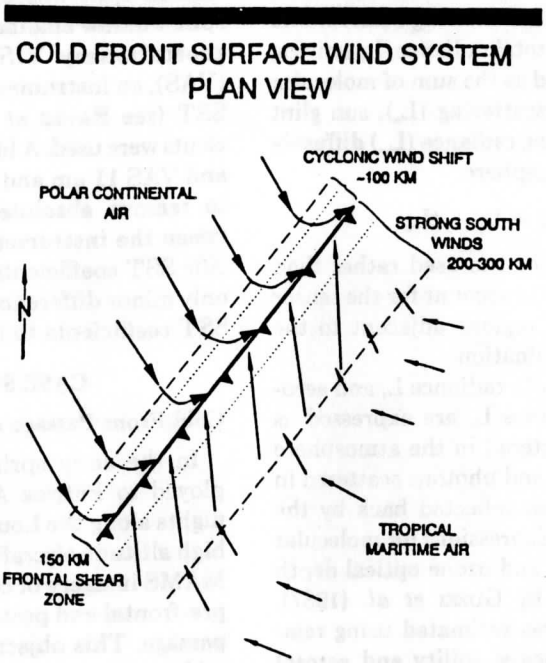

Figure 2. Winds of the cold front system (from ROBERTS *et al.*, 1987).

(1) previously deposited seafloor material (from the Atchafalaya Bay sediment plume) resuspended by storm wave action, and (2) mud freshly precipitated from the coast-hugging Atchafalaya mud stream. The extent and flow path of this mud-stream/sediment-plume is of primary importance for understanding land growth (and loss) patterns along the Chenier Plain. It will be shown later than the behaviour of the sediment plume from Atchafalaya Bay is affected differently by the different phases of a cold front passage. In contrast, the Chandeleur Islands, a series of sandy barrier islands off eastern Louisiana, are sediment starved and eroding. Storm waves and surge cause erosion and destruction of this barrier island/beach/dune geomorphic complex. Images showing responses of discharge plumes from the Mississippi River birdfoot delta channels are used to further illustrate the response of coastal waters to the cold front system.

THE COLD FRONT MODEL

About 30 to 40 cold fronts pass through the Louisiana coastline each year between the months of October and April. These cold fronts have a spatially and temporally ordered system of changes in surface wind speed, wind direction, barometric pressure, temperature, and humidity (ROBERTS *et al.*, 1987). Figure 2 summarizes the wind system of a passing cold front. The cold front consists of three basic phases: (1) the pre-frontal phase (ahead of the front) in which southerly component winds dominate and warm, humid atmospheric conditions exist with generally falling barometric pressure, (2) the frontal passage phase, with strong and variable winds and a characteristic sharp shift of wind direction from a southerly to a westerly component, and (3) the post-frontal or cold air outbreak phase (behind the front) in which winds become northerly and air temperature and humidity decrease significantly with rising barometric pressure. Along the Louisiana coastline, pre-frontal phase southerly winds drive saline water into coastal bays and marshes. Onshore wave action created by the southerly winds erodes sediment starved sandy portions of the coastline while depositing sediment along muddy regions of the coastline (such as portions of the Chenier Plain). After the cold front passes, winds shift to a northerly direction driving down water levels in coastal areas and reducing onshore wave action. The dry cold air behind the front rapidly dries newly formed deposits on the shoreface, thus expediting the sediment consolidation of the coastal progradation process (HUH *et al.*, 1991). Water levels continue to drop, promoting marsh drainage and discharge of bay waters onto the continental shelf of the Gulf of Mexico. Coastal water temperatures also respond, cooling most rapidly in shallow regions.

Figure 2 represents an idealized model, a plan view of the surface wind fields associated with a cold front as it advances from NW to SE. The natural variability of cold fronts through the season includes: their orientation, direction of propagation (west to east, or north to south), strength (characterized by pressure gradient force, temperature and humidity characteristics), and speed of propagation. These factors will determine in large part the kind and amount of impact that a cold front passage will have on a coastal region. While the ordered pattern of change in a cold front passage is similar from case to case, there is much individual variability.

DATA PRODUCTS

Atmospheric Correction of Visible Radiances

MAMS visible and near infrared radiances are corrected for atmospheric effects to isolate the radiance upwelling from the water. Using mod-

elling studies, GORDON (1978), and GORDON *et al.*, (1983), developed a single scattering atmospheric correction method. The total radiance, L, arriving at the sensor is expressed as the sum of molecular scattering (L_r), aerosol scattering (L_a), sun glint (L_g), and the water leaving radiance (L_w) diffusely transmitted by the atmosphere.

$$L = L_r + L_a + L_g + tL_w$$

The diffuse transmittance t is used rather than the direct transmittance to account for the sensor receiving photons from regions adjacent to the field of view under examination.

Molecular scattered path radiance L_r and aerosol scattered path radiance L_a are expressed as the sum of photons scattered in the atmosphere directly into the sensor, and photons scattered in the atmosphere and then reflected back by the surface into the sensor. Expressions for molecular scattering optical depth and ozone optical depth (absorption) are given by GUZZI *et al.* (1987). Aerosol optical depth was estimated using relationships between surface visibility and aerosol optical depth given by Sturm (1981). Sun glint radiance L_g was estimated using sun-sensor geometry and surface wind speed data in a model by GUZZI *et al.* (1987).

After atmospheric effects have been removed, the remaining water leaving radiance is expressed as a subsurface reflectance according to ROBINSON (1985). The subsurface reflectance quantity can be regressed against *in situ* suspended sediment concentration (SSC) data; however, *in situ* data were not sufficient to establish reliable SSC regression coefficients for March 30 and April 1, 1989. Therefore, MAMS visible and near infrared reflectance images in this paper are displayed as a scaled subsurface reflectance quantity. Further discussion of the atmospheric correction of MAMS radiances can be found in GUMLEY *et al.* (1990).

Atmospheric Correction of Infrared Data

MAMS 11 μm and 12 μm infrared radiances were used to correct for atmospheric water vapor effects in estimating sea surface temperature (SST). A split window algorithm (MCMILLIN and CROSBY, 1984) was used

$$SST = T_{11} + A(T_{11} - T_{12}) + B$$

where T_{11} and T_{12} are the MAMS 11.2 μm and 12.5 μm brightness temperatures, A is a regression coefficient, and B is a bias correction. Robust values for A and B have not yet been determined for MAMS split window channels; because MAMS split window channels are similar to those of the geostationary VISSR Atmospheric Sounder (VAS), an instrument used previously to estimate SST (see BATES *et al.*, 1987), VAS SST coefficients were used. A bias correction between MAMS and VAS 11 μm and 12 μm radiances was applied to remove absolute calibration differences between the instruments. Tests using MAMS-specific SST coefficients under development showed only minor difference (<1 K) from using the VAS SST coefficients to estimate SST.

CASE STUDY RESULTS

Cold Front Passage of 31 March 1989

In the early spring of 1989, MAMS was deployed to Patrick AFB, Florida, for a series of flights along the Louisiana coast on NASA's ER-2 high altitude aircraft. The objective was to obtain MAMS imagery of coastal conditions during both pre-frontal and post-frontal phases of a cold front passage. This objective is difficult as pre-frontal mid and upper level clouds often obscure the coastline during the cold front season. However, a weak relatively cloud-free synoptic low which had formed in Texas on March 29, strengthened and proceeded with minimal cloudiness through the Louisiana coastal region with frontal passage occurring late on March 30 into early morning of March 31. MAMS was flown on the morning of March 30 twelve hours prior to frontal passage, and on the morning of April 1, about thirty-six hours after frontal passage.

The cold front propagated west to east at a high angle to that of the coastline orientation. Surface conditions created by this system are illustrated in a time series format in Figure 3 from observations made at the National Weather Service (NWS) station in Lake Charles (LCH), Louisiana. The frontal passage is well defined by the increase in surface pressure beginning about 0200 UTC on March 31 (8 pm LST, March 30). Decrease of air temperature behind the front is illustrated by the temperature minima on the days following the frontal passage (about 3–6 K). Dew point temperatures also decrease behind the front. Surface winds show maximum speeds in the 12 hours preceding and just after the frontal passage with a southwest to northerly wind shift. Thus, while MAMS flew in both the pre-frontal and post-frontal phases, it did not overfly the Louisiana coast during peak winds in either phase. Results of the wind forcing during those peak velocity periods

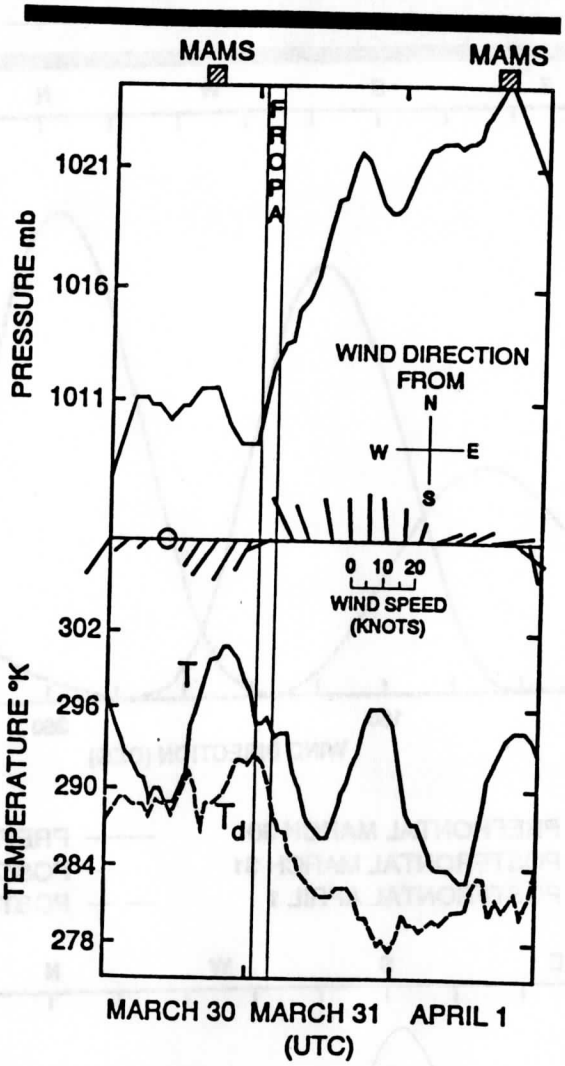

Figure 3. Surface observations of pressure, wind, temperature (T) and dew point (T_d) at Lake Charles (LCH), Louisiana, from March 30 through April 1, 1989. A cold front passage at Lake Charles is indicated by FROPA. MAMS data collection periods are indicated by blocks at top of diagram.

however are seen in the imagery because hours are required to establish the wind driven coastal and estuarine circulation.

The wind forcing by a cold front may be quantitatively evaluated by a summation of the wind energy over time as a function of wind direction. A simple kinetic energy approach is to square the wind speed and compute the component over the spectrum of wind directions. This summation is plotted as a function of wind direction in the top of Figure 4 for the NWS station at Lake Charles (LCH), Louisiana, located about 40 km inland. Energy curves are plotted for 24 hour summation periods beginning on March 30. Note that surface wind speeds are likely to be significantly greater over the open nearshore waters than over land (Hsu, 1981). Maximums in the southwesterly (pre-frontal; March 30) and northerly (post-frontal day 1; March 31) directions are obvious and represent the strongest portions of the pre-frontal and post-frontal phase winds respectively. Wind conditions during the MAMS flight on April 1 (post-frontal day 2) were weaker and more easterly (becoming more southeasterly later in the day, signalling the transition into the next pre-frontal phase; see Figure 3). The observed coastal temperature and turbidity patterns on April 1 therefore depict coastal waters under a weaker forcing than existed at earlier times in the cold front cycle. Data collection during peak periods of wind forcing is desirable to fully understand the impact during the cold front cycle. The absolute magnitude of the cold front wind energy is best understood in comparison to that of other cold front passages. In the bottom of Figure 4, overlain on the March/April 1989 data, is the wind energy spectrum for a strong north to south propagating cold front that passed through LCH on December 22, 1990. The December 1990 energy in the pre-frontal phase is more than twice that of the March/April 1989 case. Energy in the 24 hours following cold front passage (post-frontal day 1) is similar for each case, however post-frontal day 2 energy for the December 1990 case far exceeds that of the March/April 1989 case. This comparison shows that the March 1989 case involved only a modest level of wind energy. There is a need to collect data on more cold front passage cases so that understanding can be advanced on how factors such as cold front strength, speed of propagation,

Figure 4. Cumulative surface wind energy for 24 hour periods of pre-frontal, post-frontal day 1, and post-frontal day 2 as a function of wind direction for observations at Lake Charles, Louisiana, on March 30–April 1, 1989 (top and bottom), and December 21–23, 1990 (bottom). Wind energy, primarily southerly in pre-frontal conditions (solid lines), shifts to northerly directions after frontal passage (dashed lines). Note the scaling change in the bottom graph, which is presented as a comparison of the wind energy from a strong (December 21–23) and a modest (March 30–April 1) cold front case. →

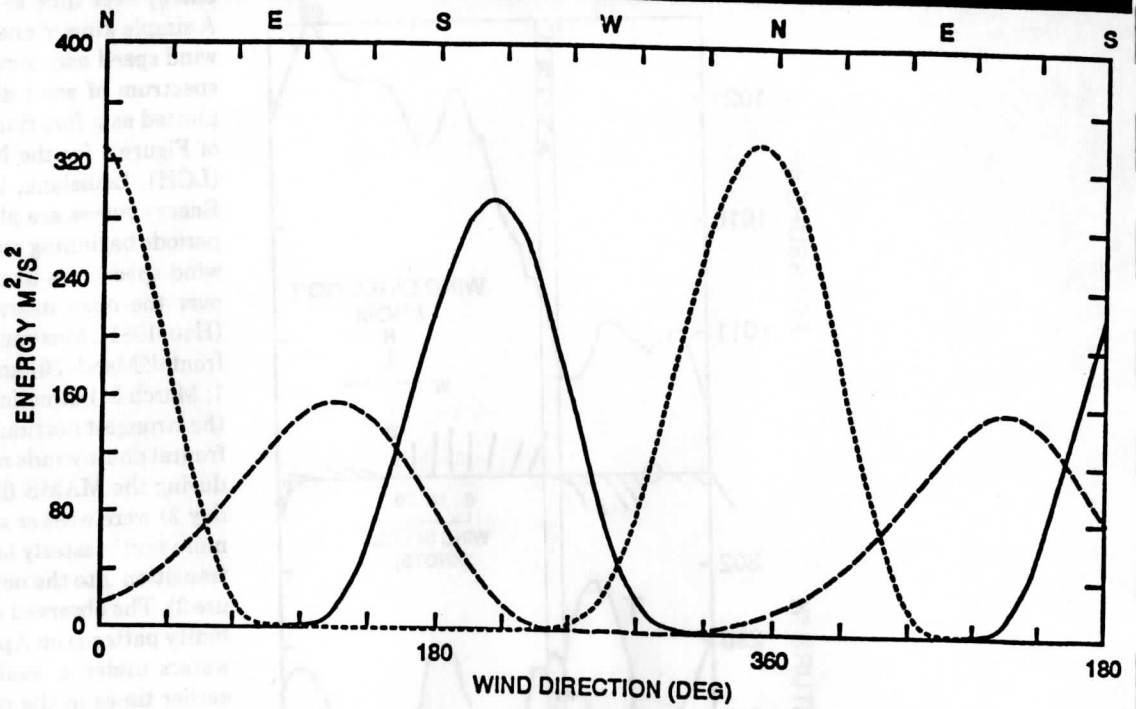

PREFRONTAL MARCH 30
POSTFRONTAL MARCH 31
POSTFRONTAL APRIL 1
PREFRONTAL DEC 21
POSTFRONTAL DEC 22
POSTFRONTAL DEC 23

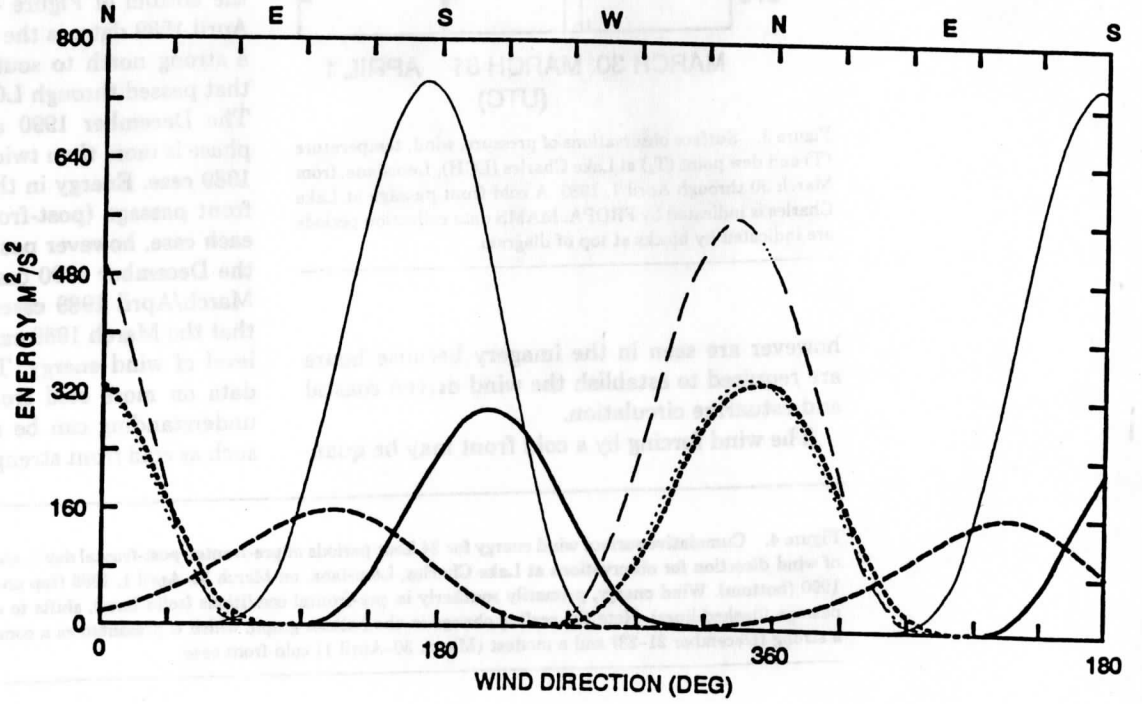

and angle of approach affect the response of the coastal environment. These factors affect the coastal wave and current generation in addition to sea level setup and setdown.

Response of Sediment Plumes

The sediment load of the Mississippi River is split between two distributaries, the Mississippi River delta and the Atchafalaya River delta. The Atchafalaya River (including the Red River flow) discharge is 30% of the volume and 50% of the suspended sediment load of that in the Mississippi River (MOSSA and ROBERTS, 1990). The Atchafalaya Bay sediment discharge plume is a primary source of depositional material for the western Louisiana coastal zone including the Chenier Plain region. Cold front passages create a "pulse" of increased Atchafalaya Bay discharge onto the continental shelf. Whether the sediments in the discharge plume are deposited directly onto the shoreface or onto the subaqueous bottom, coastal progradation relies on an influx of this material. Because of this, it is useful to determine the response of the Atchafalaya Bay sediment plume to cold front systems. The Atchafalaya Bay sediment plume is shown in Figure 5 for the MAMS flights on March 30 and April 1. Southwesterly winds on March 30 (top) retarded the westward flow of the plume (yellow/red in Figure 5) towards the Chenier Plain, creating a damming effect which forced the sediment plume southward out of the Atchafalaya Bay into the Gulf of Mexico (beyond the southern extent of the MAMS imagery). This restricted the flow of depositional material towards the Chenier Plain. Under these conditions, only resuspended bottom sediments (by wave action) are available for deposition on the Chenier Plain shoreface. Otherwise, with low sediment content, wave action is an erosive force on the Chenier Plain coastline. On April 1 (bottom), with easterly winds, the plume extended westward along the Chenier Plain coast, transporting high levels of suspended sediment to that area. Very little of the plume extended southward on April 1. This is seemingly a direct response of the sediment plume to surface winds, exhibiting an important dependence of the coastal environment on cold front systems.

The main channel of the Mississippi River carries about 70% of the Mississippi River's sediment load to the Gulf of Mexico. The modern Mississippi birdfoot (Balize) subdelta, some 600–800 yr old, has prograded to near the edge of the continental shelf. Sediment carried to the Gulf is visible as narrow, linear plumes emanating from the various outlet points of the delta. The sediment is dispersed, gradually settling out of the plumes into relatively deep waters. Thus, little or no coastal progradation is taking place near the Mississippi River delta. The pattern of sediment plumes around the birdfoot delta are shown in Figure 6. Like the response in the Atchafalaya Bay region on March 30, sediment outflow appears to be blocked from the southwest, resulting in pooling of high turbidity water (green/yellow) on the southwest side of the delta. On April 1, northeasterly to easterly winds concentrate turbid water on the northeast side of the delta, while the turbid water on the southwest side appears to have largely dispersed. Plumes on the southwest side of the delta suggest that the turbid water has dispersed downwind.

Coastal Circulation Response

The rise and fall of water levels as well as the winds in coastal regions affects coastal circulation patterns. Astronomical tides cause water levels to rise and fall on a regular and predictable basis. Because the Louisiana coast is a microtidal coast (astronomical tides have a range of only about 0.5

Figure 5 (top). MAMS images of subsurface reflectance in the Atchafalaya Delta/Chenier Plain area (refer to map in Figure 1) on March 30 (top) and April 1 (bottom), 1989. North is towards the top of the page. Relatively clear water is purple/blue; highly turbid water is yellow/red. Land is shaded white. The data is subsampled to 300 m resolution to display the entire flight track in the image. On March 30, southwesterly winds retard sediment flow towards the west, forcing the sediment plume out into the Gulf of Mexico to the south; on April 1, easterly winds force the plume westward along the coast, reducing its southward extent into the Gulf of Mexico.

Figure 6 (bottom). MAMS subsurface reflectance at the Mississippi birdfoot delta (refer to map in Figure 1) on March 30 (left) and April 1 (right). North is towards the top of the page. Land is shaded white. Relatively clear water is blue; turbid water is green to yellow. The data is subsampled to 200 m resolution. On March 30, southwest surface winds caused sediment to pool on the southern and western sides of the delta. With northeast surface winds on April 1, sediment is concentrated on that side of the delta while sediment pools on the southwest side have largely dispersed.

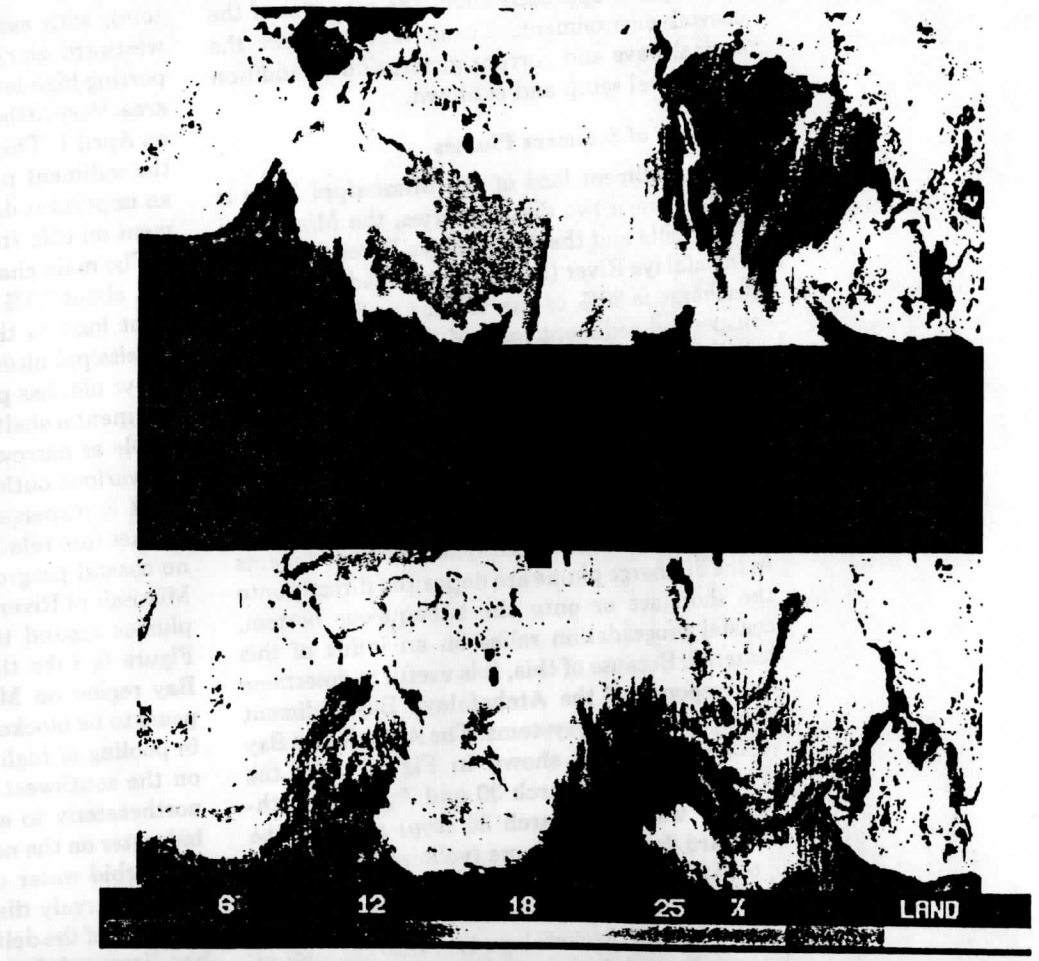
6
12
18
25
%
LAND

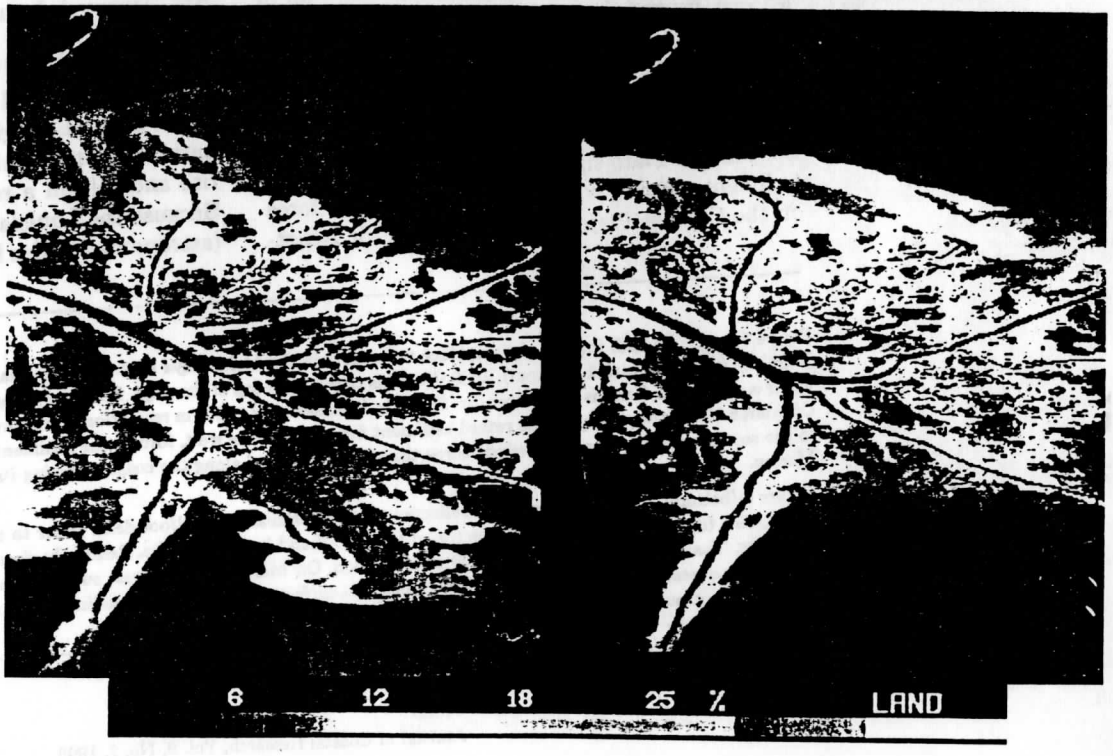
6
12
18
25
%
LAND

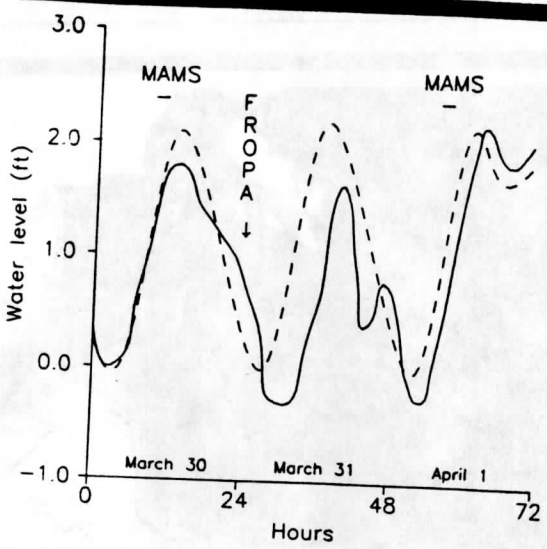

Figure 7. Predicted (dashed) and observed (solid) water levels at Eugene Island, Louisiana. Values are differences from their respective low water on the morning of March 30. Data plotted begins at midnight local time on March 30. Predicted tide data is taken from tables compiled by the U.S. Coast and Geodetic Survey. Observed water level data courtesy of U.S. Army Corps of Engineers, New Orleans District. MAMS data collection periods indicated by bars at top. Time of frontal passage at Eugene Island indicated by FROPA.

meters), winds of a cold front system induce relatively large, but lower frequency changes in water level. Onshore winds, the pre-frontal southerlies, and decreasing barometric pressure set up sealevel along the coast. This increases bay and estuary water levels, temporarily "damming up" the inflowing rivers. Offshore winds, the post-frontal northerlies, and rising barometric pressure set down coastal water levels, spilling river, marsh, bay and estuarine waters seaward onto the continental shelf. The actual water level is the result of the combined influence of astronomical tides and surface winds. The different but regular time scales of these two forces, (diurnal *vs.* 3–6 days) add to water level variability as they go in and out of phase. The response of water level to the cold front winds of March 30–April 1 can be seen in water level data collected at Eugene Island in the Atchafalaya Bay (Figure 7). Predicted astronomical tide data for Eugene Island is also shown. During southerly winds on March 30, water level closely follows the predicted tidal range until about midday (12 hours before the frontal passage) when water levels begin to drop more slowly than the predicted tides. After frontal passage during the night of March 30–31, winds become more northerly and water level drops quickly while tides are predicted to increase. A subdued high water level on March 31 follows, this all occurring under the strong northerly winds that followed the frontal passage (see Figure 3). Water level and predicted tides work back into agreement with each other when the northerly winds weaken on April 1. Interestingly, water level range exceeds predicted tide range when winds turn back out of the southeast later in the day on April 1. This is a case where wind and astronomical tide forcings were out of phase. Had they been in phase, the range of the observed water level plot probably would have doubled.

While it is difficult to discern the various scales of motion which are surely present in a "snapshot" of a coastal scene, some circulation patterns in the Atchafalaya Bay are identifiable in Figure 8. Figure 8 demonstrates small scale (<1 km) circulation changes affected by cold front passages. The SST imagery shows an arm of cold (dark) water (point A) flowing eastward from Atchafalaya Bay into Four League Bay on March 30. Thin, warmer (lighter) streamlines off the Atchafalaya delta (point B) also indicate flow towards Four League Bay. It is also somewhat apparent that cooler bay water extends south and east (point C) around Point Au Fer Island out of the bay. This pattern is also visible in the subsurface reflectances for March 30 in Figure 5. On April 1, with easterly winds, cold streamlines near the Atchafalaya delta (point B) appear to be draining southward towards the Gulf, bypassing Four League Bay. An arm of warmer marsh drainage water appears to be cutting between Atchafalaya Bay and the entrance to Four League Bay (point A). Evidence of this relatively clear marsh drainage also exists in the subsurface reflectance data (thin, blue streamline in Figure 5). Cold Atchafalaya Bay waters extend westward (point C) out of the Bay in agreement with the pattern shown for April 1 in Figure 5.

Circulation patterns in the Chandeleur Islands/birdfoot delta region are depicted using SST imagery in Figure 9. On March 30 an extended coastal zone of cold (dark) water exists on the northeast (lee) side of the delta. Water on the southwest (windward) side appears diffuse and shows little in the way of circulation patterns. On April 1, the coastal zone on the northeast (windward) side of the delta has a smaller seaward extent. On the

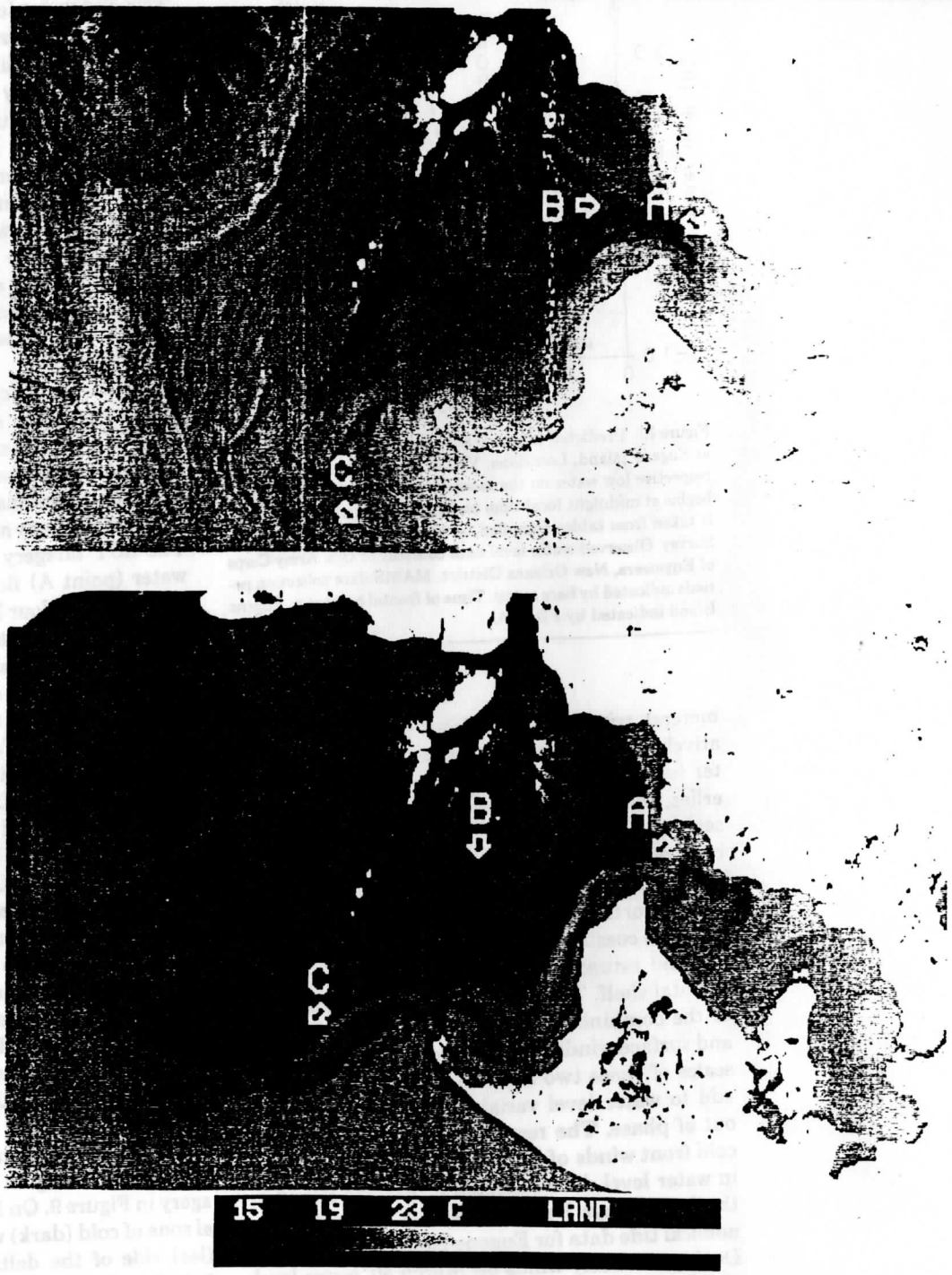

Figure 8. MAMS SST imagery in the Atchafalaya Delta area (refer to Figure 1 for map) on March 30 (top) and April 1 (bottom). Land is shaded white. Dark shades are cold. North is towards the top of the page. Thermal contrast shows evidence of flow in the water on each day. Arrows indicate direction of flow. See text for discussion.

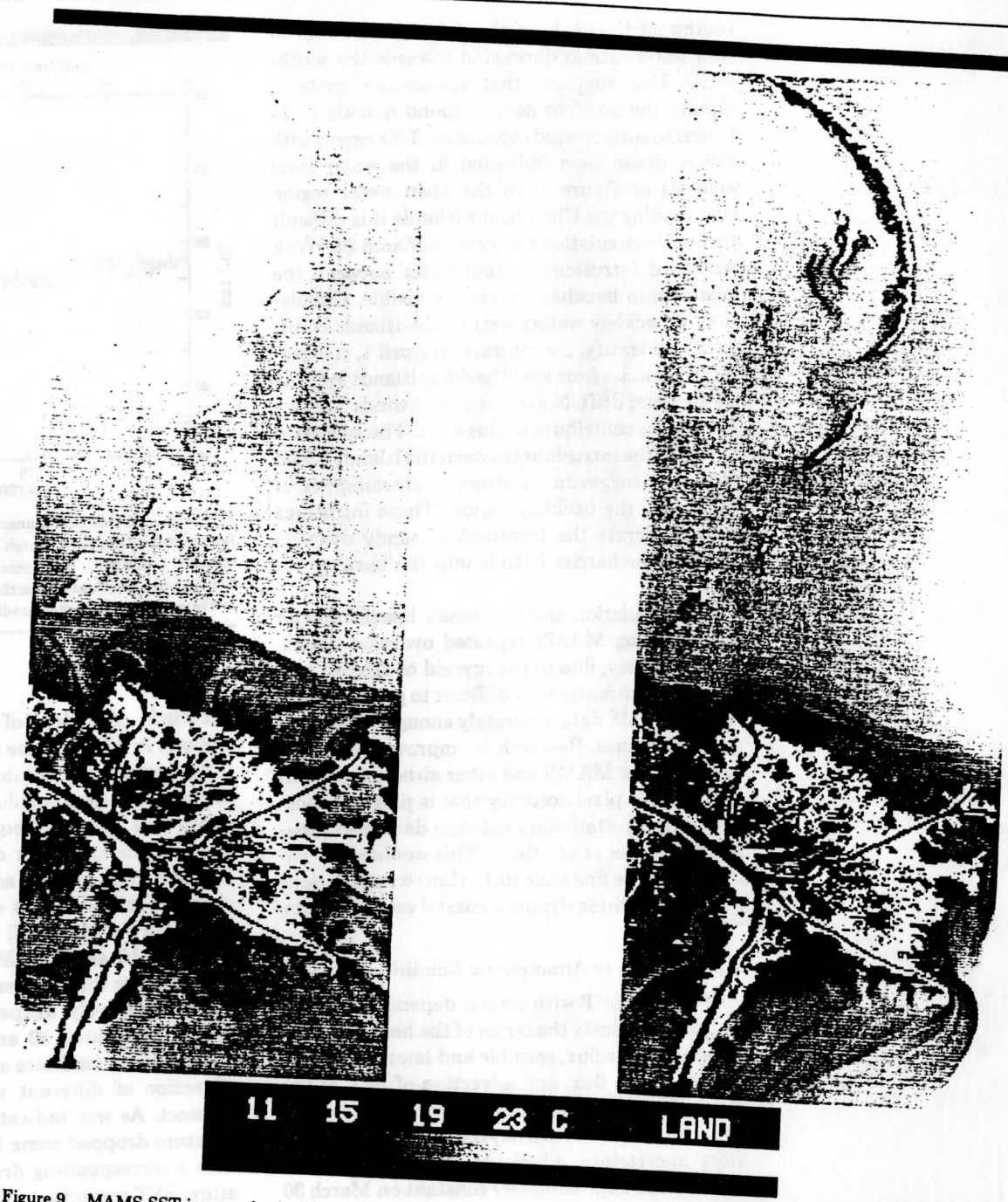

Figure 9. MAMS SST imagery in the Mississippi birdfoot delta/Chandeleur Islands area (refer to Figure 1 for map) on March 30 (left) and April 1 (right). North is towards the top of the page. Dark shades are cold. Land is shaded white. The data is subsampled to 300 m resolution. The coastal front around the birdfoot delta (bottom of each image) is indicated by a strong thermal gradient. On the northeast side of the delta, the coastal front extends much further out on March 30 than it does on April 1. Also note cooler SST's in the shallow waters on the western side of the Chandeleur Islands (top center of each image) on April 1 *vs.* March 30. Thermal contrast also shows evidence of flow in the water on each day.

southwest (lee) side of the delta, streamlines of cold water extend downwind towards the southwest. This suggests that circulation patterns around the birdfoot delta respond quickly (<24 hours) to surface wind conditions. This agrees with the response time indicated in the water level analysis of Figure 7. In the open water region surrounding the Chandeleur Islands it is difficult to discern circulation patterns on March 30. Weak westward intrusions of cool water between the islands into backbay waters are visible. Circulation in backbay waters west of the islands is difficult to identify. By contrast on April 1, cool water streamlines from small backbay islands indicate a southward drift. Northeast to east winds on April 1 probably contribute to this drift. The westward extent of the intrusions between the islands is also increased suggesting a stronger entrainment of water into the backbay region. These intrusions may accelerate the transport of sandy deposits between the barrier islands into the backbay region.

The circulation analysis would benefit greatly by animating MAMS repeated overpass scenes. Unfortunately, due to the myraid of aircraft motions, it is currently very difficult to geometrically rectify MAMS data accurately enough to animate multiple scenes. Research to improve image rectification (for MAMS and other airborne sensors) to the single pixel accuracy that is presently possible with geostationary satellite data is in progress (RICKMAN *et al.*, 1989). This would allow animation of the fine scale (0.1–5 km) water motions that exist in these dynamic coastal environments.

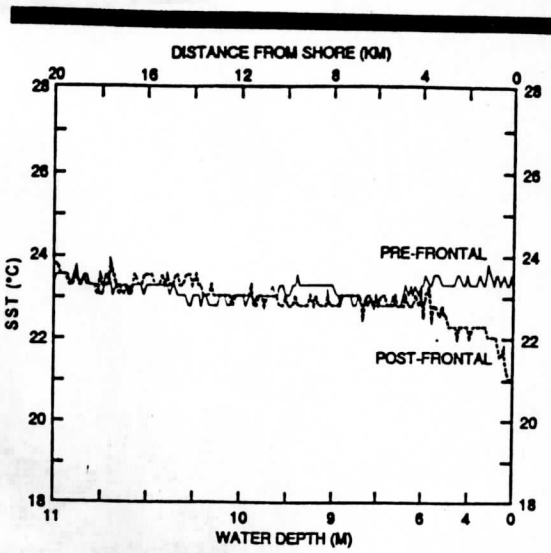

Figure 10. MAMS SST transects along the Chenier Plain coast for pre-frontal phase on March 30 (solid) and post-frontal phase on April 1 (dashed). SST increases towards shore in the warm pre-frontal conditions of March 30, and decreases towards shore in the colder post-frontal conditions on April 1.

SST Response to Atmospheric Conditions

Change of SST with time is dependent on several fluxes, namely the terms of the heat exchange equation: solar flux, sensible and latent heat flux, radiative heat flux, and advection of heat in the water column. For carefully chosen locations, solar flux (clear skies both days) and, with somewhat more uncertainty, advection of heat can be assumed to be approximately constant on March 30 and April 1. This leaves sensible, latent, and radiative heat fluxes, which all vary as a function of atmospheric conditions, as responsible for most of the SST change from March 30 to April 1. Strictly speaking, SST represents the temperature of the water's skin, not the entire water column as is specified in the heat exchange equation. However, if the water column is well mixed, as in the windy conditions of cold front passages, then changes in SST become representative of changes in the entire water column. Knowing that the heat content of the water column is a function of water depth and assuming equal fluxes over a spatial domain, shallow water columns should heat and cool the most rapidly as atmospheric conditions change. This idea was examined in the MAMS SST data for March 30 and April 1.

Figure 10 shows a MAMS SST transect extending from the Chenier Plain coast outward into the progressively deeper waters of the Gulf of Mexico on March 30 and April 1. The location was chosen to minimize ambiguities resulting from advection of different water types through the transect. As was indicated in Figure 3, air temperature dropped some 3 to 6 K over this period with a corresponding drop in dew point temperature. SST response to the atmospheric variation is related to water depth in Figure 10. Little response is apparent in waters deeper than about 6 meters. As water depth decreases towards the shore, the response increases. A maximum cooling of about 2.5 K occurs within a few hundred meters of shore. This quick response to changing atmospheric conditions is a result of the lower heat content of shallow waters. In deeper waters, ver-

tical mixing and larger stored heat content maintain the SST at a nearly constant temperature. A similar response can be seen in Figure 9 around the Chandeleur Islands. Near the islands, water temperatures are significantly cooler on April 1 than on March 30. Deeper waters show little change. Decreases of about 2–3 K from March 30 to April 1 have also been seen in MAMS SST data in the shallow Barataria Bay region of the Louisiana coast as well as in inland lakes.

CONCLUSIONS

MAMS has been used to study the response of Louisiana coastal waters to atmospheric forcings associated with individual cold front passages. Linking atmospheric forcings to dynamic responses in the coastal environment is an important approach for understanding processes of coastal change. One hundred meter resolution images collected during the pre-frontal and post-frontal phases of a March, 1989 cold front event are among the first high resolution images known to the authors to document the coastal response to a cold front. The wind, pressure, temperature, and humidity characteristics of the cold front passage force changes in the coastal environment. Atmospherically corrected visible and near infrared imagery show that sediment flowing out of the Atchafalaya Bay is deflected downwind by post-frontal winds, displacing the source of depositional material for coastal progradation. Coastal circulation patterns vary in response to wind, water level, and river discharge, all forced or modulated by cold front winds. SST imagery provides information on timing and extent of the temperature response of shallow coastal regions to atmospheric conditions. These are reliable in the absence of significant thermal advection and horizontal mixing of water types.

Coastal waters evolve continuously during the cold front event. The MAMS data shown in this paper provide a discrete look at the continuous responses to a single cold front event. Coastal circulation, plume dispersal, and sea surface temperature patterns during peak forcing conditions on March 31 would likely have revealed even stronger responses to the winds during the post-frontal phase of the cold front (as is indicated in Figure 7 by the response of water level to the winds just after frontal passage) had the MAMS instrument been flown on that day. Also of interest is the response of coastal waters and sediments to cold fronts of varying intensity, propagation speed, and angle of approach. Further, the question of cumulative impact over a winter season, especially as compared to the impact of tropical storms and hurricanes, has received very little attention. Preliminary work (Huh *et al.*, 1978) suggests that coastal and continental shelf waters evolve continuously in response to the seasonal succession of cold front passages, with chilled shelf waters spreading progressively seaward from inshore to shelf edge.

ACKNOWLEDGEMENTS

The authors gratefully acknowledge NASA funding under Grants NAGW-2052, to Louisiana State University, from Geology Programs, under Dr. Miriam Baltuck for surface truth, and NAGW-1745 to the University of Wisconsin, from Atmospheric Programs, under Dr. James Dodge for MAMS ER-2 data collection and analysis. Special appreciation is extended to the NASA Ames Research Center's High Altitude Missions Branch; without their tireless efforts, it would not have been possible to collect the excellent MAMS data set used in this paper.

LITERATURE CITED

Bates, J.J.; Smith, W.L.; Wade, G.S., and Woolf, H.M., 1987. An interactive method for processing and display of sea-surface temperature fields using VAS multispectral data. *Bulletin of the American Meteorological Society*, 68, 602–606.

Gordon, H.R.; Clark, D.K.; Brown, J.W.; Brown, O.B.; Evans, R.H., and Broenkow, W.W., 1983. Phytoplankton pigment concentrations in the Middle Atlantic Bight: Comparison of ship determinations and CZCS estimates. *Applied Optics*, 22, 20–36.

Gordon, H.R., 1978. Removal of atmospheric effects from satellite imagery of the oceans. *Applied Optics*, 17, 1631–1636.

Gumley, L.E.; Moeller, C.C., and Menzel, W.P., 1990. Monitoring of Mississippi delta coastal geomorphology using high resolution Multispectral Atmospheric Mapping Sensor (MAMS) data. *5th Australasian Remote Sensing Conference* (Perth, Australia), pp. 738–745.

Guzzi, R.; Rizzi, R., and Zibordi, G., 1987. Atmospheric correction of data measured by a flying platform over the sea: Elements of a model and its experimental validation. *Applied Optics*, 26, 3043–3051.

Hsu, S.A., 1981. Models for estimating offshore winds from onshore meteorological measurements. *Boundary Layer Meteorology*, 20, 341–351.

Huh, O.K.; Wiseman, W.J., Jr., and Rouse, L.J., Jr., 1978. Winter cycle of sea surface thermal patterns, northeastern Gulf of Mexico. *Journal of Geophysical Research*, 83(C9), 4523–4529.

Huh, O.K.; Roberts, H.H., Rouse, L.J., and Rickman, D.A., 1991. Fine grain sediment transport and deposition in the Atchafalaya and Chenier Plain sedi-

mentary system. *Coastal Sediments '91: Proceedings of Specialty Conference* (June 25–27, 1991, Seattle, Washington), American Society of Civil Engineers, New York, pp. 817–830.

JEDLOVEC, G.J.; BATSON, K.B.; ATKINSON, R.J.; MOELLER, C.C.; MENZEL, W.P., and JAMES, M.W., 1989. Improved capabilities of the Multispectral Atmospheric Mapping Sensor (MAMS). NASA Technical Memorandum 100352, Marshall Space Flight Center, Huntsville, Alabama, 71pp.

KEMP, G.P., 1986. Mud Deposition at the Shoreface: Wave and Sediment Dynamics on the Chenier Plain of Louisiana. Ph.D. Dissertation, Louisiana State University, 146p.

MCMILLIN, L.M. and CROSBY, D.S., 1984. Theory and validation of the multiple window sea surface temperature technique. *Journal of Geophysical Research*, 89(C3), 3655–3661.

MOELLER, C.C.; GUMLEY, L.E., MENZEL, W.P., and STRABALA, K.I., 1989. High resolution depiction of SST and SSC from MAMS data. *Fourth Conference on Satellite Meteorology and Oceanography* (AMS, Boston, Massachusetts), pp. 208–212.

MOSSA, J. and ROBERTS, H.H., 1990. Synergism of riverine and winter storm related sediment transport processes in Louisiana coastal wetlands. *Transactions of the Gulf Coast Association of Geological Societies*, XL, 635–642.

RICKMAN, D.; OCHOA, M.C.; HOLLADAY, K.W., and HUH, O.K., 1989. Georeferencing airborne imagery over new deltas in Louisiana. *Photogrammetric Engineering and Remote Sensing*, 55, 1161–1165.

ROBERTS, H.H.; HUH, O.K.; HSU, S.A.; ROUSE, L.J., JR., and RICKMAN, D., 1987. Impact of cold-front passages on geomorphic evolution and sediment dynamics of the complex Louisiana coast. *Coastal Sediments '87, Proceedings of a Specialty Conference* (May 12–14, 1987, New Orleans, Louisiana). American Society of Civil Engineers, New York, pp. 1950–1963.

ROBINSON, I.S., 1985. *Satellite oceanography—An introduction for oceanographers and remote-sensing scientists*. Chichester, United Kingdom: Ellis Horwood, 150p.

STURM, B., 1981. The atmospheric correction of remotely sensed data and the quantitative determination of suspended matter in marine water surface layers. *In:* CRACKNELL, A.P. (ed.), *Remote Sensing in Meteorology, Oceanography, and Hydrology*. Chichester, United Kingdom: Ellis Horwood, pp. 163–197.

MONITORING OF MISSISSIPPI DELTA COASTAL GEOMORPHOLOGY USING HIGH RESOLUTION MULTISPECTRAL ATMOSPHERIC MAPPING SENSOR (MAMS) DATA

L.E. Gumley(1), C.C. Moeller(2), W.P. Menzel(2)

(1) Remote Sensing and Satellite Research Group
Department of Applied Physics
Curtin University of Technology
GPO Box U1987, Perth WA 6001, Australia

(2) Cooperative Institute for Meteorological Satellite Studies
University of Wisconsin-Madison
1225 W. Dayton St., Madison WI 53706, USA

INTRODUCTION

The coastal delta regions of large rivers are subject to dramatic and continuous geomorphic change. The outflow and dispersal of sediment from rivers in delta regions allows landforms to be built up along the coastline, while the passage of weather systems such as hurricanes can cause severe erosion and degradation to existing landforms. Recent observations (Roberts et al., 1987) suggest that the winds, waves and currents generated by the passage of winter cold fronts over the Mississippi River delta region have a measurable and significant effect on the geomorphology of the coastline. It is suggested that while cold fronts impart less kinetic energy to the land and water surface than do hurricanes and tropical storms, their uniform northwesterly direction of approach and relatively higher frequency during the winter season allows them to cause greater coastal geomorphic change than the more intense but less frequent tropical weather systems. An important indicator of geomorphic change in a river delta region is the amount, distribution, and movement of riverborne sediment which is transported from upstream of the river delta. Since both coastal deposition and erosion processes are directly linked to the distribution and movement of sediment laden water in the delta region, monitoring of sediment distribution offers information about the change in the geomorphology of the coastline over space and time (Egleme, 1985).

The techniques of remote sensing have been used in previous investigations of ocean and river borne sediment loading. Visible wavelength scanning sensors mounted on both aircraft and spacecraft have quantitatively mapped sediment loading in coastal regions and lakes (Lathrop et al., 1987, Egleme, 1985, Collins et al., 1984) by relating the visible radiance sensed above the water surface to the sediment loading of the water. An important step in the determination of water surface parameters from visible wavelength data is the process known as atmospheric correction, or removal of atmospheric effects (Gordon, 1978). This process accounts for the transmission and scattering properties of the atmosphere which influence the visible radiance measured by a scanning sensor above the water surface. This paper presents a method for the removal of atmospheric effects from visible wavelength multispectral scanner data, and then briefly describes the utility of the combination of derived visible and infrared imagery in monitoring the geomorphology of the Atchafalaya Bay region.

MULTISPECTRAL ATMOSPHERIC MAPPING SENSOR (MAMS)

The MAMS is a scanning spectrometer flown on a high altitude NASA ER-2 aircraft (Jedlovec et al., 1989). It measures upwelling radiance in 8 visible and 3 infrared bands with 100 meter spatial resolution. The 8 visible bands span the spectral region from 0.42 to 1.05 μm, and the infrared bands are centered at 3.7, 11.2 and 12.5 μm. The relatively high spatial resolution of the data, and the combination of multi-wavelength visible and infrared bands permits investigation of atmospheric and surface features that are not resolved by current satellite sensors (Jedlovec, 1987; Menzel et al., 1986).

The MAMS scans over a cross track angle of 86 degrees, which for an aircraft altitude of 20 kilometers gives a cross track scan width of approximately 38 kilometers. 716 pixels are recorded per scan line, of which half are sampled to avoid overlap. Every second scan line is sampled to avoid overlap in the direction of flight. Calibration of the visible bands is done before and after instrument deployment by viewing a well calibrated integrating sphere. Calibration data for the infrared bands are recorded onboard during flight by viewing two temperature controlled black body sources during the acquisition of each scan line. Image data for the visible bands are recorded in 256 levels, while the infrared data are recorded in 1024 levels. More detailed technical information on the MAMS may be found in Jedlovec et al. (1989).

SINGLE SCATTERING ATMOSPHERIC CORRECTION

A complete treatment of the atmospheric correction problem requires consideration of the complex multiple scattering processes that occur in the atmosphere. On the basis of modelling studies, Gordon (1978, 1983) developed an atmospheric correction method that considers single scattering only, where the scattering effects due to molecules and aerosols are treated independently. The total radiance L_t arriving at the sensor is expressed as the sum of components arising from molecular scattering (L_r), aerosol scattering (L_a), sun glint (L_g), and the water leaving radiance (L_w) diffusely transmitted by the atmosphere. L_t may then be written as

$$L_t = L_r + L_a + L_g + t\,L_w\,, \qquad (1)$$

where all quantities are dependent on wavelength. The diffuse transmittance t is used rather than the direct transmittance to account for the sensor receiving photons from regions adjacent to the field of view under examination.

MOLECULAR SCATTERED PATH RADIANCE

The scattering and absorption of visible photons by gaseous components of the atmosphere depends on the optical depth of the species. In the visible portion of the spectrum where the scattering molecules are small compared to the wavelengths of photons, the scattering process is known as Rayleigh scattering. Because of the near uniformity throughout the atmosphere of the molecular components that affect visible radiation, it is possible to develop good approximations of their optical properties in order to calculate the molecular scattered path radiance. Molecular scattering optical depth is determined using an expression dependent on sensor altitude derived by Guzzi et al. (1987) and given by

$$\tau_r = H_r(h_o)\ 0.0088\ \lambda^{(-4.15\ +\ 0.2\lambda)}$$
$$H_r(h_o) = 1 - \exp(-0.1188h_o - 0.00116h_o^2)$$

h_o : sensor altitude (km)

λ : wavelength (μm)

The principal absorber of visible radiation in the atmosphere is ozone. The optical thickness due to ozone absorption may be calculated on the basis of observations of ozone distribution in the atmosphere. An expression dependent on sensor altitude is also used for ozone absorption optical depth derived by Guzzi et al. (1987) and given by

$$\tau_o = H_o(h_o)\ 0.03\ \exp[-277(\lambda - 0.6)^2)$$
$$H_o(h_o) = 1 - 1.0183\ /\ (1 + 0.0183\ \exp(h_o/5))$$

Although the MAMS is typically flown at an altitude of 20 kilometers, and as such is above most of the scattering depth of the atmosphere, the expressions developed here are generalized to apply to an aircraft sensor flying at any altitude. The molecular scattered path radiance (L_r) is expressed as the sum of single scattered contributions such that $L_r = L_r(1) + L_r(2)$. $L_r(1)$ accounts for photons scattered in the atmosphere towards the sea surface and

then reflected from the sea surface into the sensor, while $L_r(2)$ accounts for photons scattered by the atmosphere into the sensor without interacting with the ocean surface.

$L_r(1)$ = $1/(4\pi\cos\theta)\ F_o\ T_o\ \tau_r(1)\ (\rho(\theta) + \rho(\theta_o))\ P_r(\psi_+)$
$L_r(2)$ = $1/(4\pi\cos\theta)\ F_o\ T_o\ \tau_r(2)\ P_r(\psi_-)$
F_o : Solar spectral irradiance determined from the LOWTRAN7 database (Kneizys et al., 1988), corrected for the ellipticity of the Earth's orbit around the sun
T_o : Ozone transmittance from space to the surface, and the surface to the sensor = $\exp(-(\tau_o(1)/\cos\theta_o + \tau_o(2)/\cos\theta))$, $\tau_o(1)$ is the ozone optical depth from space to the surface, $\tau_o(2)$ is ozone optical depth from the surface to the sensor
$\tau_r(1)$: Molecular optical depth from space to the surface
$\tau_r(2)$: Molecular optical depth from surface to the sensor
$\rho(\theta)$: Fresnel reflectance of the water surface at angle of incidence θ
$P_r(\psi)$: Rayleigh scattering phase function at scattering angle ψ = $0.7629\ (1 + 0.9324\cos^2(\psi))$ (Maul, 1985)
ψ_+,ψ_- : Scattering angles
ψ_+ = $\cos^{-1}(\cos\theta_o\cos\theta - \sin\theta_o\sin\theta\cos(\phi - \phi_o))$
ψ_- = $\cos^{-1}(-\cos\theta_o\cos\theta - \sin\theta_o\sin\theta\cos(\phi - \phi_o))$
θ_o : Solar zenith angle
θ : Sensor zenith angle
ϕ_o : Solar azimuth angle
ϕ : Sensor azimuth angle

AEROSOL SCATTERED PATH RADIANCE

At visible wavelengths, the scattering of photons by atmospheric aerosols is described by Mie theory, since the size of the aerosols is comparable to the wavelength of the interacting photon. For a given aerosol distribution specified in terms of size, shape, and refractive index, it is possible to calculate the scattering properties by the application of Mie theory. In practice the calculation of the contribution to the total visible radiance (L_t) by aerosol scattered path radiance (L_a) is complicated because of the non-uniformity of aerosol optical depth due to changes in aerosol type and spatial/temporal distribution. It is not possible to develop a generalized parameterization of aerosol optical depth which is universally applicable. Estimates of aerosol optical depth must be made specifically for each geographic location, and each set of observing conditions.

In the case of CZCS atmospheric correction (Gordon, 1983), the ocean is a treated as a complete absorber of solar radiation at a wavelength of 0.670 μm. Thus in the absence of sun glint, molecular and aerosol scattering are the only contributors to the radiance sensed above the surface. Since the molecular scattering contribution can be estimated accurately, the residual radiance at 0.670 μm is the contribution to the total radiance from aerosol scattering. For a given aerosol scattered radiance, it is possible to calculate the aerosol optical depth. Then by assuming a constant relationship between the aerosol optical depth at 0.670 μm and the aerosol optical depth at the shorter CZCS wavelengths, it is possible through the use of an iterative scheme to calculate the aerosol scattering effect throughout the image with reasonable accuracy, with no other independent measurement of the aerosol optical depth.

Visual examination of MAMS imagery over Atchafalaya Bay at wavelengths of 0.665 μm and 0.740 μm shows obvious features at the water surface due to high sediment loading. Thus the implementation of a CZCS-type aerosol scattering correction is not possible, as the water is not a complete absorber at the longer visible wavelengths around 0.670 μm. As a first attempt to estimate the effect of aerosol scattering, it is assumed that the aerosol optical depth is constant over the area being examined. For MAMS imagery this corresponds to a strip 38 km wide and several hundred kilometers long. It should be noted that this

approximation is not optimal for a quantitative atmospheric correction, and methods for aerosol correction over sediment laden coastal waters require further investigation.

An estimate of aerosol optical depth is derived from observations of surface visibility. Although meteorological visibility (which depends on the horizontal attenuation coefficient) is the defining parameter required for aerosol optical depth, here observer estimates of horizontal visibility are used, as attenuation measurements were unavailable. The altitude dependent aerosol optical depth is then given (Sturm, 1981) by

τ_a = $(3.912/V - 0.0116)\ (0.55/\lambda)^{\alpha-3}\ [H_1(1 - \exp(-5.5/H_1)) + 12.5\ \exp(-5.5/H_1) + H_2\ \exp(-5.5/H_1)\ (1 - \exp(-(h_o-18)/H_2))]$

V : meteorological visibility range (km)

α : exponent of Junge distribution ≈ 3.8

H_1 = $0.886 + 0.0222\ V$ (km)

H_2 = 3.77 km

As with the molecular scattered path radiance, the aerosol scattered path radiance L_a is expressed as the sum of two single scattered contributions. The terms are given by

L_a = $L_a(1) + L_a(2)$

$L_a(1)$ = $(1/4\pi(\cos\theta_o + \cos\theta))\ F_o\ T_o\ (\rho(\theta) + \rho(\theta_o))\ P_a(\psi_+)$ * $(1 - \exp(-\tau_a(1)\ (1/\cos\theta_o + 1/\cos\theta)))$

$L_a(2)$ = $(1/4\pi(\cos\theta_o + \cos\theta))\ F_o\ T_o\ P_a(\psi_-)\ (1 - \exp(-\tau_a(2)\ (1/\cos\theta_o + 1/\cos\theta)))$

$\tau_a(1)$: Aerosol optical depth from space to surface

$\tau_a(2)$: Aerosol optical depth from surface to sensor

$P_a(\psi)$: Aerosol phase function at scattering angle w - Henyey Greenstein two-term type as defined by Gordon (1987)

= $a\ f(\psi,g_1) + (1 - a)\ f(\psi,g_2)$

$f(\psi,g)$ = $(1 - g^2)\ (1 + g^2 - 2g\ \cos\theta)^{-3/2}$

a = 0.983

g_1 = 0.82

g_2 = -.0.55

SUN GLINT RADIANCE

The roughening of the ocean surface by surface winds causes reflection to occur in directions other than the specular direction. Thus the sun glint radiance detected by a sensor is heavily dependent on both the surface wind speed and the sun-sensor geometry. The calculation of the sun glint radiance based on a statistical estimate of the probability of reflection at a given angle, given a surface wind speed. Guzzi et al. (1987) present the following method for calculating the sun glint radiance. The sun glint radiance is given by

L_g = $(1/4\pi)\ F_o\ T_o\ \rho(\omega)\ g(\omega,\beta,v)\ \exp(-\tau(1)/\cos\theta_o)\ \exp(-\tau(2)/\cos\theta)$

$g(\omega,\beta,v)$= $p(\beta,v)\ \cos\omega/(4\cos^3\beta)$

$p(\beta,v)$: Probability function for direct reflection by the sea surface

= $1/(\pi r^2)\ \exp(-\tan^2\beta/r^2)$

r^2 = $0.003 + 0.00512\ v^2$

v : Surface wind speed (ms^{-1})

β = $\cos^{-1}((\cos\theta + \cos\theta_o)/2\cos\omega)$

ω = $\cos^{-1}(0.5(1 + \cos\psi))^{1/2}$

ψ = $\cos^{-1}(\cos\theta_o\ \cos\theta - \sin\theta_o\ \sin\theta\ \cos(\phi - \phi_o))$

$\tau(1)$: Combined molecular, ozone and aerosol optical depth from space to surface

$\tau(2)$: Combined molecular, ozone and aerosol optical depth from surface to sensor

In most cases where the wind speed is low, and the scan plane of the sensor is perpendicular to the solar azimuth plane, the sun glint radiance is negligible. However a high sun elevation angle, or high wind speed can cause very high sun glitter radiances which will in some cases

saturate the sensor. For this reason, it is advisable to plan the sensor flight parameters in advance to avoid sun glint, or to have some system by which the sensor can mechanically avoid viewing sun glint regions, such as was used on the CZCS.

DERIVATION OF SUBSURFACE REFLECTANCE

The remaining task is to separate the water leaving radiance (L_w) from the other terms in equation (1). From equation (1), it can be seen that

$$L_w = (L_t - L_r - L_a - L_g) / t$$

where the diffuse transmittance (t) from surface to sensor is given (Gordon et al., 1983) by

t = $\exp(-(\tau_r/2 + \tau_{oz} + \tau_a/6) / \cos\theta)$
τ_r = molecular optical depth from surface to sensor
τ_o = ozone absorption optical depth from surface to sensor
τ_a = aerosol optical depth from surface to sensor.

Thus after atmospheric corrections have been applied to the visible data, the parameter remaining is the water leaving radiance (L_w). However L_w is not a unique signature of the materials suspended or dissolved in the water, as it is influenced by the spectrum of incoming solar radiation and the sensor zenith angle as much as by the water composition. Robinson (1985) states that the subsurface reflectance ratio (R) is a more useful parameter since it takes into account variations in the solar spectrum and also the sensor zenith angle. The subsurface reflectance is given by

$$R = E_u / E_d$$

where E_u is the upwelling irradiance at the water surface, and E_d is the downwelling irradiance at the water surface, given by F_oT where F_o is the solar spectral irradiance incident at the top of the atmosphere and T is the total transmittance along the path from the sun to the surface. Optical theory shows that for a flat surface, R is related to L_w by

$R = L_w / \{E_d [1 - \rho(\theta')] / (Q\, n^2)\}$
ρ : Fresnel reflectivity of the air-water interface at angle of incidence θ'. This causes a portion of E_u to be reflected back down into the water.
θ' : Angle of incidence beneath the water surface of a beam which exits the water surface in direction θ.
Q : Equal to pi for a Lambertian reflecting surface
n : Refractive index of sea water

The expression for R was derived for a flat surface. However Robinson (1985) asserts that as long as θ is not close to the critical angle of 48 degrees, surface roughening does not introduce much error. If the surface is roughened to the point where whitecaps appear, then the errors are much larger. The refractive index of sea water changes with salinity and temperature, but the error introduced by neglecting this effect is small when compared with the uncertainty of the atmospheric correction procedure.

ESTIMATION OF SEDIMENT PARAMETERS

The next task is to develop algorithms to estimate suspended sediment from derived subsurface reflectances. A standard technique used is regression analysis (Lathrop et al., 1986; Collins et al., 1984) where the subsurface reflectance is the independent variable and the desired suspended sediment is the dependent variable. In order to perform this regression analysis, it is first necessary to acquire a set of in-situ measurements with collocated subsurface reflectances.

In order to accomplish this objective, MAMS flights over the Mississippi Delta and Atchafalaya Bay have been conducted in a continuing program since early 1987. In conjunction with the MAMS flights, measurements of suspended sediment concentration (SSC), Secchi disk depth (SDD), and sea surface temperature (SST) have been made at ground based locations in Atchafalaya Bay.

SSC measurement involves filtering a water sample taken from the surface layer to determine the proportion of sediment per volume. At each field location, 1 liter water samples are taken. A portion of this 1 liter sample, typically less than 0.25 liters, is then filtered through a pre-weighed 100/40 μm millipore filter. The filters are then dried at 80°C and weighed again to determine the suspended sediment weight, and thus the suspended sediment concentration may be obtained. Egleme (1985) reports SSC values in the Atchafalaya Bay region of up to several hundred milligrams per liter. Secchi disk depth measurement involves lowering a highly reflective white disk of specified dimensions into the water and finding the depth at which it just becomes invisible. For clear waters, this may be many meters, but for turbid waters it is typically less than a meter. SST measurement is done using a bucket sample and a thermometer.

Regression analysis of the in-situ samples and collocated subsurface reflectances is used to generate estimates of suspended sediment concentration and Secchi disk depth. The regression relationship used is

$$S = C_0 + C_1R_1 + C_2R_2 + C_3R_3 + ... + C_nR_n$$

over n spectral bands (Whitlock et al., 1982), where S is the derived sediment parameter, C_i are the regression coefficients, and R_i are subsurface reflectances for spectral band i. SST values are derived from the MAMS 11.2 μm and 12.5 μm infrared channels using the split window algorithm of the form

$$SST = T_{11} + a (T_{11} - T_{12}) + b$$

where T11 and T12 are the 11.2 μm and 12.5 μm brightness temperatures, a is a coefficient determined by regression, and b is a bias correction (Bates et al., 1987). Results of the application of regression analysis to the MAMS atmospherically corrected subsurface reflectances are detailed in Gumley (1990).

FEATURES OBSERVED IN DERIVED MAMS IMAGERY

Examination of atmospherically corrected visible imagery along with infrared SST imagery shows features which yield information about the distribution of sediment and the effect of atmospheric events such as cold front passages. MAMS flights over the Atchafalaya Bay region from 1987 to the present have revealed seasonal, daily, and hourly changes in features related to the geomorphology of the coastal region. Current research effort is directed at understanding and interpreting the features observed in the MAMS imagery.

A strong correspondence was noted between MAMS visible subsurface reflectance and sea surface temperature (SST) in Atchafalaya Bay on 27 January 1988. Boundaries delineating the cooler sediment laden waters of the Bay and the warmer, clearer waters of the Gulf of Mexico are apparent in the MAMS imagery. It was also noticed that at the small scale, some features were observed in the SST imagery which appeared to indicate a response to solar warming of the Bay waters which may be affected by the bottom topography. The presence of four different water sources were inferred in the Atchafalaya Bay area. These were

(1) Drainage from coastal marshes (low visible reflectance, high SST),
(2) River water discharge (high reflectance, low SST),
(3) Groundwater discharge from delta lobes (low reflectance, low SST),
(4) Gulf of Mexico shelf water (low reflectance, high SST).

This type of information could be used to develop maps of water drainage or transport in the Atchafalaya Bay region.

Subsurface reflectance images of Atchafalaya Bay on 30 March 1989 and 1 April 1989 show a dramatic change in shallow water temperatures and coastal front zones in response to wind direction and temperature changes associated with a cold front passage. The change in the observed reflectance pattern gives an indication that remotely sensed sampling on a daily basis is necessary to accurately monitor changes in the sediment distribution in Atchafalaya Bay.

CONCLUSIONS AND FURTHER WORK

An atmospheric correction algorithm has been developed for Multispectral Atmospheric Mapping Sensor (MAMS) visible wavelength data, and the resulting imagery used to estimate sediment parameters in Atchafalaya Bay, Louisiana. Molecular and aerosol single scattered radiance and sun glint radiance contributions to the total sensed MAMS visible radiance have been computed for MAMS data acquired over Atchafalaya Bay, Louisiana. Images of visible wavelength subsurface reflectance in Atchafalaya Bay show a high level of detail at the 100 meter resolution of the MAMS data, and indicate the potential for mapping the distribution of sediment outflow from the Atchafalaya River. The combination of visible and infrared data allows information to be determined about water sources, and the coastal processes showing a response to changes in the atmospheric environment.

A continuing program of MAMS flights and in-situ measurements aims to establish the database necessary for use in regression estimation of sediment parameters. Further work will be directed at interpreting the features seen in the derived visible and infrared imagery, and relating these to the geomorphic changes of the coastline and atmospheric events such as cold front passages. The atmospheric correction algorithm will also continue to evolve as the aerosol scattering correction is updated to use better estimates of aerosol optical depth, and the effect of multiple scattering is investigated.

Acknowledgements. This work received support from the National Aeronautics and Space Administration under grant NAGW-1745. Special recognition for their efforts goes to the ER-2 team at NASA Ames Research Center.

REFERENCES

Bates, J.J., Smith, W.L., Wade, G.S., Woolf, H.M. (1987). An interactive method for processing and display of sea-surface temperature fields using VAS multispectral data. Bull. Am. Met. Soc., **68**.

Collins, M., Pattiaratchi C. (1984). Identification of suspended sediment in coastal waters using airborne thematic mapper data. Int. J. Remote Sensing, **5**, 635-657.

Egleme, M.L. (1985). Landsat-4 based models for suspended sediment concentrations in central Louisiana coastal waters. MS thesis, Louisiana State University, Baton Rouge LA.

Gordon, H.R., Clark, D.K., Brown, J.W., Brown, O.B., Evans, R.H., Broenkow, W.W. (1983). Phytoplankton pigment concentrations in the Middle Atlantic Bight: comparison of ship determinations and CZCS estimates. Appl. Opt., **22**, 20-36.

Gordon, H.R., (1978). Removal of Atmospheric Effects from Satellite Imagery of the Oceans. Appl. Opt., **17**, 1631-1636.

Gumley, L.E. (1990). Atmospheric correction of Multispectral Atmospheric Mapping Sensor (MAMS) data and estimation of sediment parameters in Atchafalaya Bay, Louisiana. MS thesis, University of Wisconsin-Madison, Madison WI.

Guzzi, R., Rizzi, R., Zibordi, G. (1987). Atmospheric correction of data measured by a flying platform over the sea: elements of a model and its experimental validation. Appl. Opt., 26, 3043-3051.

Jedlovec, G.J., Batson, K.B., Atkinson, R.J., Moeller, C.C., Menzel, W.P., James,M.W. (1989). Improved Capabilities of the Multispectral Atmospheric Mapping Sensor (MAMS). NASA Technical Memorandum 100352, George C. Marshall Space Flight Center, Huntsville AL.

Jedlovec, G.J. (1987). Determination of Atmospheric Moisture Structure from High Resolution MAMS radiance data. PhD thesis, Department of Meteorology, University of Wisconsin-Madison, Madison WI.

Kneizys, F.X., Shettle, E.P., Abreu, L.W., Chetwynd, J.H. Anderson, G.P., Gallery, W.O., Selby, J.E.A., Clough, S.A. (1988). Users Guide to LOWTRAN 7. AFGL-TR-88-0177, Air Force Geophysics Laboratory, Hanscom AFB MA.

Lathrop, R.G., Lillesand, T.M. (1986). Use of Thematic Mapper Data to Assess Water Quality in Green Bay and Central Lake Michigan. Photogrammetric Engineering and Remote Sensing, 52, 671-680.

Maul, G.A. (1985). Introduction to Satellite Oceanography. Martinus Nijhoff Publishers, Boston MA.

Menzel, W.P., Jedlovec, G.J., Wilson, G.S. (1986). Verification of small-scale water vapor features in VAS imagery using high resolution MAMS imagery. Preprint Volume, Second Conference on Satellite Meteorology/Remote Sensing and Applications, May 13-16 1986, Williamsburg VA, 108-112.

Roberts, H.H., Huh, O.K., Hsu, S.A., Rouse, L.J., Jr., Rickman, D. (1987). Impact of cold-front passages on geomorphic evolution and sediment dynamics of the complex Louisiana coast. Coastal Sediments '87, WW Div./ASCE, New Orleans LA, 1950-1963.

Robinson, I.S. (1985). Satellite Oceanography - An introduction for oceanographers and remote-sensing scientists. Ellis Horwood Limited, Chichester UK, p150.

Sturm, B. (1981) The atmospheric correction of remotely sensed data and the quantitative determination of suspended matter in marine water surface layers. In: Cracknell, A.P. (ed.), Remote sensing in meteorology, oceanography and hydrology. Ellis Horwood, Chichester UK, 163-197.

Whitlock, C.H., Kuo, C.Y., LeCroy, S.R. (1982). Criteria for the use of regression analysis for remote sensing of sediment and pollutants. Remote Sensing of Environment, 12, 151-168.

HIGH RESOLUTION DEPICTION OF SST AND SSC FROM MAMS DATA

Christopher C. Moeller
Liam E. Gumley
Kathleen I. Strabala

Cooperative Institute for Meteorological Satellite Studies
University of Wisconsin
1225 West Dayton Street
Madison, Wisconsin 53706

W. Paul Menzel

NOAA/NESDIS Advanced Satellite Products Project
1225 West Dayton Street
Madison, Wisconsin 53706

1. INTRODUCTION

Monitoring the coastal environment is of great importance to the maintenance of the delicate balance that exists where water meets land. Coastal processes displace and deposit tons of material each year, with important implications on the physical and biological systems of these areas. The Gulf coast of Louisiana is a particularly dynamic area of coastal change. The presence of the Mississippi River Delta and the new Atchafalaya River Delta serve as sources of sediment rich fresh water. Roberts et al. (1987) have summarized various responses of portions of the Louisiana coastline depending on how this sediment is distributed. A need to monitor these responses is indicated.

Close monitoring of coastal (or ocean) environments is greatly enhanced through the use of high resolution remote sensing data. Instruments such as Landsat, Coastal Zone Color Scanner, and the Airborne Thematic Mapper have been used to obtain high resolution estimates of suspended sediment concentration (SSC), chlorophyll, and salinity in coastal environments (see, for example, Rimmer et al., 1987; Holligan et al., 1983; Khorram, 1982). The Multispectral Atmospheric Mapping Sensor (MAMS) is also well suited for water quality measurements. The aircraft mounted instrument carries eight visible/near infrared and three infrared channels, which sense upwelling radiance at 100m resolution. The visible/near infrared data can be used to determine estimates of SSC. Additionally, the MAMS infrared channels with their split window combination can be used to determine high resolution estimates of sea surface temperature (SST). High resolution SSC and SST estimates may be useful in determining water origin and identifying flows as well as inferring information about sea depth.

This paper presents MAMS high resolution estimates of SSC and SST and interprets these estimates to identify physical features and mechanisms of the coastal waters of Louisiana. MAMS data from a 27 January 1988 daytime flight along the Louisiana coastline is used in this study.

2. MAMS INSTRUMENT CHARACTERISTICS

The MAMS instrument is a 12 channel scanner which flies onboard high altitude aircraft at about 20 km. The MAMS scans across a total path width of about 36 km at 100m resolution.

The MAMS spectral bands are summarized in Table 1. Channels 1-8 are similar to those of the Airborne Thematic Mapper. Of the four infrared channels, two are used as redundant channels. The infrared data is collectable at 10 bit precision.

Table 1. - MAMS spectral channels

channel	bandwidth (@ 50% response)
1[a]	0.42 - 0.45
2	0.45 - 0.52
3	0.52 - 0.60
4	0.57 - 0.67
5	0.60 - 0.73
6	0.65 - 0.83
7	0.72 - 0.99
8	0.83 - 1.05
9	3.47 - 3.86
10	3.47 - 3.86
11	10.55 - 12.24
12	12.32 - 12.71

a) not available when 10 bit infrared data are collected

MAMS infrared data is calibrated by viewing two blackbodies of known temperature with the assumption that the detector response is linear with respect to radiance. The blackbodies are viewed on each scan. Visible calibration is accomplished in the laboratory with the use of an integrating sphere at periodic intervals throughout the year, often just prior to instrument deployments. Detailed information is available on the MAMS in Jedlovec et al. (1989), and Menzel et al. (1986).

3. DATA ALGORITHMS

3.1 SST

The MAMS 11μm and 12μm channels are used in a split window algorithm of the form:

$$SST = T11 + a(T11 - T12) + b$$

where T11 and T12 are the 11μm and 12μm brightness temperatures, a is a coefficient determined through regression, and b is a bias correction. This form of an SST algorithm has been used extensively with VAS data by Bates et al. (1987) and with NOAA AVHRR data by McClain et al. (1985), and has shown high correlation to NOAA fixed buoys.

The coefficients a and b can be determined by regressing in-situ ship and buoy SST against collocated T11 and T12 data. However, because of a lack of collocated in-situ points along the Louisiana coastline on 27 January, a value of a=1.4846 from a VAS SST algorithm was used here. This is acceptable because of the similarity of the VAS and MAMS 11μm and 12μm channels (see Jedlovec et al., 1988). The value of b could not be reliably determined using 27 January data, however a small number of ground truth SSTs were collected on 22 January. These were used as guidance for the value of b. In order to improve the application of the VAS coefficient, a radiance bias between the VAS and MAMS 11μm and 12μm channels was also applied. These were generated by collocating 74 VAS footprints (8 km resolution) over the MAMS data of 27 January; spectral and viewing angle differences were taken into account. The bias for each channel was applied to the MAMS data as a correction before the SST algorithm was applied.

3.2 SSC

The MAMS visible data are used to calculate an image that is closely related to the SSC. In order to accomplish this, the radiance signal scattered upward out of the water must be separated from an atmospheric solar scattering contribution and a direct ocean surface reflected contribution.

The atmospheric contribution, or path radiance, is due to scattering of photons into the sensor field of view by air molecules (Rayleigh scattering) and aerosols (Mie scattering). Radiance is also reflected into the sensor from the ocean surface (sun glint). Procedures for correction of these effects have been established for NIMBUS-7 Coastal Zone Color Scanner imagery (Gordon et al., 1983; Viollier et al., 1980). For this study, we have considered only the Rayleigh scattering component of the path radiance, and the sun glint radiance. Procedures for evaluating the aerosol scattered component are currently under development.

The total signal, L_t, received by the sensor at a particular wavelength is given by

$$L_t = L_r + L_a + L_g + t^*L_w$$

where L_r : Rayleigh scattered path radiance
L_a : aerosol scattered radiance (presently neglected)
L_g : sun glint radiance
L_w : water leaving radiance
t : diffuse transmittance from sea to sensor

The Rayleigh path radiance L_r is given by (Gordon et al., 1983).

$$L_r = \{F_0 T_{o3}(\theta_0,\theta) t_r(\uparrow) P_r(\theta_+)[r(\theta_0) + r(\theta)]\} /4\pi\cos(\theta) + \{F_0 T_{o3}(\theta_0,\theta) t_r(\uparrow) P_r(\theta_-)\} /4\pi\cos(\theta)$$

where F_0 : Solar spectral irradiance incident at top of atmosphere
T_{o3} : Ozone transmittance $= \exp[-t_{o3}(1/\cos(\theta) + 1/\cos(\theta_0))]$
t_{o3} : Ozone optical depth
θ_0 : Solar zenith angle
θ : Sensor zenith (scan) angle
$t_r(\downarrow)$: Rayleigh optical depth for space to sea surface
$t_r(\uparrow)$: Rayleigh optical depth for sea surface to sensor
$P_r(\theta)$: Rayleigh scattering phase function $= 0.7629[1 + 0.9324\cos(\theta)]$
$\cos(\theta_-) = -\cos(\theta)\cos(\theta_0) - \sin(\theta)\sin(\theta_0)\cos(\phi - \phi_0)$
$\cos(\theta_+) = \cos\theta_- + 2\cos\theta\cos\theta_0$
ϕ_0 : solar azimuth angle (east of north)
ϕ : sensor azimuth angle (defined as the azimuth of a vector from the point on the sea surface being examined to the sensor; east of north)
$r(\theta)$: Fresnel reflectance of ocean surface at angle θ (refractive index of sea water = 1.341)

The term containing θ_- describes the path radiance due to photons which are scattered by the atmosphere into the sensor without interacting with the ocean surface. The term containing θ_+ describes the path radiance due to photons which are scattered by the atmosphere towards the ocean surface, and then specularly reflect from the surface into the sensor, as well as photons which are specularly reflected from the surface, and then scattered by the atmosphere into the sensor. The ocean surface is assumed to be flat for this reflectance calculation. The sun glint radiance L_g is given by (Viollier et al., 1980).

$$L_g = F_0 T_{o3} T_r r(\theta) p(\theta)$$

where T_r : Molecular (and aerosol if known) transmittance $= \exp\{-[t_r(\downarrow)/\cos(\theta_0) + t_r(\uparrow)/\cos(\theta)]\}$
θ : Sun glint reflection angle
$p(\theta)$: Probability function for direct reflection of sun radiance at angle θ depending on wind speed at the ocean surface (Cox and Munk, 1954).

The sun glint term takes into account the effect of surface wind causing capillary waves on the ocean which tend to reflect solar radiance in directions other than the specular direction. The water leaving radiance can thus be calculated by

$$L_w = (L_t - L_r - L_g)/t$$

where $t = \exp[-(t_r/2 + t_{o3})/\cos(\Theta)]*T_a$

T_a = aerosol transmittance (assumed to be 1.0 here)

Estimation of SSC requires regression of in-situ measured SSC's against collocated water leaving radiances. Previous studies (Collins and Pattiaratchi, 1984) have shown that a useful model is a linear multiple regression of the form

$$\log_e(SSC) = C_0 + C_1R_1 + C_2R_2 + C_3R_3$$

where C_i are regression coefficients and R_i represents water leaving radiances in visible channels. In practise, the C values are determined from the in-situ SSC data. However, no in-situ data were available for the 27 January flight. As a result, the three MAMS visible channels centered at 0.48μm, 0.56μm, and 0.62μm are given equal weight in this model. Regression using in-situ data may alter the scale of the SSC values obtained, but the spatial features in the imagery will not be significantly changed. The model used coefficients $C_0 = 0.3$, $C_1 = C_2 = C_3 = 0.2$. This produced unscaled SSC indicator values in the range 0.0-10.0; these may be related to in-situ measurements of SSC in the Atchafalaya Bay region which have been shown to range from about 50 mg/liter up to about 600 mg/liter (Egleme, 1985).

4. EVALUATION OF CAPABILITY AND INTER-COMPARISONS

On 27 January 1988, the MAMS instrument was flown along the Louisiana coastline. Figure 1 shows a portion of the flight and identifies locations along the route. The MAMS collected 10 bit data for channels 9-12. Clear skies with light northeasterly winds (~5 knots) prevailed along the entire coastline yielding excellent data collection conditions between 1400 and 1700 GMT. The flight came in the wake of a strong cold air outbreak on the morning of 25 January 1988. Although northerly winds had diminished, the coastline was still under the influence of cold high pressure which followed the cold front.

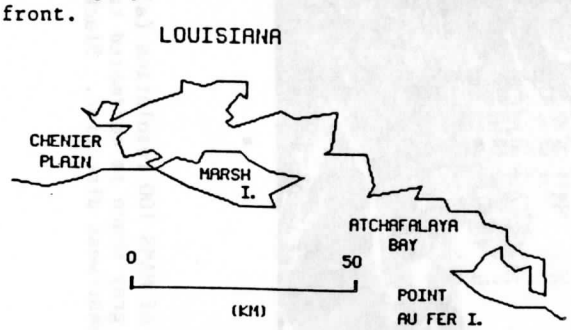

Fig. 1. Atchafalaya Bay region of Louisiana coastline.

In processing the MAMS data, corrections were applied to the infrared calibration when it deviated significantly from time averaged means (spike noise). The navigation was also checked against observable landmarks and corrected for biases, which produced accuracy to within about .5 km rms (Jedlovec et al., 1989).

Single sample noise was calculated for channels 11 and 12. Noise values in channels 11 and 12 were 0.10K and 0.13K, respectively. By applying these noise values to the SST algorithm the accuracy of the SST calculation was estimated to be on average about .25k. This SST error value is well within the error given by Bates et al. (1987) for various VAS algorithms. It is noted, however, that Bates' error estimates were for comparisons to actual SST and therefore may include significant ground truth measurement error.

As a further check on the MAMS infrared data, a comparison was performed between the MAMS 11μm data and collocated NOAA 10 AVHRR 11μm data (1 km resolution) for 27 January. In total 95 collocations were found. Corrections were made for spectral differences and viewing angle differences via a simulated radiance calculation. Results showed that the MAMS 11μm data was highly correlated (r=.91) with the AVHRR 11μm data. In a similar comparison with VAS (74 collocations), the correlation was significantly less (r=.55), probably owing to the large difference in resolution between the instruments. Near coastlines even a single pixel offset in the VAS navigation can make a large difference in the observed 11μm brightness temperature.

Images of SST and SSC were processed for the MAMS flight tracks of 27 January. The SST and SSC images for a flight track over the Atchafalaya Bay are shown together in Fig. 2. In both images, dark shades represent lowest values. Simulated radiance calculations indicated that no limb correction would be necessary for the 11μm and 12μm data. Sun glint was also found to be zero for the visible data.

Figure 2 shows a high degree of variability in both the SSC and SST products. SST variability is about 10K with each grey shade representing .25K of variability. Through the use of the sparse ground truth available from 22 January 1988 and that given by Egleme (1985), the SSC grey shades can be assigned a variability of about 50 mg/l for each grey shade in the image.

The SSC image indicates that high SSC water exists in the bay with significantly lower SSC values outside of the bay. High SSC water flows from the mouth of the Atchafalaya River and fans out into the bay. The low SSC water represents water originating from the gulf. As the high SSC water streams outward it is affected by prevailing currents. Roberts et al. (1987) have reported that this sediment can travel westward along the coast and be deposited as fluid mud on the face of the Chenier Plain. Evidence of this type of flow is present in the SSC depiction with an apparent wide band of relatively high SSC water flowing westward out of the bay past Marsh Island. Streamers of SSC within the bay are possibly tracers of flows within the bay. However no ground truth data was collected to verify these flows.

The contrast in SST from within the bay to gulf waters also acts as an indicator of the water origin, especially when coupled with the contrast in SSC values. It is expected that the bay waters would be cooler for two reasons. First, the river water flowing into the bay with its continental origin is cooler than the gulf water in the winter. Second, from simple heat

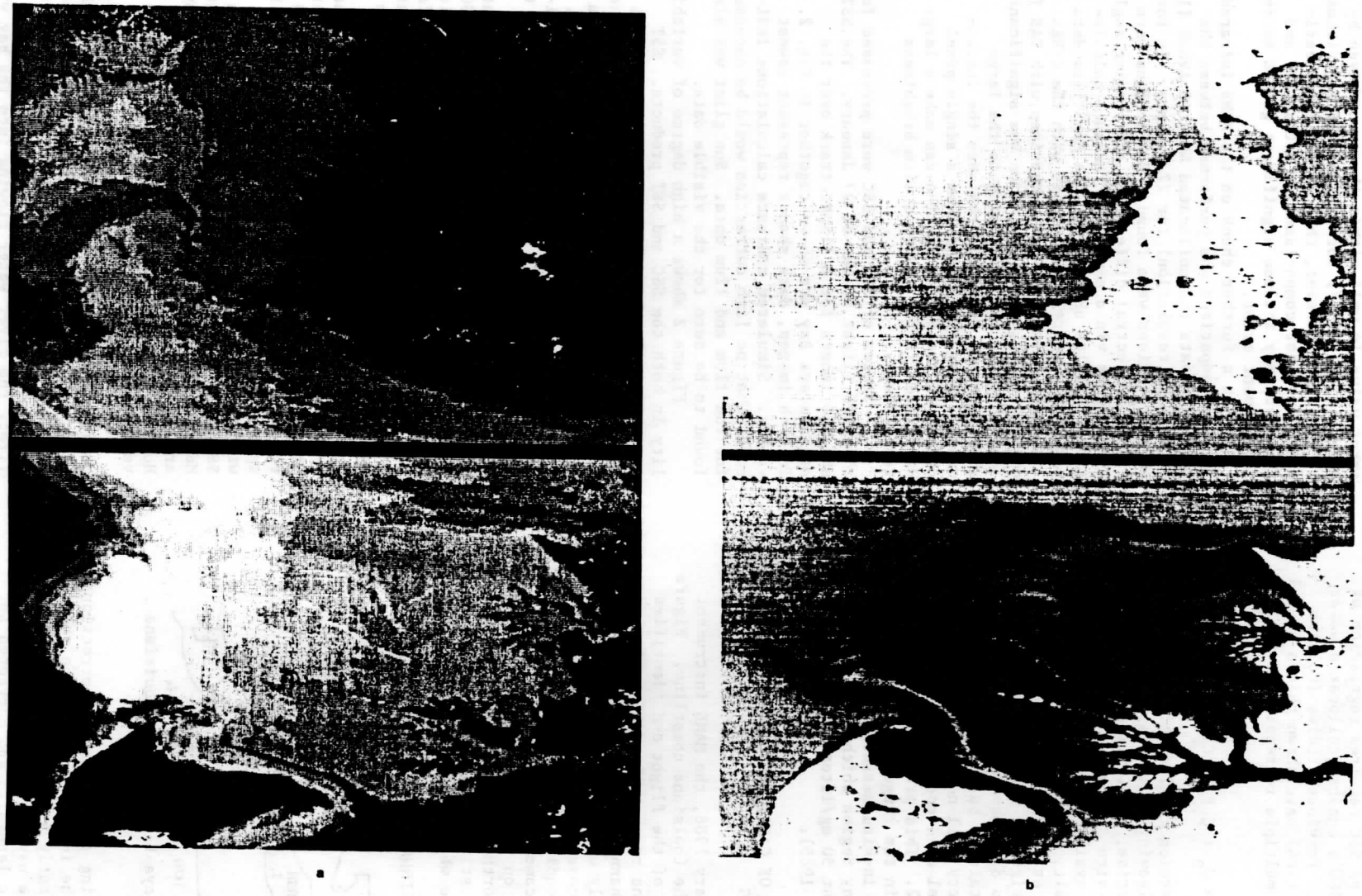

Feb. 2. Images of MAMS 100 resolution (a) unscaled SSC, (b) SST in Atchafalaya Bay region. Each SST gray shade represents .25k. Each SSC gray shade is estimated to represent 50 mg/l. North is towards top of page. Images are compressed by factor of 2 in east-west direction. Black line is missing data.

capacity considerations, the shallowest waters would be cooled the most when cold air outbreaks occur. Bathymetry charts show the shallowest waters of the region to be in the Atchafalaya Bay with depth increasing to the south. This agrees with an inference of sea depth from the SST depiction of Fig. 2. In addition, as in the SSC depiction, several streamers are apparent in the bay. These once again may be indicators of flow. Several of these streamers show significant temperature contrast with surrounding water. For instance, the SW/NE oriented streamer just to the west of Point Au Fer Island shows a decided warm core. This may indicate a flow of gulf water into the bay and/or a greater water depth in the streamer. Interestingly, a streamer of low SSC water occurs at the same location, which lends credence to the idea that this streamer water is of a different nature than the surrounding water. Other streamers of both warm and cold water are evident throughout the bay; they may be indicating areas of deeper and shallower water. However, it is difficult to verify this with bathymetry charts in an area of dynamic deposition and erosion like the Atchafalaya Bay. Nonetheless, if depth information may be inferred from the SST depiction, then daily, weekly, or even seasonal high resolution SST data could be useful in tracking the shifting of shoals in these waters.

A correlation of the SSC and SST fields was calculated in the Atchafalaya Bay region. Land areas were excluded from the correlation. An inverse correlation of r=-.57 was found. Warm SSTs correlated to low SSCs. This is a good indication that the warm SST/low SSC water of the gulf and the cold SST/high SSC water of the Atchafalaya River maintain their characteristics as they are advected in the region. This would seem to underscore the possibility of tracking these different water types through time. It is noted that this correlation improved when data further out in the gulf (warm SST, low SSC) was added to the computation.

5. CONCLUSIONS

The capability of the MAMS instrument to produce high resolution (100m) depictions of SSC and SST has been demonstrated. MAMS SST displays a spatial variability of better than .5k while SSC fields display realistic variability. The high variability in the Atchafalaya Bay of the Louisiana coastline depicted in these products is a strong testimonial to the value of such data. There are indications of SSC advection, water depth, water origin, and flow. In addition, an inverse correlation between SST and SSC is observed indicating a potential ability to track these features.

The MAMS will continue to be flown along the Louisiana coastline. An effort to monitor temporal changes along the coast as well as improve the SSC and SST algorithm coefficients will be made. Daily as well as seasonal changes will be investigated with an emphasis on the relationship between weather patterns (such as cold front passages) and the geomorphology of the Louisiana coastline.

REFERENCES

Bates, J. J., W. L. Smith, G. S. Wade, and H. M. Woolf, 1987: An interactive method for processing and display of sea-surface temperature fields using VAS multispectral data. Bull. of Amer. Met. Soc., 68, 602-606.

Collins M., and C. Pattiaratchi, 1984: Identification of suspended sediment in coastal waters using airborne thematic mapper data. Int. J. Remote Sensing, 5, 635.

Cox C., and W. Munk, 1954: Statistics of the sea surface derived from sun glitter. J. Mar. Res., 14, 198.

Egleme, L. E., 1985: Landsat-4 based models for suspended sediment concentrations in central Louisiana coastal waters. M.S. Thesis, Louisiana State University, 124 pp.

Gordon, H. R., D. K. Clark, J. W. Brown, O. B. Brown, R. H. Evans, and W. W. Broenkow, 1983: Phytoplankton pigment concentrations in the Middle Atlantic Bight: comparison of ship determinations and CZCS estimates. Appl. Optics, 22, 20.

Holligan, P. M., M. Viollier, C. Dupouy, and J. Aiken, 1983: Satellite studies on the distributions of chlorophyll and dinoflagellate blooms in the western English Channel. Contin. Shelf Res., 2, 81.

Jedlovec, G. J., 1988: Determination of low-level precipitable water variability from split window channel radiance data. Preprints Third Conference on Satellite Meteorology and Oceanography, AMS, Boston, 89-94.

Jedlovec, G. J., K. B. Batson, R. J. Atkinson, C. C. Moeller, W. P. Menzel, and M. W. James, 1989: Improved capabilities of the Multispectral Atmospheric Mapping Sensor (MAMS). NASA Technical Memorandum (in print), Marshall Space Flight Center, Huntsville, AL, 71pp.

Khorram, S., 1982: Remote sensing of salinity in the San Francisco Bay delta. Remote Sensing Environ., 12, 15.

McClain, E. P., W. G. Pichel, and C. C. Walton, 1985: Comparative performance of AVHRR-based multichannel sea surface temperatures. J. Geophys. Res., 89(C6), 11587-11601.

Menzel, W. P., G. J. Jedlovec, and G. S. Wilson, 1986: Verification of small scale features in VAS imagery using high resolution MAMS imagery. Second Conference on Satellite Meteorology/ Remote Sensing and Applications, AMS, Boston, 108-111.

Rimmer, J. C., M. B. Collins, and C. B. Pattiaratchi, 1987: Mapping of water quality in coastal waters using Airborne Thematic Mapper data. Int. J. Remote Sensing, 8, No. 1, 85-102.

Roberts, H. H., O. K. Huh, S. A. Hsu, L. J. Rouse, Jr., and D. Rickman, 1987: Impact of cold-front passages on geomorphic evolution and sediment dynamics of the complex Louisiana coast. Coastal Sediments '87, WW Div./ASCE, New Orleans, 1950-1963.

Viollier, M., D. Tanré, and P. Y. Deschamps, 1980: An algorithm for remote sensing of water color from space. Boundary Layer Meteorol., 18, 247.

RESPONSE OF THE LOUISIANA COASTAL ENVIRONMENT TO A COLD FRONT WIND SYSTEM

Christopher C. Moeller
University of Wisconsin Cooperative Institute for Meteorological Satellite Studies
Madison, WI 53706

Oscar K. Huh
Louisiana State University Coastal Studies Institute
Baton Rouge, LA 70803-7527

Liam E. Gumley
Curtin University of Technology Remote Sensing and Satellite Research Group
Perth, Australia

W. Paul Menzel
NOAA/NESDIS Advanced Satellite Products Project
Madison, WI 53706

1. INTRODUCTION

The role of cold front weather systems in coastal geomorphology has only begun to be studied. Cold fronts, because of their higher frequency of occurrence and their uniform direction of approach, are thought to be affecting the coastal environment more on a cumulative basis than the occasional tropical event. Roberts et al. (1987) have outlined responses of various portions of the Louisiana coastline to passing cold fronts. These include deposition and erosion at different parts of the coastline, suspended material transport, and water level setup and wave action which alternately cause inland marsh inundation and drainage. Kemp (1986) has suggested that wave action associated with winter storms transports fluid mud in coastal waters, promoting progradation of shoreface where fluid mud is present. Understanding the mechanisms of coastal change and their response to cold front systems is necessary in order to develop effective coastal management programs.

The Multispectral Atmospheric Mapping Sensor (MAMS) has been used to study the impact of a cold front wind system which passed through the Louisiana coastal zone on March 31, 1989. MAMS data was collected in daytime cloud-free conditions during the pre-frontal phase on March 30 and the post-frontal phase on April 1. MAMS has been used in previous work along the Louisiana coastline (Moeller et al., 1989) and is well suited to monitor the coastal environment because of its 100 meter resolution in 12 spectral channels. The 12 visible/infrared channels are shown in Table 1. MAMS flies onboard NASA's ER2 high altitude aircraft, scanning a 37 km swath from an altitude of 20 km. Calibration of infrared channels is accomplished by viewing two onboard blackbodies of known temperature during each scan. Visible calibration is accomplished by laboratory procedure. For detailed information on the MAMS spectrometer, see Jedlovec et al. (1990).

2. LOUISIANA COAST AND THE COLD FRONT MODEL

Fig. 1 shows the Louisiana coastal region. The Atchafalaya Bay is a region of new delta growth and is a focal point of the study.

Table 1. - MAMS spectral channels

channel	bandwidth (@ 50% response)
1[a]	0.42 - 0.45
2	0.45 - 0.52
3	0.52 - 0.60
4	0.57 - 0.67
5	0.60 - 0.73
6	0.65 - 0.83
7	0.72 - 0.99
8	0.83 - 1.05
9	3.47 - 3.86
10	3.47 - 3.86
11	10.55 - 12.24
12	12.32 - 12.71

a) not available when 10 bit infrared data are collected

Suspended sediment is transported by the Atchafalaya River, a distributary of the Mississippi River, into the Atchafalaya Bay where it is transported by existing currents. Significant deposits of this material have been found along the Chenier Plain to the west, which acts as a catchment of sediment flowing westward out of the Atchafalaya Bay. The Mississippi River delta is also of interest as well as barrier islands in sediment starved waters to the northeast of the delta.

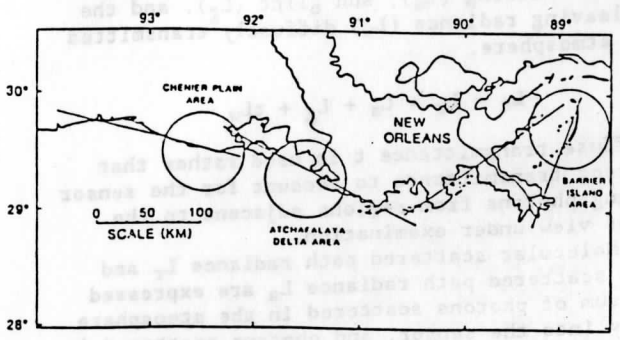

Fig. 1. Louisiana coastal region with MAMS flight tracks and areas of interest in the study.

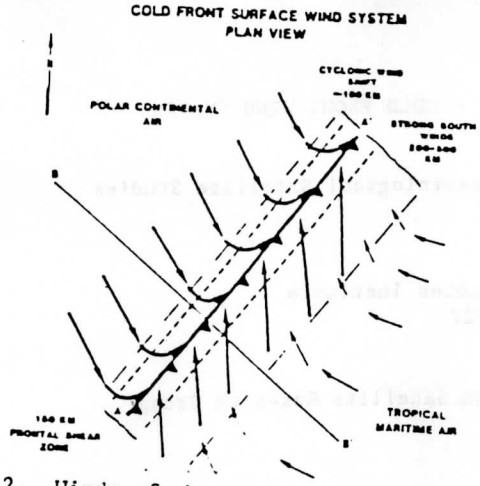

Fig. 2. Winds of the cold front system (from Roberts et al 1987).

About 30 to 40 cold fronts pass through the Louisiana coastline each year between the months of October and April. Fig. 2 summarizes the wind system of a passing cold front. In the pre-frontal phase southerly surface winds drive saline water into coastal bays and marshes. Onshore wave action created by the southerly winds erodes sediment starved portions of the coastline while depositing suspended material from sediment rich waters onto other regions of the coastline. After the cold front passes, winds shift to a northerly direction driving down water levels in coastal areas and reducing onshore wave action. The dry cold air behind the front rapidly dries newly formed deposits on the shoreface, thus expediting the coastal growth process. Water levels continue to drop, promoting marsh drainage and outflow of bay waters onto the continental shelf of the Gulf of Mexico. Coastal water temperatures also respond, cooling most rapidly in shallow regions.

3. DATA PRODUCTS

3.1 Atmospheric Correction of Visible Radiances

MAMS visible and near infrared radiances are corrected for atmospheric effects to isolate the radiance upwelling from the water. Using modelling studies, Gordon (1978, 1983) developed a single scattering atmospheric correction method. The total radiance, L_t, arriving at the sensor is expressed as the sum of molecular scattering (L_r), aerosol scattering (L_a), sun glint (L_g), and the water leaving radiance (L_w) diffusely transmitted by the atmosphere.

$$L_t = L_r + L_a + L_g + tL_w$$

The diffuse transmittance t is used rather that the direct transmittance to account for the sensor receiving photons from regions adjacent to the field of view under examination.

Molecular scattered path radiance L_r and aerosol scattered path radiance L_a are expressed as the sum of photons scattered in the atmosphere directly into the sensor, and photons scattered in the atmosphere and then reflected back by the surface into the sensor. Expressions for molecular scattering optical depth and ozone optical depth (absorption) are given by Guzzi et al. (1987). Aerosol optical depth was estimated using relationships between surface visibility and aerosol optical depth given by Sturm (1981). Sun glint radiance L_g was estimated using sun-sensor geometry and surface wind speed data in a model by Guzzi et al. (1987).

After atmospheric effects have been removed the remaining water leaving radiance is expressed as a subsurface reflectance according to Robinson (1985). The subsurface reflectance quantity can be regressed against in-situ suspended sediment concentration (SSC) data, however in-situ data were not sufficient to establish reliable SSC regression coefficients for March 30 and April 1, 1989. Therefore, images in this paper are displayed as a scaled subsurface reflectance quantity. A discussion of the atmospheric correction of MAMS radiances can be found in Gumley et al. (1990).

3.2 Atmospheric correction of infrared data

MAMS 11μm and 12μm infrared radiances were used to correct for atmospheric water vapor effects in estimating sea surface temperature (SST). A split window algorithm (McMillin and Crosby, 1984) used

$$SST = T_{11} + A\,(T_{11} - T_{12}) + B$$

where T_{11} and T_{12} are the 11.2μm and 12.5μm brightness temperatures, A is a regression coefficient, and B is a bias correction. Because MAMS split window channels are similar to those of VAS, VAS SST coefficients were used with a bias correction between MAMS and VAS 11μm and 12μm radiances applied.

4. CASE STUDY RESULTS

4.1 Cold Front Passage of March 31, 1989

The cold front passage of March 31 propogated west to east at a high angle to that of the coastline orientation. This is opposite to a front traveling north to south with the frontal boundary oriented parallel to the coastline. To illustrate the characteristics of this system, temperature, dew point, wind, and pressure data are shown in a time series format in Fig. 3 for the NWS station at Lake Charles (LCH), LA. The

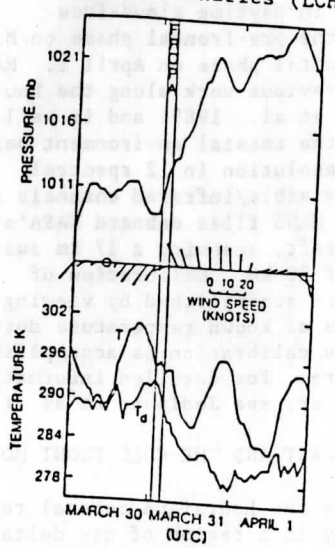

Fig. 3. Surface observations of pressure, wind, temperature (T) and dew point (Td) at Lake Charles (LCH), Louisiana from March 30 through April 1, 1989. A cold front passage is indicated by FROPA.

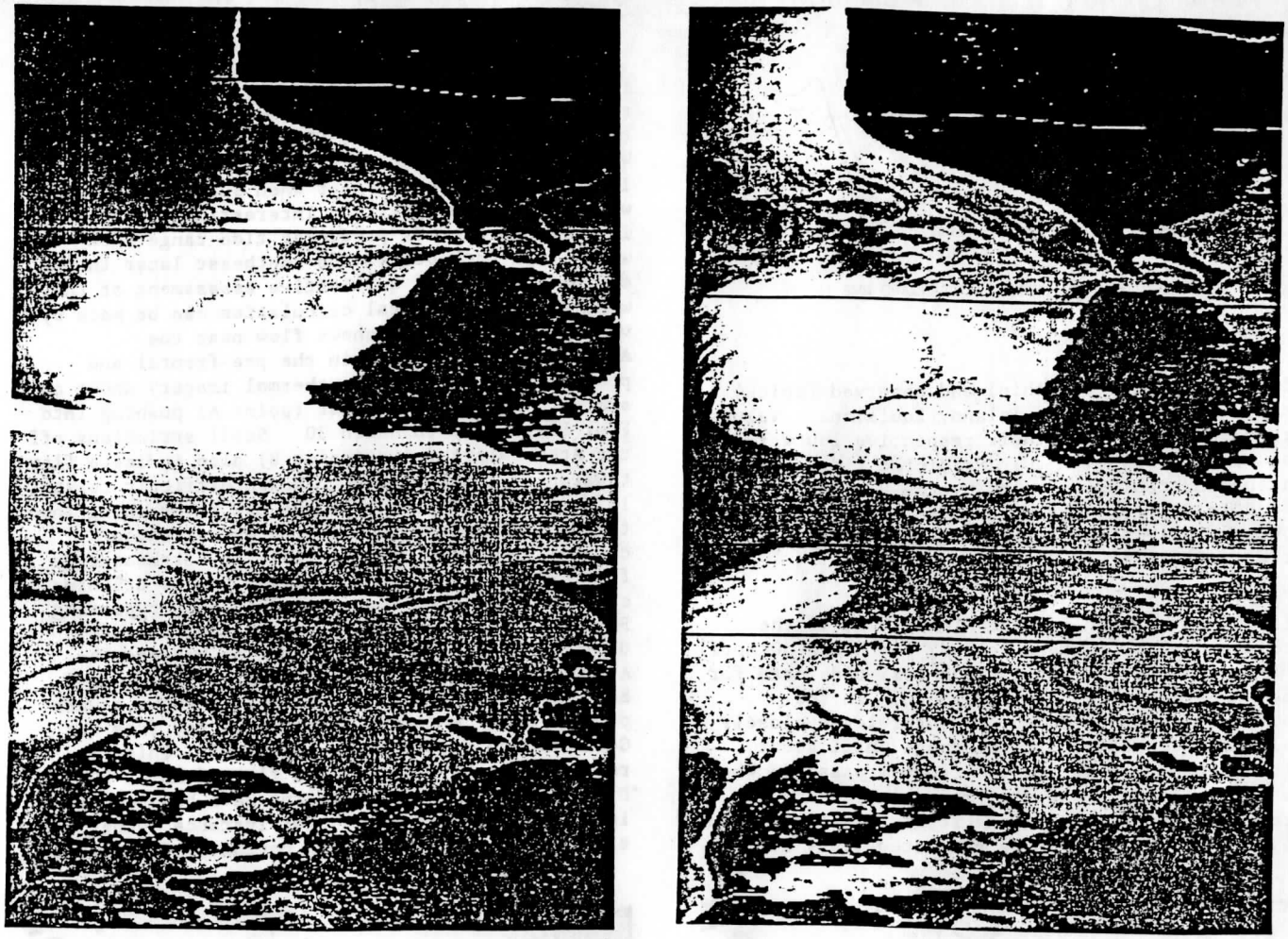

Fig. 4. MAMS images of subsurface reflectance on March 30 (left) and April 1 (right) 1989. High reflectances are bright. Land is artificially shaded dark. On March 30, southwesterly winds retard sediment flow towards the west (top), forcing the sediment plume out into the Gulf of Mexico to the south (left); on April 1, northeasterly winds force the plume westward along the coast, reducing its southward extent into the Gulf of Mexico.

frontal passage is well defined by the increase in surface pressure beginning about 0200 UTC on March 31. Decrease of air temperature behind the front is best illustrated by the lower maximum temperature on the 31st vs. the 30th (about 5 K). Dew point temperatures also decrease behind the front. Surface winds show maximum speeds in the 12 hours preceding and just after the frontal passage with a southwest to northerly wind shift. These conditions of the cold front passage cause the forcing on the coastal environment. Linking these forcings to responses in the environment is a tool for understanding coastal change.

4.2 Response of the Coastal Environment

The Atchafalaya Bay sediment plume is a primary source of depositional material for the western Louisiana coastal zone including the Chenier Plain region. Whether deposited directly onto the shoreface or onto the subaqueous bottom, coastal progradation relies on the presence of an influx of sedimentary material. Because of this, it is important to monitor the response of the Atchafalaya Bay sediment plume to cold front wind systems. The Atchafalaya Bay sediment plume is shown in Fig. 4 for the MAMS flights on March 30 and April 1. Southwesterly winds on March 30 retarded the flow of the plume towards the Chenier Plain, creating a damming effect. This cuts off the flow of depositional material towards the Chenier Plain. Under these conditions, coastal waters along the Chenier Plain must rely on wave action resuspending bottom sediments for material for coastal progradation. Otherwise, with low sediment content, wave action is an erosive force on the coastline. On April 1, in northeasterly flow, the plume flowed westward, hugging the Chenier Plain coast and restoring the influx of sediment to that area. This direct response of the sediment plume to surface winds exhibits an important dependence of the coastal environment on cold front wind systems.

4.3 Coastal Circulation Response

Coastal circulation patterns are a function of several factors including astronomical tides, water levels, offshore currents, and subaqueous terrain. Winds of the cold front system also affect water levels in coastal regions, increasing bay and estuary water levels when winds blow inshore (southerly winds in the case of the Louisiana coast) and driving down water levels in offshore wind conditions. Some indication of this

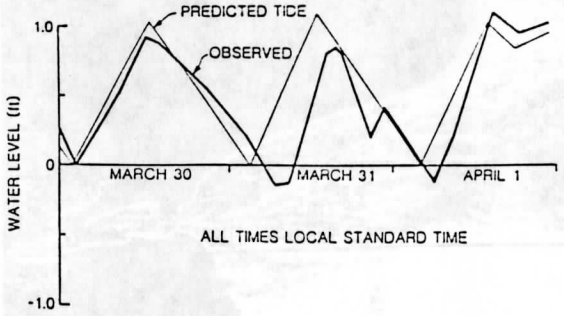

Fig. 5. Predicted (thin) and observed (thick) water levels at Eugene Island, Louisiana. Values are differences from their respective low water on the morning of March 30. Predicted tide data is taken from tables compiled by the U.S. Coastal Geodetic Survey. Observed water level data courtesy of U.S. Army Corps of Engineers, New Orleans District.

effect can be seen in water level data of the Atchafalaya Bay (Eugene Island) for March 30-April 1 (Fig. 5). Predicted astronomical tide data for the Atchafalaya Bay is also shown. In the southerly winds of March 30, water level closely follows the predicted tidal range until about midday (12 hours before the frontal passage) when water levels begin to drop more slowly than the predicted tides.. Following frontal passage, water level drops quickly while predicted tides are increasing. A subdued high water level follows, this all occurring in the strong northerly flow that followed the frontal passage (see Fig. 3). Water level and predicted tides begin to work back into phase with each other when surface northerly winds weaken on April 1. Interestingly, water level range exceeds predicted tide range when winds turn back out of the southeast later in the day on April 1. A qualitative assessment of the wind effect on coastal circulation can be made by viewing Fig. 6 which shows flow near the Atchafalaya Bay region in the pre-frontal and post-frontal modes. The thermal imagery shows an arm of cold (bright) water (point A) pushing into Four League Bay on March 30. Small striations off the Atchafalaya delta (point B) also indicate flow towards Four League Bay. Though difficult to see, it is likely that Four League Bay is draining into the Gulf of Mexico through the Oyster Bayou channel (point C). On April 1, in northeasterly flow, water from the Atchafalaya Bay is draining southward (point B) out into the Gulf, bypassing Four League Bay. An arm of warm (dark) marsh drainage water can be seen cutting between the Atchafalaya Bay and the entrance to Four League Bay (point A). Close scrutiny also shows a warm pool of water entering Four League Bay from the Gulf through Oyster Bayou (point C). This represents a reversal of the flow of March 30. Different circulation patterns have been observed in other MAMS data sets. For instance, under low tide conditions with strong northerly flow, water

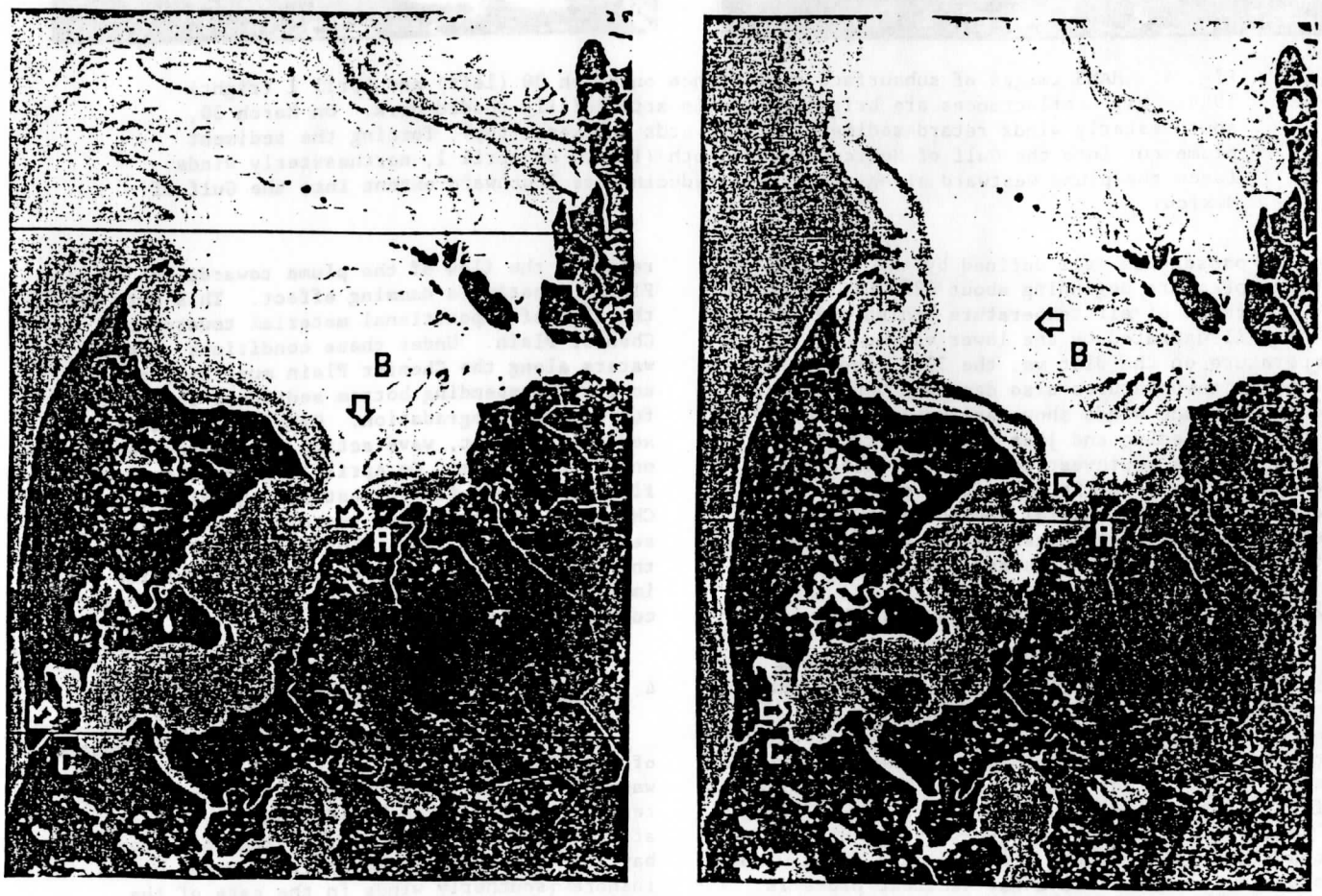

Fig. 6. MAMS thermal imagery over the Atchafalaya Bay on March 30 (left) and April 1 (right). Land is dark (warm). Note the small delta near the mouth of the Atchafalaya River. Thermal contrast shows evidence of flow (arrows) in the water on each day.

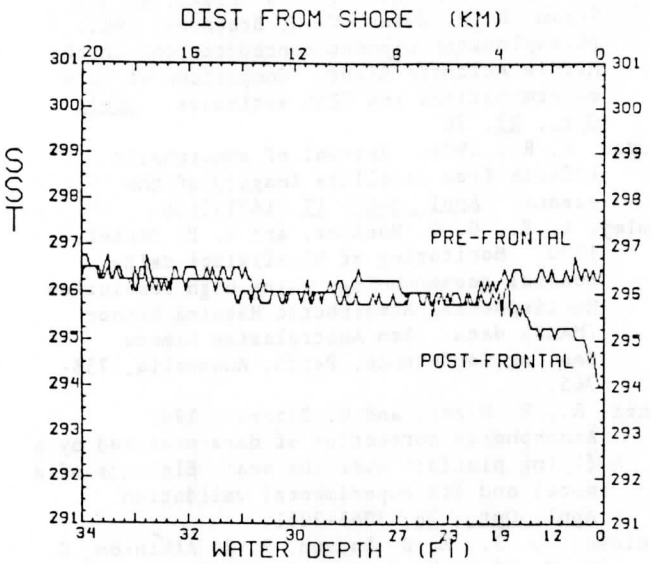

Fig. 7. MAMS SST transects in pre-frontal (March 30) and post-frontal (April 1) modes.

has been observed draining from both the Atchafalaya Bay and Four League Bay into the Gulf. The circulation response to atmospheric and tidal forcing is a subject of continuing investigation.

4.4 SST Response to Atmospheric Conditions

Fig. 7 shows a transect of MAMS SST data from the Chenier Plain coast outward into the Gulf of Mexico on March 30 and April 1. As was indicted in Fig. 3, air temperatures dropped some 5 to 7 K over this period with a corresponding drop in dew point temperatures. SST response to the atmospheric variation is related to water depth in Fig. 7. Little response is apparent in waters deeper than about 20 feet. As water depth decreases towards the shore, the response increases. A maximum cooling of about 2.5 K occurs within a few hundred meters of shore. This indicates that shallow waters respond first to changing atmospheric conditions, presumably because of a reduced thermal capacity. In deeper waters, vertical and horizontal mixing may be acting to maintain the SST at a nearly constant temperature. Decreases of about 2-3 K from March 30 to April 1 have also been seen in MAMS SST data in the shallow Barataria Bay region of the Louisiana coast as well as in inland lakes.

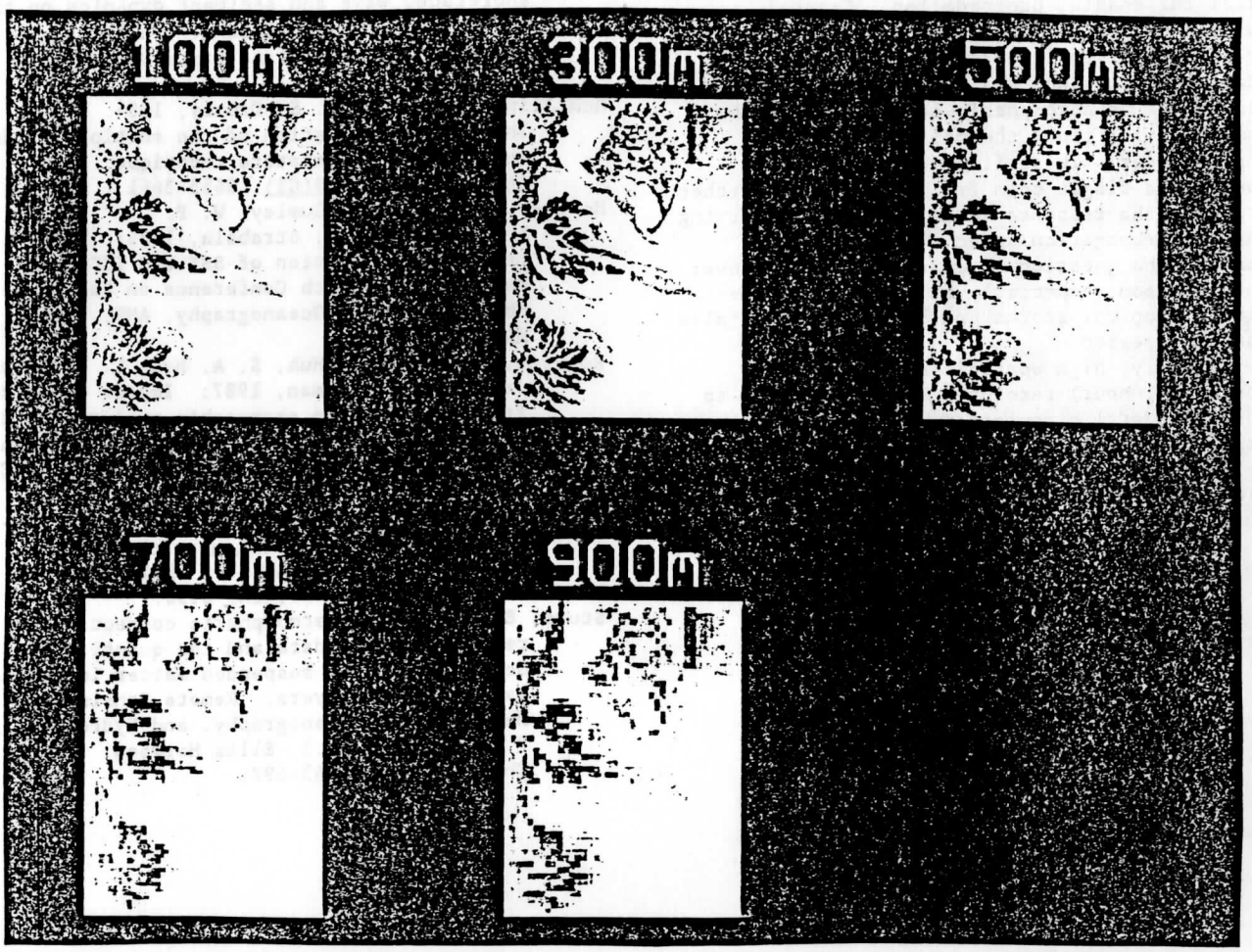

Fig. 8. MAMS thermal imagery over the Atchafalaya Bay region degraded to various resolutions. Dark shades are warm. Note blurring of small scale flow patterns as imagery is degraded.

4.5 Instrument Resolution

Instrument spatial (and temporal) resolution considerations are important in planning and designing future remote sensing systems. The impact of instrument spatial resolution in the Louisiana coast study was addressed by degrading the spatial resolution of MAMS thermal data through an averaging process. Degraded images are shown in Fig. 8. Small scale features which provide information about coastal circulation are blurred by degrading the spatial resolution. These features would likely be useful as tracers of water flow in a system which provided high temporal as well as high spatial resolution. Thermal gradients are also reduced, removing information about thermal variation and affecting the delineation of landform from water. A loss of thermal response information is likely. These findings, while qualitative, provide insight into the importance of spatial resolution considerations for future coastal studies.

5. CONCLUSIONS

MAMS has been used to study the response of Louisiana coastal waters to wind and temperature effects associated with cold front passages. Sediment flowing out of the Atchafalaya Bay is deflected towards the downwind direction by cold front winds, displacing the source of sedimentary material for coastal progradation. Coastal circulation patterns vary in response to changing water levels forced in part by cold front winds. SST data indicate that shallow coastal regions respond first to atmospheric conditions, in the absence of significant thermal advection and mixing of water. These findings outline the response to a single cold front event. Of further interest is the response to cold fronts of varying intensity, propagation speed, and angle of approach. The question of cumulative impact over a winter season, especially as compared to the impact of tropical storms and hurricanes, has also not been addressed.

Finally, high spatial (< .5 km) and temporal (< 1 hour) resolution data is needed to delineate coastal circulation patterns as well as identify thermal responses of coastal waters to changing atmospheric conditions in future coastal studies. Such data is not currently available on a routine basis.

REFERENCES

Gordon, H. R., D. K. Clark, J. W. Brown, O. B. Brown, R. H. Evans, W. W. Broenkow, 1983: Phytoplankton pigment concentrations in the Middle Atlantic Bight: Comparison of ship determinations and CZCS estimates. Appl. Opt., 22, 20.

Gordon, H. R., 1978: Removal of atmospheric effects from satellite imagery of the oceans. Appl. Opt., 17, 1631-1636.

Gumley, L. E., C. C. Moeller, and W. P. Menzel, 1990: Monitoring of Mississippi delta coastal geomorphology using high resolution Multispectral Atmospheric Mapping Sensor (MAMS) data. 5th Australasian Remote Sensing Conference, Perth, Australia, 738-745.

Guzzi, R., R. Rizzi, and G. Zibordi, 1987: Atmospheric correction of data measured by a flying platform over the sea: Elements of a model and its experimental validation. Appl. Opt., 26, 3043-3051.

Jedlovec, G. J., K. B. Batson, R. J. Atkinson, C. C. Moeller, W. P. Menzel, and M. W. James, 1989: Improved capabilities of the Multispectral Atmospheric Mapping Sensor (MAMS). NASA Technical Memorandum 100352, Marshall Space Flight Center, Huntsville, AL, 71pp.

Kemp, G. P., 1986: Mud deposition at the shoreface: wave and sediment dynamics on the Chenier Plain of Louisiana. Ph.D. dissertation, Louisiana State University, 146pp.

McMillin, L. M., and D. S. Crosby, 1984: Theory and validation of the multiple window sea surface temperature technique. J. Geophys. Res., 89(C3), 3655-3661.

Moeller, C. C., L. E. Gumley, W. P. Menzel, and K. I. Strabala, 1989: High resolution depiction of SST and SSC from MAMS data. Fourth Conference on Satellite Meteorology and Oceanography, AMS, Boston, MA, 208-212.

Roberts, H. H., O. K. Huh, S. A. Hsu, L. J. Rouse, Jr., and D. Rickman, 1987: Impact of cold-front passages on geomorphic evolution and sediment dynamics of the complex Louisiana coast. Coastal Sediments '87, WW Div./ASCE, New Orleans, LA, 1950-1963.

Robinson, I. S., 1985: Satellite oceanography - an introduction for oceanographers and remote-sensing scientists. Ellis Horwood Limited, Chichester, UK, p150.

Sturm, B., 1981: The atmospheric correction of remotely sensed data and the quantitative determination of suspended matter in marine water surface layers. Remote Sensing in Meteorology, Oceanography, and Hydrology, A. P. Cracknell (Ed.), Ellis Horwood, Chichester UK, 163-197.

Reprinted from Coastal Sediments '91 Proceedings
Specialty Conference/WR Div./ASCE
Seattle, WA/June 25-27, 1991

FINE GRAIN SEDIMENT TRANSPORT AND DEPOSITION IN THE ATCHAFALAYA AND CHENIER PLAIN SEDIMENTARY SYSTEM

Oscar K. Huh[1] Harry H. Roberts[1] L. J. Rouse[1]
and
Doug A. Rickman[2]

ABSTRACT: The most extensive land loss and land accretion processes in the U.S. are occuring in the Mississippi River Delta Plain. Some 40 square miles of valuable marshlands are lost annually. However, discharge of one third of the Mississippi River waters through the Atchalfalaya Basin is now rapidly building land, deltas in Atchafalalaya Bay and prograding mudbanks along the Chenier Plain. Studies of these coastal processes is underway combining field work with the data from remote sensing systems. Remote sensing systems being used include the NOAA Satellite AVHRR, the Multispectral Atmospheric Mapping System, the Calibrated Airborne Multispectral Scanner, SPOT satellite imagery and color aerial photography.

Storms, both winter cold front passages and the occasional hurricane actually build up the muddy coasts by heaving fluid mud onto the shoreface where it becomes stranded. The deposit consists of a centimeter or so of sand/shell overlain by a 6-8 cm layer of mud. The mud begins dewatering by evaporation and by percolation through the sand/shell lamina. It becomes sun dried, dessicates, hardens, cracks into mudcrack cobbles which resist wave erosion. The transition from fine to very coarse grained sediment stabilizes newly accreted sediment against the coast. This process has caused recent progradation (1987-1990) of up to 200 m per year along the Chenier Plain coast west of Morgan City, La. Newly formed land is quickly colonized by marsh grasses. Cold front passages and hurricanes have essentially the same effect, with hurricanes just creating larger mud layers.

INTRODUCTION

Land loss and marsh deterioration are major problems for the State of Louisiana. The dynamic coastal environments are in a state of flux by natural processes of delta development operating on an array of time scales. Added to this are the extensive leveeing(flood protection), oil and gas development and dredging for navigation, and other smaller scale anthropogenic changes. The richness of resources, extent of settlements, and competing activities have inevitably created major environmental and legal problems. Recent studies have shown that our lack of understanding of the natural processes of land

1) Coastal Studies Institute, Louisiana State University, Baton Rouge, La. 70803.
2) Science and Technology Laboratory, NASA Stennis Space Center, Bay St. Louis, Ms.

loss and land building in a deltaic environment seriously hinder our ability to manage these environmental problems effectively or avoid creating new ones.

A few studies are focused on the important and desirable processes, those of land building. For these the sediment load of the Mississippi and Atchafalaya Rivers is considered a commodity, the raw material for coastal processes that build land. The main channel of the Mississippi, discharging into the birdfoot delta has extended to the continental shelf edge, dumping its sediment load into the deep Gulf where it is essentially a commodity lost to Louisiana. Particularly since both natural and man made leveeing largely prevents deposition in the shallow bays and estuaries adjacent to the delta. In fact we have reached the end of the delta lobe building cycle for the present Mississippi Delta and a switch to the Atchafalaya Basin/river channel is in progress. If not for intervention by the Corps of Engineers with the old river control structure, the major part of the Mississippi River flow would be through the Atchafalaya distributary channel.

This paper is focused on the land building processes associated with that 1/3rd of the discharge that flows through the Atchafalaya river system. The Atchafalaya discharges into an estuary and broad continental shelf(150 km). Thus the relatively small volume of sediment builds land as it accumulates, having little space to fill before shoaling occurs. Observations and measurements from remote sensing systems provide invaluable technological capabilities in the study of coastal sedimentation and land building processes.

REMOTE SENSING SYSTEMS AND OPERATIONS

The large areal extent and difficulty of accessing this wilderness coastal region make the remote sensing approach particularly useful for study of these environments. Both aircraft and satellite systems are being employed. They provide a time series of maps of water temperature color/albedo, plant cover, and coastal geomorphology. The coastal waters of this region are a mosaic of water types, many with contrasting temperature, turbidity and depth. The systems being used are optical (visible and infrared) and are so weather/atmosphere/sunlight dependant. The atmospheric conditions best for the use of such systems characteristically occurs with the cold, dry, cloud free continental air that follows cold front passages over the coast. Cold fronts also are important in driving environmental changes, including differentiating coastal and estuarine water types by temperature and turbidity, plus eroding/depositing sediment.

The remote sensing systems used include the NOAA Satellite Advanced Very High Resolution Radiometer (AVHRR), the Multispectral Atmospheric Mapping System (MAMS), SPOT satellite imagery, the Calibrated Airborne Multispectral Scanner (CAMS), and aerial photography. CAMS and MAMS are airborne systems flown on a Lear Jet (at 2 Km and 12 km alt.) and ER-2 (U-2 type, 20 km alt.). The characteristics of these systems are specified in table I. The AVHRR in circa 860 km sun sunchronous orbit and multiple daily passes (4-6) is used to follow the movement of weather systems and map the water temperature and turbidity at scales of 2-10s of kms. The high resolution visible sensor(HRV) of the French SPOT satellite can provide digital imagery on geomorphology and water reflectance at 10m resolution panchromatic, or 20 m multispectral. These two satellite systems are of course, orbit bound, whereas the MAMS and CAMS are used in scheduled missions. The MAMS is a MODIS (planned earth observing system sensor) simulator, with a 100m resolution. CAMS, on a Lear Jet stationed at Bay St. Louis, MS, is routinely flown at the altitudes noted above with 6m and 30m resolution respectively. For all data acquisitions surface measurement (surface "truth") teams deploy for essential surface and atmospheric measurements. False color infrared photography is acquired with each

TABLE I Specifications of Remote Sensing Systems

System	NOAA Satellite AVHRR	SPOT Satellite HRV	LearJet CAMS	ER-2 MAMS	Spect. Band
	Channel	Channel	Channel	Channel	
Spectral Bands	1. .58-.68 2. .7-1.1 3. 3.5-3.9 4. 10.5-11.5 5. 11.5-12.5	1. .50-.59 2. .61-.68 3. .79-.89	1. .45-.52 2. .52-.60 3. .60-.63 4. .63-.69 5. .69-.76 6. .76-.90 7. 1.55-1.75 8. 2.08-2.35 9. 10.50-12.50	1. .42-.45 2. .45-.52 3. .52-.60 4. .57-.67 5. .60-.73 6. .65-.83 7. .72-.99 8. .83-1.05 9. 3.47-3.86 10. 3.47-3.86 11. 10.55-12.24 12. 12.32-12.71	Blue Green yel/org Red NIR NIR Therm IR
Spatial Resolution	1.1km	20m	5m @ 2km 30m @ 12km	100m	
Swath Width @ ALT	2800km @ 860km	60km @ 840km	2.33km @ 2km 14km @ 12km	37km @ 20km	

MAMS and CAMS overflight, which provides higher spatial resolution often needed for positive identification of some object or feature seen in the scanner data.

Aircraft overpass missions involve careful planning, with launch decisions based on weather, solar elevation and stage of the tide. Clear sky conditions are the first requirment and therefore accurate coastal marine weather forcast is of primary importance. Solar elevation is critical in two ways, if it is too high, there is a serious, image degrading sun glint spot in the middle of the scene. Such sun spots obscure important water column, shoreline, and coastal detail. Sunspot calculations for coastal hydrographic surveys show that at 35 degrees solar elevation less than an 8th of the photograph/image is affected. Above that large portions of the image get obliterated. If solar elevation is too low, there is insufficient illumination of the water column to provide good color rendition of the coastal waters. See Table II illustrating sunlight transmittance into the sea versus solar altitude. We selected 20 degrees solar elevation as our lower limit and 35 degrees as our upper limit for overflights. Solar elevation is operationally forecast using Smithonian table 170, List R.J. 1984.

Table II Transmittance of Sunlight into the Sea

Solar Altitude	% Transmittance 0 $msec^{-1}$ Winds	%Transmittance 4 $msec^{-1}$ Winds
90	97.9%	97.9%
60	97.8%	97.8%
40	96.5%	96.3%
30	93.9%	93.5%
20	86.5%	86.3%
10	65.0%	70.8%
0	0%	50.7%

Data from Austin, 1974 Seawater Ref. index 1.341

In this low relief coastal region, stage of the tide is also a critical factor. High water in these muddy environments provides little information on the geomorphology of the shore face, shoals, marshes, and beaches. Water types are still detected however by temperature and turbidity. This region is microtidal, range circa 0.3-0.5 m, but the meteorological tides, i.e. wind setup, can dominate and even reverse the astronomical influence on the coastal water level. The ideal condition is a morning or afternoon with a low astronomical tide and strong offshore winds. Under these conditions spectacular imagery and photography are obtained from the Atchafalaya and Chenier Plain coasts.

The field measurement program component of each mission includes: (1) atmospheric radiosonding and sun photometry (for aerosol loading), (2) small boat measurements of water temperature, color, turbidity, water sampling(for lab analysis for suspended sediment), (3) access to regional water level and meteorological data, all of which to establish the "state of the environment" during the remote sensing overpass. The atmospheric measurements provide data for atmospheric correction of the remote visible and infrared radiometric measurements. Small boat measurements are used to provide information on conditions of the environment for studies of radiometry vs. surface condtions("surface truth"). The Louisiana shelf has an extensive array of hydrocarbon drilling platforms, many of which are instrumented for meteorological measurements, figure 1. Data on the conditions of the environment through remote and insitu measurements support the surface observation and measurement program.

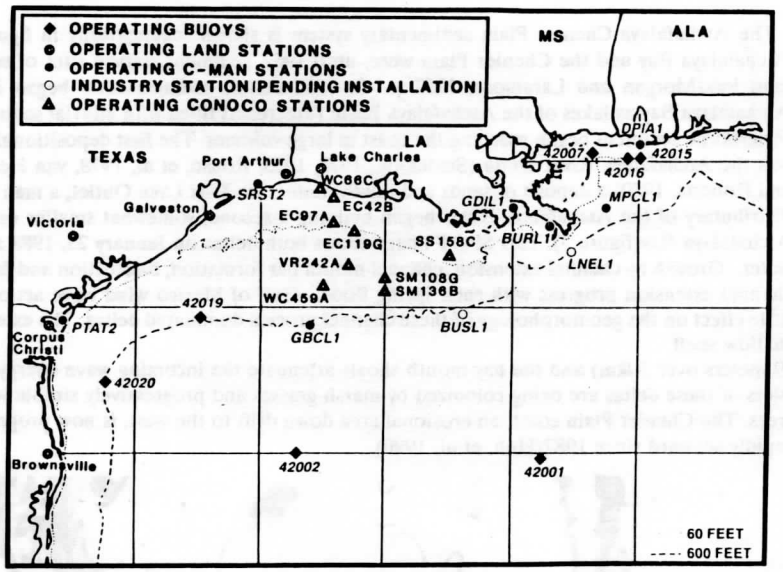

Figure 1. Location of sources of meteorological data on and near the Louisiana Continental shelf, June 1990.

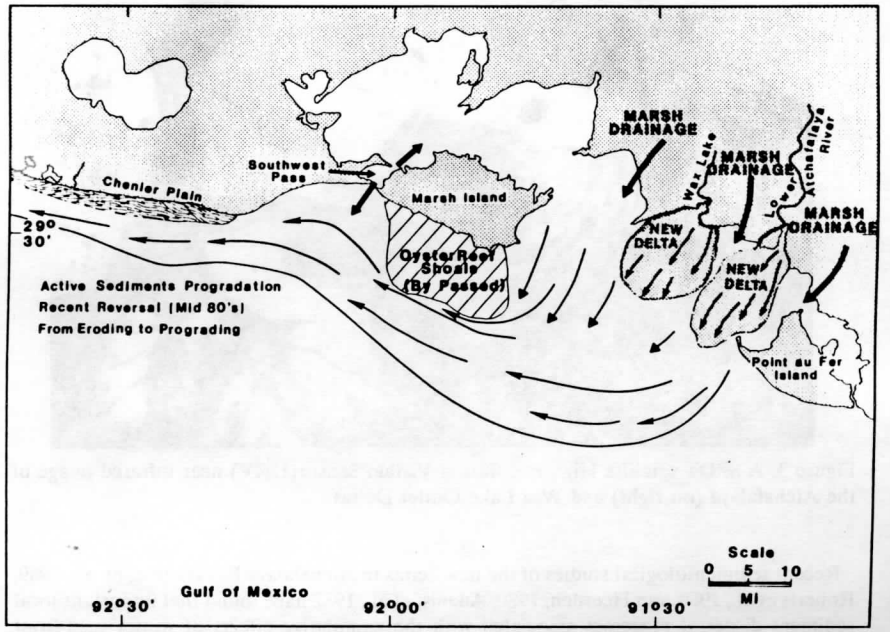

Figure 2. A diagram outlining the elements of the Atchafalaya Chenier Plain Sedimentary System.

THE SEDIMENTARY PROCESSES AND COASTAL GEOMORPHIC CHANGE

The Atchafalaya-Chenier Plain sedimentary system is shown schematically in figure 2 . Atchafalaya Bay and the Chenier Plain were, until 1952, sediment starved sites of serious land loss(Morgan and Laramore, 1957). In 1952 deltaic sedimentation began in the Atchafalaya Bay as lakes of the Atchafalaya Basin (upstream) filled with alluvial sediments. Riverborne sediment began reaching the coast in large volumes. The first depositional form was the Atchafalaya River Delta (Schlemon, 1972, 1975, Rouse, et al, 1978, van Heerden and Roberts, 1980) a deposit of sands and muds. Later, the Wax Lake Outlet, a man made distributary of the Atchafalaya River began building a second, somewhat smaller delta in Atchafalaya Bay(figure 3). This SPOT image shows both deltas on January 23, 1988 at low water. Growth by channel extension, channel mouth bar formation, bifurcation and further channel extension progress with each spring flood. Gulf of Mexico wind wave action has little effect on the geomorphology of these channel process dominated deltas. The extensive shallow shelf
(9 meters over 50km) and the bay mouth shoals attenuate the incoming wave energy. The islets of these deltas are being colonized by marsh grasses and progressively sizable willow trees. The Chenier Plain coast, an erosional area down drift to the west, is now prograding rapidly seaward since 1987(Huh, et al, 1990).

Figure 3. A SPOT satellite High Resolution Visible Sensor(HRV) near infrared image of the Atchafalaya (on right) and Wax Lake Outlet Deltas.

Recent sedimentological studies of the new deltas in Atchafalaya Bay (Rouse, et. al., 1989, Roberts et al., 1980, van Heerden, 1980, Adams, et al., 1982 have found that important local sediment dispersal processes associated with the cumulative effects of winter cold-front processes. Most recently Kemp(1986) suggested winter wave fields play an important role

in transporting fluid mud to the now prograding chenier plain coast. Although cold front passages are of lower energy than the more powerful hurricanes, their uniform directions of approach, repeated pattern of wind changes, large spatial scales, and higher frequency of occurence(30-40 each season) allow them to drive perhaps even greater cumulative change.

Figure 4 illustrates a model of a cold front weather system. The cold front passages cycle is a sequence consisting of prefrontal, frontal passage and cold air outbreak phases. Prefrontal conditions consist of warm, humid air and increasing southerly winds. These conditions set up sealevel, spill shelf water into the estuaries and promote long fetched wave attack along the coast. Stalling of the frontal system over the coast can prolong such dynamic conditions. The frontal passage phase is characterized by strong gusty and variable winds, great atmospheric turbulence. The cold air outbreak phase involves strong northerly winds, rapid cooling, set down of seas built up during the prefrontal phase, set down of sealevel and spillage of the turbid suspended sediment rich estuarine and river waters onto the inner continental shelf. The cold, dry and cloud free atmospheric conditions of the cold air outbreak phase allow acquisition of excellent quality remotely sensed data, scanner or photographic.

The fine grained sediment laden waters, thus injected onto the shelf, are seen in the remotely sensed imagery to flow from the Atchafalaya bay. It flows as either a coast hugging mud stream under low to moderate winds(Wells and Kemp, 1981) or as an offshore discharge plume from high winds of the cold air outbreak.

Studies starting in 1987 have revealed a transition from erosion to rapid progradation in the chenier plain coast in the vicinity of Fresh Water Bayou and further west for some 14 km along the coast. Figure 5 shows progradation 2 km west of Fresh Water Bayou of 400m from 1987 to 1989. Extensive colonization by plants is underway as well. This represents a transition from formation of retreating reworked ridges of sand and shell on the beach face, to formation of mudflat/salt marsh deposition prograding seaward. Where the active mudflat deposition has reached the coast, the chenier of sand and shell has been buried under the earliest stable mud deposits.

Examination of these deposits reveals the following sedimentary structures and transformations in these fine grained deposits. After a storm, a 6-8 cm thick slab of gelatinous mud is found deposited on the shoreface. It is underlain by a 1-3 cm layer of sand and shell material. The mud(with consistancy of "tofu") is actively dewatering through evaporation at the top and drainage through the sand layer at its base(see figure 6). Under the solar radiation and wind driven evaporation of the cold air outbreak days, the slab of mud dessicates forming mudcrack polyhedrons of surprising durability (figure 7). Wave action rolls, rounds, and redistributes them but they resist transport and even serve to armour the softer muds from wave attack until they harden(figure 8). Each mud-sand couplet forms from a single storm, and creates a cobble beach, a transformation from finest to coarsest grained of sediments.

The immediate source of the sediment is still a question to be answered. Circumstantial evidence suggests two sources, the Atchafalaya Mud Stream and the inner continental shelf. The typical color of the Atchafalaya muddy waters is a light yellowish to olive brown. On the inner shelf, sediment of this color has been observed to form the upper several centimeters of the bottom sediment. Beneath that layer however is a dark gray to black organic rich reducing environment, a black mud. During and after some storms, both the deposit of mud and the waters of the surf zone are dark gray to black, very different from the Atchafalaya Mud stream. Interpretation of these observations is that under strong

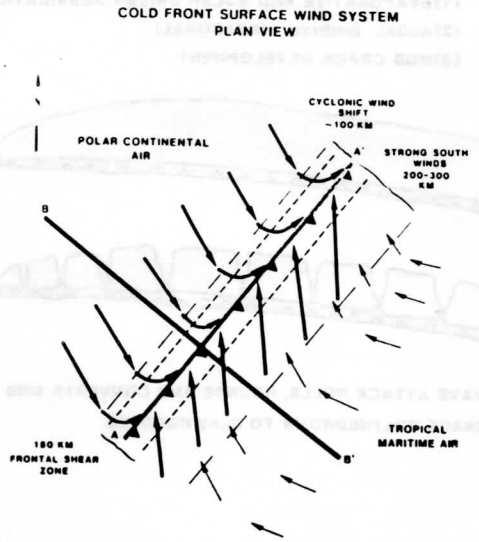

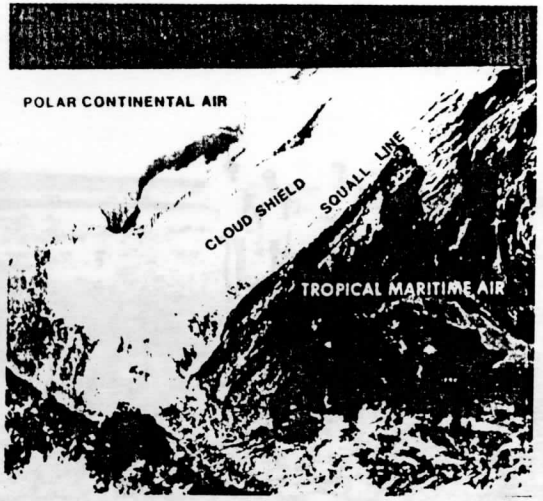

Figure 4. A cold front model, indicating components of a cold front and the associated surface wind field.

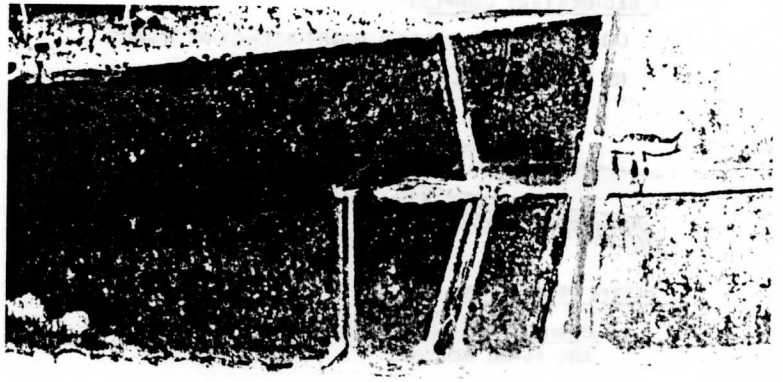

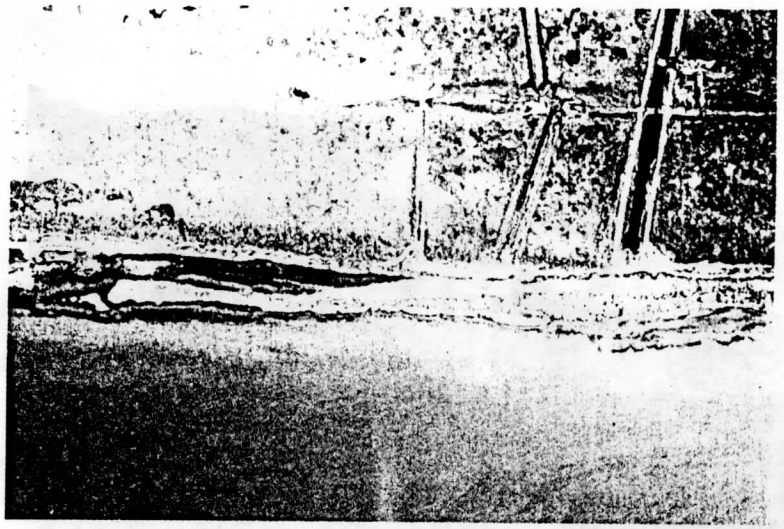

Figure 5. Land accretion between 1987-1989, a pair of pipeline canals 2 km west of Fresh Water Bayou, Vermilion Parish, La.

A SEDIMENTARY COUPLET:

(A) MUD LAYER 8 12CM (CONSISTENCY OF "TOFU")

(B) SAND-SHELL LAYER 1-3CM

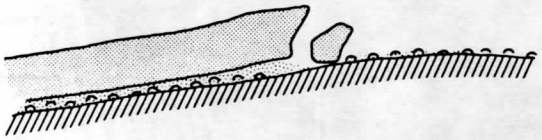

ACTIVE PROCESSES

(A) CONSOLIDATION OF MUD: BY DESSICATION AND ALGAL BONDING

(B) EROSION: SWASH EROSION OF SHELL/SAND LAYER,COLLAPSE OF UNSUPPORTED MUD LAYER. ROUNDING AND BREAKUP OF MUD LUMPS.

a

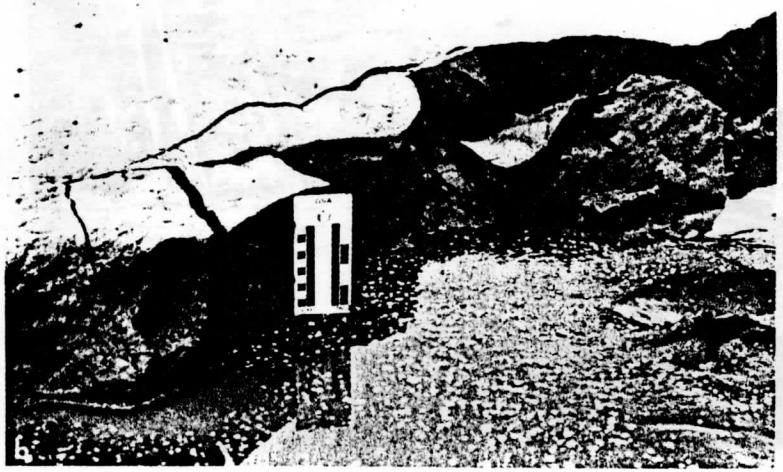

Figure 6. Storm Deposits of fine grained sediment, (a) the sedimentary couplet and processes, (b) photographic closeup of a single storm deposit.

MUD TO CLAY TRANSITION

(1)EVAPORATIVE AND SOLAR DRIVEN DESSICATION

(2)ALGAL BINDING (SEASONAL)

(3)MUD CRACK DEVELOPMENT

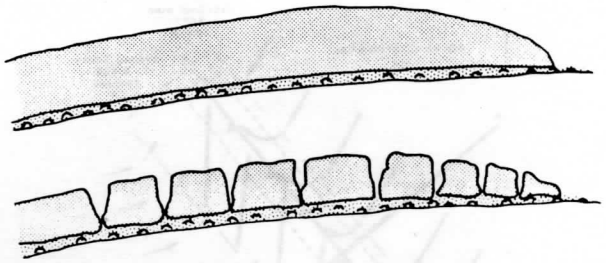

WAVE ATTACK ROLLS, ROUNDS AND CONVERTS MUD CRACK POLYHEDRONS TO CLAY COBBLES

a

Figure 7. Transformation of storm deposits, (a) transformation from very fine grained mud to cobble sized sediments, (b) photograph of recent storm deposits, Chenier plain coast.

Figure 8. Cobble beach formed from mud consolidated to clay and dessicated to "polyhedrons", (a) cobbles of mud armouring newly deposited mud, (b) a stabilized cobble beach along the chenier plain coast.

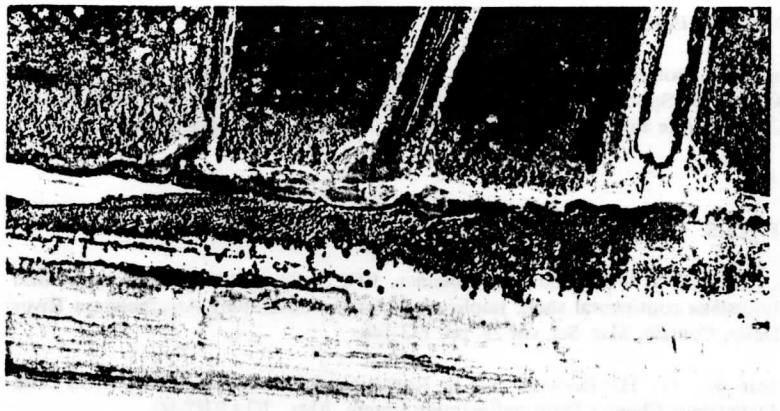

Figure 9. An aerial view of most recent(Sept. 1990) accretion along the chenier plain coast (same site as figure 5). Successive slabs of storm deposited mud are seen as along shore stripes in the newly deposited sediment.

enough wave activity the yellow brown layer on the inner shelf is stripped away and the black mud is resuspended, darkens the waters of the surf zone and is thrown up on the shore face as a deposit of black mud(see figure 8). Given time, the surface of this black mud will oxidize to a yellowish brown but fresh deposits of both colors have been observed.

Most recent deposits along this chenier plain prograding area are shown in figure 9, an aerial view. The imbricate structure is seen as a series of ledges, some cut by dendritic drainages that notch the ridges.

CONCLUSIONS

At least part of the S.W. Louisiana Chenier Plain coast is actively prograding into the Gulf of Mexico. The latest Chenier is over lain by new clay deposits. These are storm surge overwash deposits of semi-fluid mud which became stranded when the storm surge waters retreated. They are transformed from mud to clay and cobble sized polyhedrons by solar and wind driven(evaporative) dessication and consolidation. They armour and stabilize the coast from effects of further wave attack. These deposits, earliest of the transition of the Chenier Plain from an erosional to deposition phase, are most likely to be preserved in the geologic record as they are armoured from erosion by later deposits. The ultimate source of mud is unarguably the Atchafalaya River discharge, but the immediate source, whether the Atchafalaya Mudstream, the inner shelf or both is still subject of investigation. In the realm of remote sensing, caution on interpretation of water color imagery is appropriate. In most such studies, higher water albedos are indications of higher suspended sediment loads. The resuspension of the organic rich inner shelf muds would result in lower albedo of surface waters which might otherwise be interpreted as a lower suspended sediment load.

ACKNOWLEDGEMENTS

This study is supported by the Solid Earth Science Branch of NASA, contracts NAG13-4 and NAGW-2052. Special appreciation is extended to Prof. S. A. Hsu of Coastal Studies Institute for accurate weather forecasts and to the Institute field support group for insitu data.

REFERENCES

Adams, C. E., Jr., J. T. Wells, and J. M. Coleman, 1982 Sediment transport on the central Louisiana continental shelf: Implications for the developing Atdcfhafalaya River Delta, Contrib. Mar. Sci, vol 25, pp. 133-148.

Huh, Oscar K., H. H. Roberts, L. J. Rouse, and D. A. Rickman, 1990 The Atchafalaya-Chenier Plain sedimentary system, Abst. IGARRS-90

Kemp, G. P., 1986 Mud deposition at the shoreface: wave and sediment-dynamics on the Chenier Plain of Louisiana, Ph.D. Dissertation 146pp., Louisiana State University, Baton Rouge, La.

Morgan, J. P. and P. B. Larimore, 1957 Changes in the Louisiana Shoreline, Trans. gulf Coast Assoc. Geol. Soc., Vol 7, pp. 303-310.

Penland, S. and J. R. Suter, 1989 The Geomorphology of the Mississippi River Chenier Plain, Marine Geology, Vol 90, pp. 231-258.

Roberts, H. H., R. D. Adams, and R. H. W. Cunningham, 1980 Evolution of the sand-domiant subaerial phase, Atchafalaya Delta, Louisiana, Am. Assoc. Petrol. Geol. Bull, Vol 64, pp. 264-279

Roberts. H. H., O. K. Huh, S. A. Hsu, L. J. Rouse Jr., and Doug Rickman, 1989 Impact of cold-Front Passages on Geomorphic Evolution and Sediment Dynamicss of the Complex Louisiana Coast.

Rouse, L. J., H. H. Roberts, and R. H. W. Cunningham, 1978 Satellaite ogbservation of the subaerial growth of the Atchafalaya Delta. Louisiana, Geology, vol 6, pp. 405-408.

Wells, J. T., and Paul Kemp, 1981 The Atchafalaya Mud Stream and Recent Mudflat Progradation: Lousiaian Chenier Plain, Transactions-Gulf Coast Association of Geological Societies, vol. XXXI, p. 409-416.

van Heerden, L. Ll., 1989 Sedimentary responses during flood and non-flood conditions, new Atchafalaya Delta, Louisiana, M.S. Thesis, Louisiana State University, Baton Rouge, La., 75pp.

Processes of Coastal Geomorphic Development: Land Building and Land Loss along the Louisiana Deltaic Coastline

Oscar K. Huh*
H. H. Roberts*
Chris C. Moeller#
W. Paul Menzel#

ABSTRACT

The geomorphology of deltas is inherently complex and dynamic as their huge depositional rates have been sufficient to overwhelm the recent sealevel rise of 130 m. in the last 18,000 years. The complex, deltaic geomorphology of the Louisiana coast has its origins in the development of multiple delta lobes, annual floods of clay, silt and sand, levees (natural and man made), cold front passages, hurricanes, regional subsidence and shifting domains of fresh water, brackish water and salt water zones. All of these processes leave geomorphic imprints on the coast, extensively recorded in aerial and satellite imagery. The low relief environments including the intertidal zone and shallow subtidal zones of high river runoff and suspended sediment rich areas are detectable only during unusually low stands of water. Cold front passages, with astronomical tide provide the best views of the results of coastal erosion and depositional processes. The clear water sediment starved regions such as the Chandeleur Island chain are mappable under most conditions due to clear water and visibility of the predominant sandy shoals. Sealevel rise, breakup of the marsh, pond expansion, shore face erosion, landward shoreface migration, salt intrusion and regional subsidence deteriorate the sediment starved coastal environments and results are readily detectable from the air. Formation of bay head deltas, crevasse splays/subdeltas, river channel overflow, and muddy chenier plain progradation, actively build new land. Some 16 NASA color, high altitude aerial photographic missions have been overflown at low water since 1987. They provide critical information on the processes of coastal geomorphic evolution. This kind of information is crucial to coastal zone management.

* Coastal Studies Institute, Louisiana State University, Baton Rouge, LA 70803
# Cooperative Institute for Meteorological Satellite Studies, University of Wisconsin-Madison, 1225 West Dayton St., Madison WI 53706

Georeferencing Airborne Imagery Over New Deltas in Louisiana

ug Rickman
tional Aeronatuics and Space Administration, Building 1100/STL, SSC, MS 39529
Michael C. Ochoa
Lockheed Engineering and Sciences, Company Inc., LESC, SSC, MS 39529
nneth W. Holladay
partment of Mathematics, University of New Orleans, c/o LESC, SSC, MS 39529
Oscar K. Huh
astal Studies Institute, Louisiana State University, Baton Rouge, LA 70803

ABSTRACT: River deltas are geologically, ecologically, and economically very important. But our understanding of the mechanisms which affect the distribution of sediment, the fundamental constituent of all deltas, is neither complete nor sufficient. For mid-latitude coasts, recent work indicates that violent summer storms, such as hurricanes, are less important movers of sediment than the passage of winter cold fronts. Testing this idea will require the detection and description of the mechanisms involved in the movement of sediment as a response to the passage of a cold front. An experiment to do this is in progress. Designed around the CAMS scanner, flown on a Lear Model 23 jet, the research requires the integration of dozens of separate aircraft flights over several years. In an area which is dominantly water, the remainder being rapidly changing coastline and marsh, standard techniques of geometric correction are neither economically feasible nor technically practical. As a result, a fundamentally new approach to the georeferencing of aircraft imagery has been developed. Working within ELAS, the software runs on a general purpose computer. Among other things, the software uses the aircraft inertial navigation data. It is able to automatically map a three channel, 1600 line file through a 90° rotation in less than 14 minutes. With the picking of a few control points, RMS errors of less than 2/3 of a pixel may be obtained. The user is able to map to any of the standard USGS projections. It has reduced geometric correction to a task requiring hours instead of weeks of effort, while achieving previously unobtainable levels of accuracy.

INTRODUCTION

RIVER DELTAS are geologically, ecologically, and economically very important. Ancient deltas are the source of much of the world's petroleum reserves, modern deltas are sites of ma- ne hatcheries, the location of major fresh and brackish water etlands, and are the homes of millions of people.

All aspects of a delta are regulated by water flow and the material carried by the water. Of the water moved materials, ie sediment is of particular significance. Sediment – sand, silt, id clay – is the stuff of which the delta is made and maintained; it is the fundamental component on which all else, in or on a, delta depends. Therefore, it is ultimately crucial to very other aspect of the delta.

Almost all of the temperate climate deltas around the world are being actively controlled by man. This control, in the form of levees, dikes, dams, and drainage systems, alters the natural ow of water in the delta. This in turn affects sediment distri- utions. Failure to recognize the full consequences of this human intervention gives rise to a host or problems (Walker *et al.*, 1987; LaFranchi, 1987; Chen, 1983).

Given the importance of deltas to man, and the importance of sediment transport to the delta, a full understanding of the processes involved in sediment transport in the deltaic system important. The essence of current understanding has the river elivering mixed sediments to the ocean, where a delta is built hrough a variety of processes (Adams *et al.*, 1985). As a deltaic lobe grows, the path length to the sea increases. Eventually, he river cuts across the recent deposits and finds a shorter path o the sea. At the new discharge point a new lobe begins to grow. While the river continues to expand the delta, the ocean continually attempts to reshape or destroy the delta. Wave ac- ion, long shore currents, and turbidite flows contribute to this. Presumably, another major component of the reshaping processes along mid-latitude coasts is the effect of hurricanes. As a delta can be quite large, at different places in one delta, growth, erosion, and transitional stages can exist contemporaneously. Such is the case in the delta of the Mississippi River. However, our understanding of the mechanisms which affect the distribution of sediment in and from a delta is neither complete nor sufficient.

With members of the Coastal Studies Institute (CSI) of Louisiana State University, the Science and Technology Laboratory of NASA/SSC is looking at a portion of this problem. Specifically, we are studying the transport of delta-derived sediments along the Louisiana coast. Our hypothesis is that the action of winter cold fronts is a more important forcing agent in sediment transport than the action of hurricanes. Results of earlier work by the CSI workers led them to this concept (Roberts *et al.*, 1987). Testing the idea requires study of the phenomena over a wide range of scales, both in time and in space. For several reasons, the most cost effective way of obtaining the needed data is by use of imagery acquired by an airborne scanner. Aircraft acquisition can be sensitive to weather patterns, tide, and cloud conditions. An aircraft can look at the same area many times in one day with resolutions down to a few metres. Compared to spaceborne systems, airborne systems also offer a much wider range of spectral coverage. For such reasons, our research is being done using the Calibrated Airborne Multispectral Scanner (CAMS) instrument, developed and operated by STL.

The CAMS has six bands which provide continuous spectral coverage from 0.45 to 0.90 μm, two bands in the near-IR and one band in the thermal-IR (Figure 1). In the CAMS imagery one can clearly see variations in sediment load and temperature contrasts (see cover). With monitoring through time, it is possible to determine direction of water motion, rates of motion, and changes in geomorphology. However, introducing the element of time, necessary for the desired numerical analysis or

PHOTOGRAMMETRIC ENGINEERING AND REMOTE SENSING,
Vol. 55, No. 8, August 1989, pp. 1161-1165.

0099-1112/89/5508–1161$02.25/0

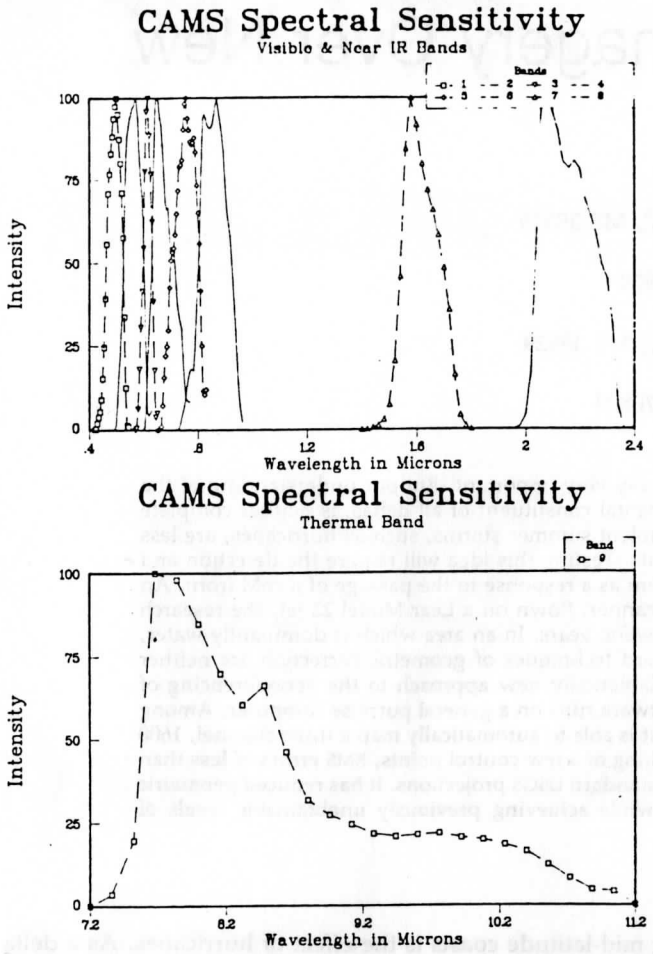

FIG. 1. Spectral curves for the CAMS scanner.

modeling, requires multiple data acquisition. This greatly complicates use of the imagery. For this reason, the scanner has two additional features, both of which are critical for the success of this project. First, as integral parts of the scanner, there are two thermal blackbodies and a calibration lamp. These function as standards of known radiance. They are scanned once every line of imagery. With the data from these, it is possible to convert the recorded digital values to absolute units measured at the sensor. Subsequently, using the appropriate atmospheric and geometric models (ELAS, 1987, module TRADE), is is possible to determine the radiance of the ground targets. Second, the scanner directly logs position and attitude information from the aircraft's inertial navigation system into each scan line of imagery.

Our experimental design requires repeated flights over the study areas. One group of flights is designed to track, coordinated with the passage of a cold front, the response of the water in and about the delta. Another set of flights is needed to observe results integrated over single and multiple years. All of this monitoring creates an enormous amount of data. To be used for computing such things as flow rates, the data must be registered to a common base. Given the nature of the study area, the precision needed, and the quantity of data, geometric correction is a major practical problem for this research.

GEOMETRIC CORRECTION

SOME PROBLEMS WITH EXISTING ROUTINES

Registration of imagery to a common base, usually a map of the Earth, is a common, fundamental need in remote sensing and GIS work. Many people have worked on the problems involved, and a number of approaches exist (Gee, 1988; Moik, 1980; Bernstein, 1983). There are two basic approaches. One approach is to numerically model the geometry of the scanner-target system, usually employing orbital elements and more or less sophisticated models of the Earth's shape. The other approach requires identification of points common to the image to be corrected and some assumed standard, usually a published map.

The points used are termed tie points or control points. Then, by employing some type of regression routine, an equation or set of equations is developed which translates image coordinates into the coordinates of the map. Various combinations of these two approaches are also used, seeking to optimize accuracy and/or minimize the manual effort required.

The complex motions possible in an aircraft and lack of specific, detailed information recording such motion has generally precluded the use of the former approach with data from airborne scanners. It is the authors' observation that most routines which may effectively be used to correct the geometry of airborne scanner imagery rely on abundant, well distributed, manually selected control points. Even these routines are not commonly available.

For this research project, much of the study site is water. Further, with almost no topographic relief, small changes in water level result in large changes in the land/water boundary. There are few mapped, well defined, man-made features in the area. Several parts of the study area are also rapidly changing; even two year old maps can be badly out of date. Manually picking numerous, well distributed control points is simply not possible for such an area.

Further, a high accuracy for the geometric correction is required for this study. Some of the features being mapped will move only a few pixels during the course of the research, which will last three years. Therefore, location errors of less than a pixel, RMS, are needed. This is an accuracy which is usually obtained only with data from satellite imaging systems.

Most routines capable of correcting aircraft data require man-days or even man-weeks of operator time. They also use many hours or days of computer time even for moderate sized files. Single data sets for this project form arrays as large as 9000 by 700 by 9. This is approximately 57 MBytes of data per data set. Most of the study sites are not oriented due north-south or east-west, and maps of the area covered look like long, thin rectangles. Because of this, the output files may be 3 to 5 times the size of the input file. Files of this size become burdensome because of I/O limitations in most computers. Because of these problems, the amount of time required to accomplish the registration of each data set must be considered.

As a result of these factors, a new approach to the digital correction of aircraft imagery was developed. It is expressly designed to avoid the problems noted above. It is part of a major software package for efficient geometric manipulation of images. A full discussion of this new approach will be reported elsewhere, after applications for copyright have been filed. The software is available as part of the ELAS package, developed by STL. Here we wish to discuss the concepts involved in that portion of the software expressly designed to handle aircraft data.

MODELING THE AIRCRAFT'S FLIGHT

The existing scanner continuously incorporates navigation data from the aircraft's inertial navigation system (INS). Currently, this is a Litton model LTN-72R, on board a Model 23 Learjet. With each scan line, the system records the position of the aircraft in longitude and latitude. These are recorded to the tenth of a minute, equivalent to approximately 177 metres at the equator. The scanner also records the true heading of the

aircraft to a tenth of a degree. Roll is not recorded; however, it is used internally by the sensor to automatically maintain the sensor nadir at a specified element in the scan line. Assuming that pitch of the aircraft is constant, enough data are available to estimate the location of each pixel on the ground. For implementation in an algorithm, the problem can be broken into parts. First, one must model the flight of the aircraft. Second, one must know the scanning characteristics of the CAMS.

Although the longitude, latitude, and true heading are recorded for each scan line, there are several reasons why these data could not be used directly. Probably the single largest problem is that the aircraft will advance forward much less than a tenth of a minute for every scan of the CAMS. Thus, many lines will have the same reported location (Figure 2). As the aircraft can fly parallel to either longitude or latitude, it may happen that the value recorded for one variable may change very slowly while the other changes much more rapidly. Data acquisition may also be accomplished over a wide range of speeds; thus, the length of time and the number of scans necessary to cover one-tenth of a minute of the Earth's surface will vary significantly. There can be systematic errors in the values written into the CAMS data stream. The most serious of these is a nearly consistent error in location as reported by the INS (Figure 2). The direction and magnitude of the error is unknown, and varies between each data set. Another problem arises because the INS and the scanner are asynchronous; data from the INS is not updated at the same rate as the scanner requires it. For a single scan line, the error could be significant. To add confusion, the data recorded from the INS can have a high level of noise. A noise value typically, but not always, appears as a radical departure, more than a few tenths of a degree, from the preceding values. Yet the aircraft's ground track and orientation in space can change over the course of a few scan lines by similar amounts. Such real differences must not be confused with noise.

Our approach to the problems of modeling the aircraft's flight is two fold. First, to remove "wild" points, the longitude, latitude, and true heading data are independently processed through a simple filter. The user supplies a value which defines the maximum change that can occur from one scan line to the next. Data for three scan lines is read. The difference between the value of the first line and the value of the second and third lines must be within the maximum change specified. If they are, the process moves forward one line and repeats. If either one of the values is outside of the limit, the value for the second line is replaced by the first value. The process then moves forward one line and repeats. The process assumes that the first two scan lines of data are good. It also asumes that the user can specify a limit to the rate of change, beyond which noise may occur, but the true behavior of the aircraft can not exceed. This has not been found to be a problem in practice.

Having removed the obviously bad values, the program attempts to smooth the data by using a local fit to a line. This functions to smooth out small scale variations, as caused by the tenth of a minute resolution of the input and the small perturbations which pass through the noise removal filter. It is assumed that the aircraft's motion is approximately linear over short time intervals; so the data for a window of up to several seconds duration is used to fit a regression line that estimates the aircraft's behavior with more precision than is available in the raw data. Window length is varied automatically by the algorithm. Looking ahead of the region used to make the regression, the routine uses the regression line to predict a value. If the predicted value is within a certain margin of the actual value, processing continues and the window's length is expanded if it is less than the preset maximum. If the prediction fails, the window's length is reduced before continuing the processing.

As the algorithm proceeds through the data, where there is little real change in the trend of values, the window will be as large as the user permits. Yet it will shrink to the smallest permitted length in order to fit around real curves in the data. The user has direct control over both the maximum and minimum window lengths. To maximize processing speed, the entire data set is stored so that the running parameters used to compute the regression line can be quickly and exactly updated when the window is moved. Thus, it is practical to read in 4 megabytes of data, obtain the needed regression, and output the navigation estimates in less than 2 minutes.

Having modeled the aircraft's flight, one can begin to determine what location on the Earth corresponds to each pixel in the image. This requires knowing specific characteristics of the scanner. Needed are the angular distance between each pixel in a single scan line, the number of the pixel at nadir, the numbering scheme for the elements, and the direction which the scanner sweeps. Also needed is knowledge of the aircraft's altitude above the terrain, as this controls the distance on the ground between the centers of the pixels.

Figure 3 illustrates the geometry involved. The regression line through the INS data indicates the ground point immediately

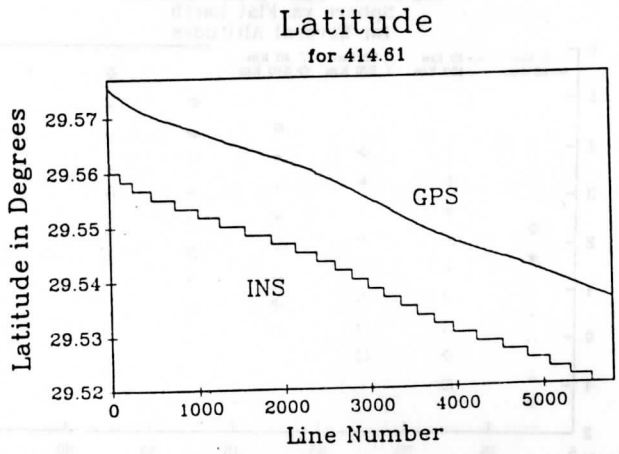

FIG. 2. INS data from the CAMS scanner. Also shown are Global Positioning System (GPS) data also recorded during this flight. Each line is 5 metres apart; therefore, a thousand scan lines covers 5 kilometres. Note the relative displacement of more than 1 kilometre between the INS and the more accurate GPS. Also note the lack of fine detail in the INS as compared to the GPS.

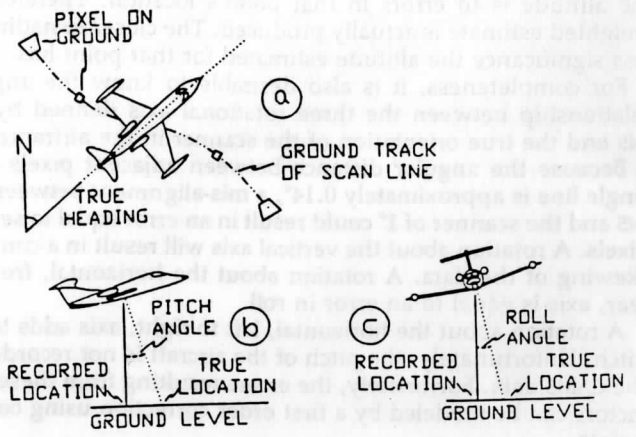

FIG. 3. Geometric relationships between a scan line and the aircraft. The ground track in (a) is drawn as if the scanner were sweeping from left to right. The change in pixel shape with scan angle is exaggerated for clarity.

under the aircraft as a function of scan line. However, due to the aircraft's pitch, the scanner is not looking straight down. If the scanner were not compensated for roll, an additional correction would also be needed. As illustrated, both of these corrections are functions of altitude and can be handled by simple geometry. A more subtle distortion is caused by the scanner sweeping through a constant angle per unit time, while looking at an essentially planar target. The distance between pixels on the ground, per unit time, is not constant. At angles far from nadir, the distance is considerably greater than for angles near nadir.

At 15, 30, and 45 degrees, assuming a size at nadir equal to 1, the distance between pixel centers is 1.07, 1.34, and 2.01. The effect of this in a scanning raster system is to cause features far from nadir on one side of the aircraft to appear displaced, or squeezed in, ahead of where they should be in the image. On the other side of the image, features are behind where they should be. Thus, a straight road appears "s" shaped.

Uncompensated Factors

There are a number of factors for which the existing algorithm makes no allowance. In each case this has been done for one of two reasons; either there are no data available to improve upon the situation, or the effect is so small as to be negligible when compared to other errors.

First, we consider those items in the CAMS for which we possess no better alternative.

Potentially, the greatest single source of error is a lack of good information about the altitude above the terrain at which the data were acquired. We currently have two options. One, we can accept the value listed on the flight log. This is a single number from a barometric altimeter, provided to the operator of the sensor by the pilot. The second option is to estimate the altitude of the aircraft from the imagery. Given the known locations of two points on the ground, seen during the sweep of a single scan line, and the element locations of the points in the image, it is a fairly straightforward task to compute the altitude of the aircraft. In practice, it is difficult to get multiple points along a single scan line. Therefore, the software uses three or more scattered points, and computes a first order regression relating element and line to ground coordinates. With this regression equation, an estimate of the location of nadir for each scan line may be obtained.

For each control point, the estimated nadir and the x,y location of the control point may be used to compute an approximate altitude. There is a relationship between accuracy and distance from nadir. The closer to nadir a point is, the more sensitive the altitude is to errors in that point's location. Therefore, a weighted estimate is actually produced. The closer to nadir, the less significance the altitude estimated for that point has.

For completeness, it is also desirable to know the angular relationship between the three rotational axis defined by the INS and the true orientation of the scanner in the airframe.

Because the angular distance between adjacent pixels on a single line is approximately 0.14°, a mis-alignment between the INS and the scanner of 1° could result in an error equal to several pixels. A rotation about the vertical axis will result in a constant skewing of the data. A rotation about the horizontal, front to rear, axis is equal to an error in roll.

A rotation about the horizontal, left to right, axis adds to the pitch. Unfortunately, the pitch of the aircraft is not recorded in the CAMS data. Fortunately, the errors resulting from these four factors can be modeled by a first order correction using control points.

There are several uncompensated error sources related to the recorded INS data. A constant displacement comes from the delay between when the INS memory is read and when the nadir element is scanned. The rate of scan also controls the size of this error. It is approximately half the error due to ignoring the aircraft's forward velocity. Effectively, it is an error which will add a constant offset of the data from their true location. There can also be systematic errors in the output of the INS. For example, the system relies on pilot input for proper initialization. Locations of ground stations are also subject to error of varying magnitude. These errors can also be corrected by first order modeling.

There are also several sources of error for which it is theoretically possible to make compensations. First, the aircraft's forward velocity or the length of time between scan lines is ignored. This should not be done if the aircraft moved forward a large distance in the time the scanner took to complete a scan line. For the CAMS, ignoring this factor results in a total error of between 0.47 and 9.5 metres. The former is for high rates of scan, the latter is for low scan rates. Half of the error will be before and half after nadir. In practice this yields an error of between one sixth and one twentieth of a pixel.

Within the algorithm, a decision must be made to define the shape of the Earth as sperical, elliptical, or an even more complex shape. Our choice of geometry has been guided by analysis of the sensitivity to the errors inherent in each option. An additional consideration was the practicality of implementing each option. For example, an error which can be ignored for the CAMS is the assumption of a flat target when computing the linear distance from nadir to an element. This cannot be done when the altitude of the scanner and the angular swath width become large enough or the instantaneous field of view (IFOV) becomes small enough. Figure 4 shows the error in distance which results from assuming a flat Earth instead of a spherical Earth. When considering the effect of the error, one should normalize by the pixel size at nadir. To illustrate, the maximum altitude from which the CAMS operates is approximately 12,000 metres; the scanner has an IFOV of 0.0025 radians. Thus, a five-metre error, as would occur at an altitude of 10 kilometres and look angle of 40 degrees, is not significant compared to the 25-metre spot size.

An elliptical shape is used when computing distances as a function of latitude. The improvement in results as compared to use of a spherical model was small, but definitely detectable even in 5-metre imagery.

Topography can also seriously affect the geometry of the image. In theory it is possible to correct the image as a function of target relief if sufficient data are available. Such data would

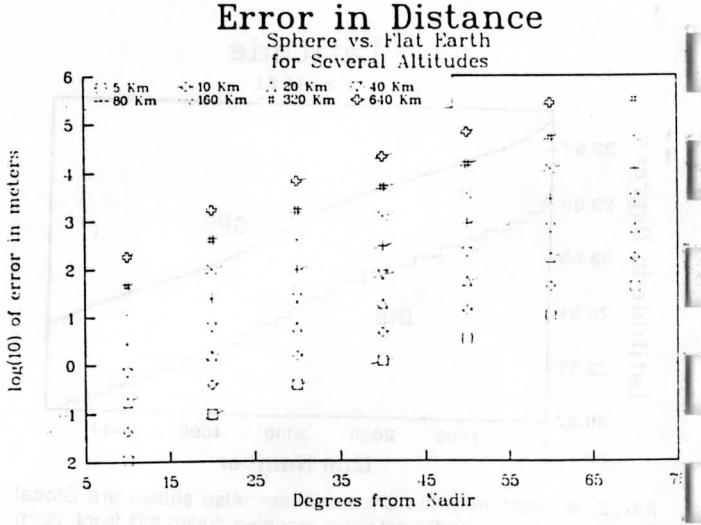

FIG. 4. Errors in distance resulting from the assumption of a flat Earth versus a spherical Earth. Plotted curves are for altitude ranging from 5 to 640 km.

ave to come from either digitized maps or distance measuring devices on board the aircraft linked to the scanner. We have contemplated such a system, but have taken no action at this me to actually create one. In the case of the study of the delta, pography is not a significant concern. Total relief in the area is approximately a few metres.

APPLICATION

The preceeding concepts have been implemented in the ELAS software package. An example of the use of the techniques is hown in Plate 1. The map is a composite of the USGS 15' sheets, ated, 1957. The CAMS data were acquired 22 January (center) and 23 January (bottom) 1988, at 2210 GMT and 1657GMT, respectively. Data acquisition was done at the altitude of approximately 12 km, with a ground resolution at nadir of 30 metres. n order to obtain coverage of this area in a single pass, the aircraft had to fly an "S" shaped path. The unusual shape of the data segments is due to clipping the imagery to remove ignetting and for presentation. Vignetting of the telescope occurs when the aircraft executes sharp manuvers during data acquisition. Mapping of the 23 January data was done with the automated georeference software. It accurately overlays the map lata wherever there has been no significant change. Recording of the INS was not proper during acquisition on the 22nd; therefore, it was approximately mapped to the data of the 23rd using a piecewise B-spline algorithm, controlled by points which were manually picked. Both sets of imagery have been processed to visually enhance features and patterns in the water. Calibration techniques have not been applied; therefore, color significance between images is only approximate.

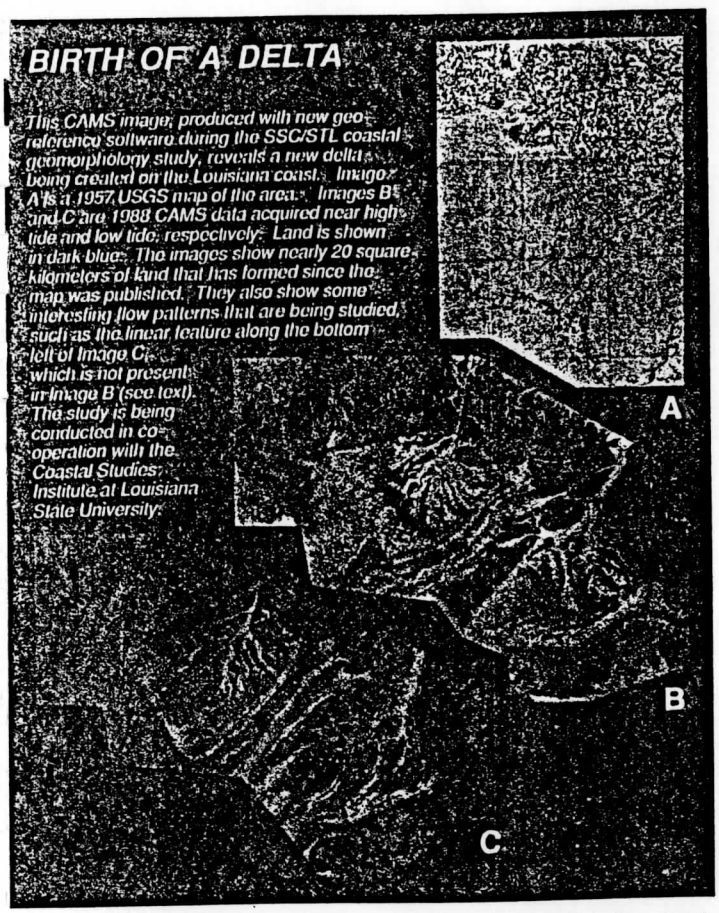

PLATE 1. Geometrically corrected CAMS imagery, Atchafalaya Bay, Louisiana. The topographic map is a composite of the USGS 15' series sheets for the area, dated 1957. For a description of the CAMS imagery, see the text.

Examination of the images shows several of the features important to the geologic study. The dominate point is the development of two new deltas in just a few years. These have a land area at low tide of approximately 20 Km^2. The differences between the two CAMS images is due to position in the tidal cycle. The data on the 22nd were acquired when the tide was coming in, while the data from the 23rd was acquired when the tide was going out. The effect on the flow patterns and the amount of exposed sediment is very dramatic. Of particular interest is the northwest-southeast linear feature in the left center portion of the two images. First indentified in these images, members of the Coastal Studies Institute have now found a submarine margin of the deltas in this location. Integrated with previous and more recent imagery, these data will be used to measure the growth of these new deltas.

SUMMARY

A study of the Mississippi River delta using data from the CAMS has begun. In the course of this research, multiple data sets will be acquired and will need to be geometrically integrated. As this was not practical with previous software, a new system has been developed. Implemented inside ELAS, the programs take advantage of the inertial navigation data from the aircraft. These are filtered, a regression curve is fitted to them, and the location of the nadir point is modeled as a function of scan line number. Employing specifications of the scanner and an estimate of the aircraft's altitude, an estimate of the ground location of each pixel can be made. An examination of the uncompensated errors shows that many of them can be modeled to a very high degree of accuracy by first-order equations. Other problems or errors are generally not significant, especially in the context of the current project. Thus, by the addition of a few control points, a very accurate mapping of the imagery can be obtained.

REFERENCES

Adams, C. E., J. T. Wells, and J. M. Coleman, 1985. *Sediment Transport in Relation to a Developing River Delta: Models in Geomorphology* (ed., M.J. Woldenberg, Alan,), U. of Boston Press, pp. 171–189

Bernstein, R., C. Colby, S. W. Murphrey, and J. P. Snyder, 1983. Image Geometry and Rectification, *Manual of Remote Sensing*, (R. W. Colwell, Editor-in-Chief), American Society of Photogrametry, Falls Church, Virginia pp. 873–922.

Chen, A., 1983. Dammed if They Do and Dammed if They Don't, *Science News*, Vol. 123, No. 13, pp. 204–206.

ELAS, 1987. *Earth Resources Laboratory Applications Software. Vol II, User Reference*, Earth Resources Lab. Report No. 183, Stennis Space Center, NASA; SSC, Mississippi 39529, pp. 1–23.

Gee, H.R., 1988. New Model for the Geometric Correction of Multispectral Scanner Data: Conference 933, SPIE Proceedings Vol. 933, Orlando, Florida.

LaFranchi, H., 1987. Louisiana's Disappearing Wetlands: *Christian Science Monitor* 9 April, p. 1.

Moik, J. G., 1980. *Digital Processing of Remotely Sensed Images*, NASA SP-431, National Aeronautics and Space Administraton, Washington D.C.; 329 p.

Roberts, H. H., O. K. Huh, S. A. Hsu, L. J. Rouse, and D. Rickman, 1987. Impace of Cold-Front Passages on Geomorphic Evolution and Sediment Dynamics of the Complex Louisiana Coast, *Coastal Sediments '87*, WW Div./ASCE, New Orleans, Louisiana 12-14 May 1987. pp. 1950–1963.

Walker, H. J., J. M. Coleman, H. H. Roberts, and R. S. Tye, 1987. Wetland Loss in Louisiana: *Geografiska Annaler*, Vol. 69, pp. 189–200.